12-2018

Carbon Fibers with Enhanced Mechanical Properties Derived from Lignin-Based Precursors

Jing Jin
Clemson University, lovevzw@hotmail.com

CARBON FIBERS WITH ENHANCED MECHANICAL PROPERTIES DERIVED FROM LIGNIN-BASED PRECURSORS

A Dissertation
Presented to
the Graduated School of
Clemson University

In Partial Fulfillment
of the Requirements for the Degree
Doctor of Philosophy
Chemical Engineering

---

by
Jing Jin
December 2018

Accepted by:
Dr. Amod A. Ogale, Committee Chair
Dr. Douglas E. Hirt
Dr. Mark C. Thies
Dr. Igor Luzinov

ABSTRACT

Carbon fibers are known for their outstanding specific strength and modulus, and they have been commercially used in structural and lightweight composites. However, the main barriers to the large-scale commercial application of carbon fibers are the high cost of petroleum-based precursor polyacrylonitrile (PAN) and the environmental concerns associated with its conversion to carbon fibers. Toxic by-products such as hydrogen cyanide (HCN) are generated during the stabilization step of PAN-based carbon fibers. Other precursors being used today, carbonaceous pitch and rayon, either are too expensive or produce carbon fibers with low strength. Among bio-derived feedstocks, lignin is of increasing interest as a precursor for producing carbon fibers. Most of early research studies utilizing lignin focused on the melt-spinning of hardwood lignins because of their better spinnability. Softwood lignin is difficult to melt-spin, but can be dry-spun with partial acetylation. Tensile strength for most of lignin-based carbon fibers was below 1.0 GPa, which is much lower than that needed for high-performance composites. In this dissertation, the primary research goal was to develop lignin precursors to produce carbon fibers with improved mechanical properties.

In the first part of this study, lignin/PAN (L/P) polymer blend was used as the precursor to produce carbon fibers. As-received softwood kraft lignin and PAN were blended to form precursor with lignin content as high as 50 wt%. Rheological measurements established that increasing lignin content in the spinning solution reduced shear viscosity and normal stress, indicating a decrease of viscoelastic behavior. The

lignin/PAN blend solutions were wet-spun into fibers, but lignin leaching occurred during coagulation that resulted in macro-void formation within initial L/P fibers. To eliminate the macro-voids within L/P fibers, out-diffusion of lignin during wet-spinning was reduced by controlling the coagulant composition. It was confirmed by UV–vis spectroscopy that an insignificant amount of lignin leached out from fibers into coagulant when 0.2% initial lignin content was incorporated into the coagulant. Thus, void-free, equi-component, L/P- derived carbon fibers were successfully produced. Using Raman spectroscopy and wide-angle X-ray diffraction, it was observed that higher lignin content led to a lower degree of graphitic crystallinity. For lignin contents of 25 to 50 wt%, the tensile strength of resulting carbon fibers was 1.2 GPa and not significantly affected. However, the modulus decreased from 148 GPa to 106 GPa, because the higher lignin content disturbed the formation of a well-layered turbostratic carbon structure.

The second major component of this research study focused on producing carbon fibers using fractionated-solvated lignin precursors (FSLPs) by dry-spinning. The FSLPs were generated via a process, Aqueous Lignin Purification using Hot Acids (ALPHA), recently developed by Thies and co-workers *(1)*. Three purified lignin fractions of increasing molecular weight were dry-spun into fibers. The spinning conditions were systematically investigated with the goal of enhancing draw-down of the precursor fibers. The solution viscosity was estimated at about 2 Pa·s (shear rate of 2×10^5 s^{-1}). Larger draw-down ratios could be obtained for the higher MW FSLPs. Within the range of conditions investigated in this study, a solution concentration of 50-55 wt% and a temperature range of 30-45 °C were identified as the window of optimal spinnability.

Thermo-oxidative stabilization of lignin fibers was successfully performed under constant load conditions to obtain about 400% extension within fibers, whereas carbonization was performed under constant-length conditions.

Finally, the microstructure and properties of FSLPs-based carbon fibers were studied. From Raman spectroscopy and X-ray diffraction analysis, it was observed that an increase in the molecular weight of lignin fractions led to a better layered microstructure within the resulting carbon fibers. At low carbonization temperatures (1000-1600°C), the lignin-based carbon fibers displayed a low degree of graphitic crystallinity, as measured by Raman spectroscopy, XRD, and TEM. Carbonization temperatures above 2000 °C improved the ordering of the layer planes, but FSLP-based carbon fibers still displayed a low degree of graphitization. The mechanical and electrical properties of FSLP-based carbon fibers were also investigated. Carbon fibers produced at 1000°C from the highest MW FSLP possessed the highest average tensile strength of 1.39±0.23 GPa and a modulus of 98±5 GPa, representing the best-quality lignin-based carbon fibers reported in the literature to date. When the fibers were carbonized at higher temperatures (>1300°C), a reduction in tensile strength was observed due to the generation of surface defects. However, the tensile modulus and electrical conductivity increased as the carbonization temperature increased because of the improved graphitic crystalline structure.

In summary, the results from this study established a route for wet-spinning void-free lignin/PAN fibers and dry-spinning fractionated lignin precursors with increasing molecular weight, leading to carbon fibers with enhanced properties.

DEDICATION

This work is dedicated to my family and everyone who supported and assisted me: my parents, and my PANG's family.

ACKNOWLEDGMENTS

I would like to express my sincere gratitude to the following people who supported and helped me to successfully complete this work and reach graduation.

My dissertation advisor, Dr. Amod Ogale, for his guidance, encouragement and support over the last six years. Thanks for this opportunity to work in carbon fiber group.

My committee members, Dr. Doug Hirt, Dr. Mark Thies, and Dr. Igor Luzinov, for their knowledge, advice, support and many encouragement.

Members of the present and past group members: Dr. Meng Zhang, Dr. Marlon Morales, Dr. Sam Lukubira, Dr. Byron Villacorta, Dr. Steve Tang, Bushra Rahman, Ozgun Ozdemir, Victor Bermudez and Sagar Vishnudas, from whom I not only learned a lot, but also had a good time working with. Thanks for making me feel part of a team.

My many undergraduate assistants, especially Eric Hair who did so much to help me clean and organize the labs.

Dr. Thies research group: Junhuan Ding, Dr. Adam Klett and Graham Tindall for their professional contribution to part of my work.

Army Research Lab, Center for Advanced Engineering Fibers and Films (CAEFF), and National Science Foundation for sponsoring the research.

Dr. Taghi Darroudi and Dr. Haijun Qian, Electron Microscopy Lab, for teaching me about electron microscopy and helping me anytime I needed.

Dr. Colin McMillen, Department of Chemistry, for his effort and professional support in the X-ray diffraction analysis conducted in this study.

Bill Coburn for all the time he spent on fixing what I needed and setting up what I needed set up.

ChBE faculty and staffs, Dr. Mark Roberts, Dr. Sapna Sarupria Dr. Joseph Scott and Dr. Rachel Getman for their help during my early PhD studies, as well as Mrs. Diana Stamey, Mrs. Joy Rodatz and Mrs. Terri McAllister for the friendship and making ChBE department like a home.

My family for their endless love and support throughout my life. Especially my parents, Yuanlin Jin and Jie Sun, without whom I could not have done any of this.

My Clemson friends, Qiuchen Wang, Hongye Wang, Mingzhe Jiang, Juan Wang, Xiaozhen Yu, Difeng Gao, and Yinye Gan for your friendship throughout six years. Thank you for being there for me.

TABLE OF CONTENTS

Table of Contents (Continued)

Page

Table of Contents (Continued)

Page

Table of Contents (Continued)

Page

LIST OF TABLES

List of Tables (Continued) Page

LIST OF FIGURES

Figure Page

List of Figures (Continued) Page

List of Figures (Continued) Page

List of Figures (Continued) Page

List of Figures (Continued) Page

List of Figures (Continued) Page

CHAPTER ONE
INTRODUCTION

1.1 Introduction to carbon fibers

Carbon fibers (CFs) possess excellent strength and stiffness, low density, good chemical stability and high thermal and electrical conductivity. Consequently, carbon fibers are used primarily as reinforcing fibers in high performance composites *(2, 3)*. In Table 1.1, the properties of different reinforcing materials are summarized. Because of the type of carbon fiber precursor and the processing method employed, the properties of resulting carbon fibers can vary over a wide range. High strength carbon fibers possess tensile strengths as high as 7 GPa, which is approximately five to seven times higher than steel. High-modulus carbon fibers have the highest modulus of 900 GPa; in addition, thermal conductivities of 1000 W m^{-1} K^{-1} have been achieved for such carbon fibers, with adequate thermal treatment. Overall, carbon fibers find applications where strength, stiffness, and low weight are critical requirements, and where high temperature and chemical resistance are important.

Table 1.1 Physical and mechanical properties of reinforcement materials *(4, 5)*.

Material	Specific Gravity	Strength (GPa)	Specific Strength (GPa)	Modulus (GPa)	Specific Modulus (GPa)	Thermal Conductivity (W/m-K)	Electrical Resistivity (μΩ-m)
Steel	7.9	1-1.5	0.1-0.2	200	25	17	0.72
Alumina	2.7	0.5	0.2	76	28	188	0.003
Kevlar fibers	1.45	2-3	~1.5-2	130	93	0.04	N/A
E-Glass fibers	2.60	3.5	1.4	76	29	10.4	10^{18}-10^{19}
C-Glass fibers	2.49	3.3	1.3	69	28	13	10^{18}-10^{19}
Rayon-based CFs	1.5	0.3-0.7	0.1-0.5	55-62	37-41	4	N/A
PAN-based CFs, T-300	1.76	3.6	2	231	131	10.4	17
PAN-based CFs, T-1000	1.80	6.7	3.9	294	164	32	14
Pitch-based CFs, P-100	2.15	2.41	1.2	759	353	520	1.5
Pitch-based CFs, K-1100	2.2	3.1	1.4	931	423	1000	2.2

Unlike polymers, carbon does not melt, and so it cannot be directly spun into fibers. Therefore, carbon fibers have to be produced from suitable precursors. The precursor material, in its solution or molten form, is first processed into precursor fibers. This spinning step is followed by a stabilization step, where precursor fibers get cross-linked into a thermoset so that the individual fibers sticking to each other. Finally, the stabilized fibers are carbonized in an inert environment at temperatures above 1000°C to obtain carbon fibers. A schematic of carbon-fiber manufacturing process is shown in Figure 1.1.

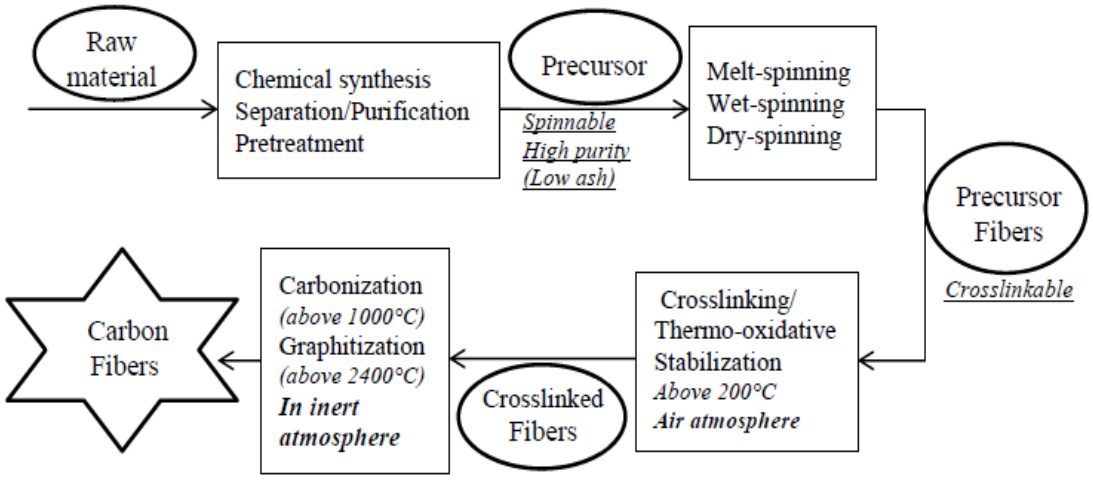

Figure 1.1 Process steps needed for producing carbon fibers. Adapted from reference *(6)*.

Carbon fibers were first produced by Thomas Edison using cotton fibers and bamboo as precursors, which melt then converted into carbon for lamp filaments *(7)*. However, the technical breakthrough for carbon fibers with good mechanical properties started in the late 1960s after the introduction of the process for producing carbon fibers from polyacrylonitrile (PAN) *(5, 8)*. Today, PAN fiber is still the most dominant precursor for the manufacture of high-strength carbon fibers. Later carbon fibers were also produced from pitch *(9)*. Since then, fiber quality has continued to improve and new precursors have been developed. In 2014, the global carbon-fiber market reached about $2 billion; the prediction is for the market to grow to $4.3B in 2021 *(10)*. However, the use of carbon fibers in general engineering and transportation is dominated by cost constraints and high production-rate requirements *(7)*. For such applications, such as automotive, there is need to reduce the cost while maintaining or improving fiber

properties. Thus, investigating sustainable, low-cost precursors, such as biomass to lower the cost of carbon fibers has become a priority in many research areas *(11)*.

1.2 Carbon-fiber precursors

1.2.1 Polyacrylonitrile (PAN)

More than 90% of commercial high-strength carbon fibers used in structural applications are produced from PAN precursors *(5, 12)*. Production of PAN-based carbon fibers includes the polymerization of PAN copolymer, fiber spinning and post-draw before stabilization in air, and carbonization in an inert environment, as illustrated in Figure 1.2 *(13)*.

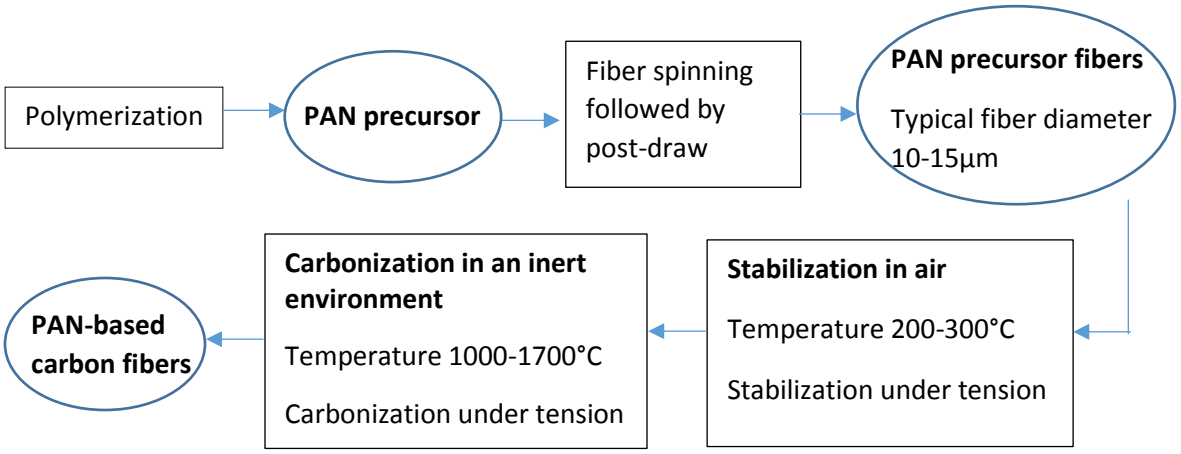

Figure 1.2 Schematic of PAN-based carbon-fiber manufacturing process.

Nearly all PAN precursors are copolymerized with a small amount of another monomer. Regular textile grade PAN contains 15% copolymer, whereas carbon fiber grade PAN contains lower than 8%. Common copolymers include acrylic acid, methacrylic acid, itaconic acid, vinyl acetate, methacrylate, and acrylamide, etc *(5, 10)*.

These PAN copolymers undergo a different mechanism during stabilization as compared to PAN homopolymer, allowing for a slower exothermic reaction and reduction in molecular defects, leading to higher mechanical properties in the resulting carbon fibers *(14)*.

PAN has been spun into fibers via a variety of spinning techniques, such as melt-spinning, wet-spinning, dry-spinning, dry-jet wet-spinning and gel-spinning. PAN polymer has a degradation temperature starting above 250°C, which is lower than its melting temperature – estimated at above 400°C. Therefore, the melt-spinning of PAN is restricted because PAN degrades before it melts *(5)*. By the addition of plasticizers or suitable copolymers, the melting temperature can be lowered, allowing melt-spinning *(15-17)*. In dry spinning, PAN copolymer is dissolved into a suitable solvent, which has low vapor pressure. PAN solution is extruded into hot gas chamber to evaporate the solvent. Due to the constraints of suitable solvent, hot gas temperature and composition, it is difficult to control mass transfer rate in the dry spinning process of PAN *(18)*.

Wet-spinning techniques involving the use of a solution that is extruded into a coagulation medium, and is the most commonly used method for PAN precursor. Variants of this process include wet-spinning, dry-jet wet-spinning and gel-spinning *(10, 19)*. Wet-spinning is the most common technique, consisting of a submerged spinneret in a coagulation bath where the extruded polymer solution fibers solidify as the solvent diffuses out of the fibers. Dry-jet wet spinning is a modification of wet-spinning, which involves raising the spinneret 1-2 cm above the coagulation bath. It introduces the extruded polymer solution into an air gap before going into coagulation bath. Gel-

spinning allows the spinning dope to remain in a gel-like state during extrusion by using high molecular weight PAN and low spinning temperature *(20)*. After coagulation, the precursor fibers are post-drawn and washed in series of stages in order to increase molecular orientation within the fiber, which can enhance the mechanical properties *(21)*.

The thermo-oxidative stabilization step involves the heating of PAN precursor fibers in a temperature range of 180 to 300°C under tension in an air atmosphere *(22, 23)*. In this stabilization process, PAN fiber is converted to an infusible ladder structure, which is able to withstand high temperatures without melting. There are two important reactions that occur during the stabilization process: dehydrogenation and cyclization reactions, which convert C≡N bonds to C=N bonds, as shown in Figure 1.3. When the temperature increases to 600°C, the cyclized structure links up in the lateral direction, forming planar hexagons containing nitrogen atoms *(24)*. The stabilized fibers are subsequently carbonized at high temperatures, typically below 1700°C in an inert atmosphere *(12, 22)*. Tension is still applied on the fibers in order to prevent shrinkage and the loss of preferred molecular orientation. In these two heat-treatment processes, toxic by-products such as hydrogen cyanide (HCN) are generated, raising environmental concerns about the manufacture of carbon fibers from PAN.

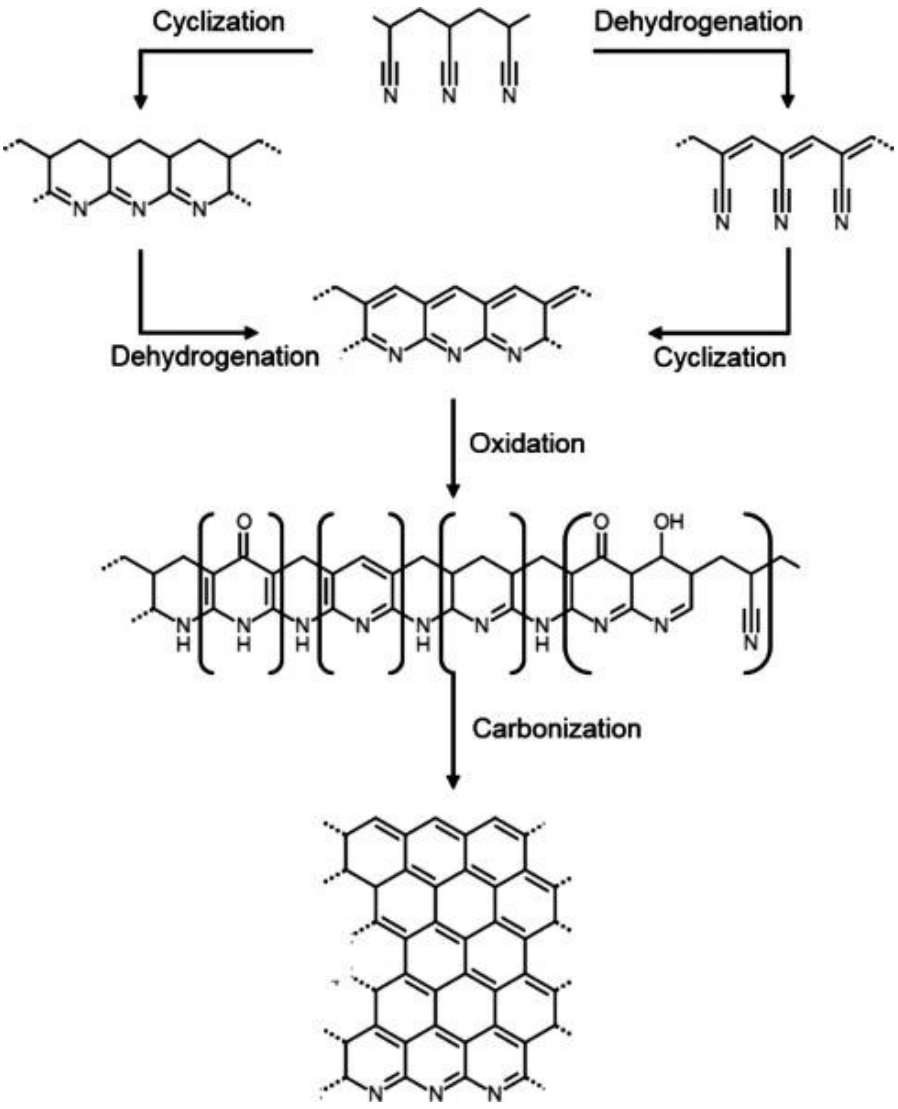

Figure 1.3 Mechanisms of structural changes within PAN fibers during stabilization and carbonization. Adapted from reference *(22)*.

PAN-based carbon fibers display a kidney-bean cross-sectional shape because of the finite diffusion rates in wet-spinning, as shown in Figure 1.4. The microstructure of PAN-based carbon fibers is fibrillar. Within the fibrillar structure, the ribbon-like undulations have the highest amplitude in the center and the lowest near the surface *(12)*.

Also, the layer planes of PAN-based carbon fiber have no regular 3-D order. 3-D schematics of the microstructure of PAN-based carbon fiber are displayed in Figure 1.5. Based on these studies, PAN-based carbon fibers contain extensively folded and interlinked turbostratic layers of carbon, which are not highly aligned with the fiber axis. Thus, they have low degree of graphitization.

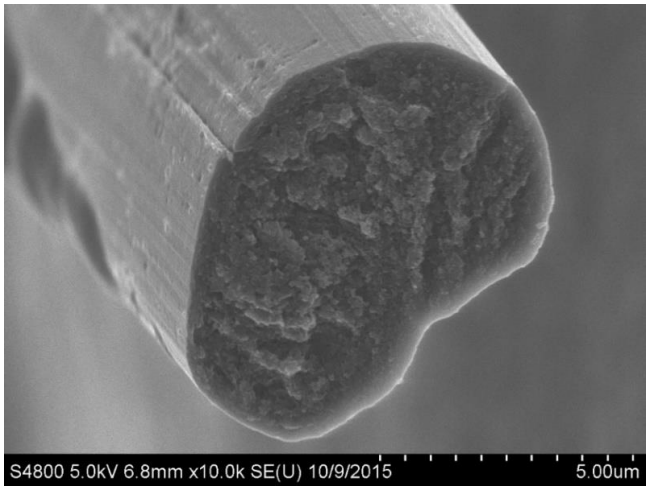

Figure 1.4 Representative SEM micrographs of PAN-based carbon fiber.

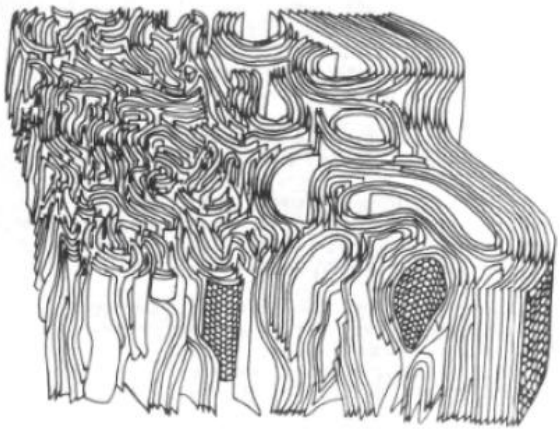

Figure 1.5 Schematic of microstructure of PAN-based carbon fiber. Adapted from reference *(5)*.

1.2.2 Mesophase pitch

Mesophase pitch is usually produced from a highly aromatic coal or petroleum pitch. For the production of high performance carbon fibers, the pitch must be transformed into a mesophase, an oriented liquid crystalline phase *(25)*. The raw pitch can be converted into mesophase by heating to temperatures ranging from 400 ºC and higher for up to 40 hours *(26)*. Solvent extraction is another method to obtain mesophase pitch *(27)*. The extraction can remove the smaller disordering molecules, and the higher molecular weight insoluble fraction can be polymerized by heating it to 230-400 ºC *(25)*. A typical mesophase pitch precursor molecule is illustrated in Figure 1.6, with molecular weight about 1000 g/mol.

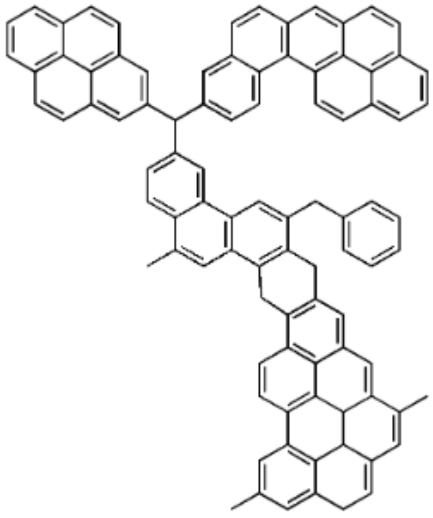

Figure 1.6 A typical chemical structure of aromatic hydrocarbon found in mesophase pitch. Adapted from reference *(28)*.

Because it is a thermotropic liquid crystalline material, mesophase pitch precursor can be melt-spun into fibers. In melt-spinning, the mesophase pitch precursor is fed into an

extruder where it is heated, and then pumped into a die head, and extruded through the spinneret. The as-spun fiber is drawn and cools down in air after it exits the spinneret, as illustrated in Figure 1.7. The melt-spinning of pitch is difficult because the viscosity of molten pitch is extremely temperature-dependent, so spinning requires precise control of conditions. Because mesophase is actually a liquid-crystalline solution, the melt-spun fibers achieve a high degree orientation during extrusion within the die *(29)*. Contrary to PAN precursor fibers, the microstructure within mesophase pitch fibers consists of highly oriented polyaromatic microdomains *(30)*, is displayed in Figure 1.8.

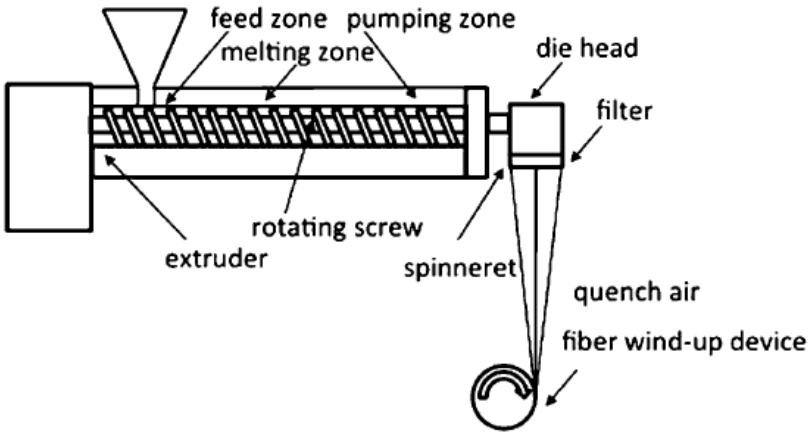

Figure 1.7 Schematic of melt-spinning process used to produce mesophase pitch fibers. Adapted from reference *(5)*.

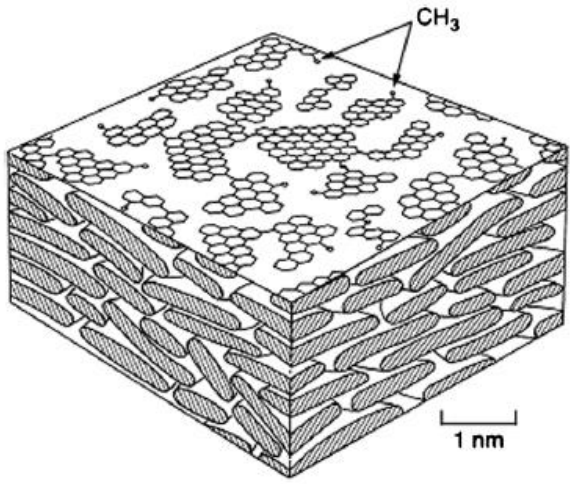

Figure 1.8 Schematic model of carbonaceous mesophase pitch. Adapted from reference *(31)*.

The thermo-oxidative stabilization of as-spun pitch fibers is performed in air at temperatures ranging from 200 to 300ºC for a period of 3-30 hours, leading to thermosetting of the mesophase pitch fibers *(5)*. The stabilization temperature needs to be lower than its softening point to avoid fiber fusion. Also, the temperature and duration of stabilization depend on fiber diameter, because in-diffusion of oxygen (air) is a transient process. Subsequent carbonization and graphitization steps are conducted between 1200 and 3000 ºC in an inert atmosphere *(5)*. Because the mesophase pitch fiber is already highly oriented as disks, the heat treatment does not affect molecular alignment to any appreciable extent *(32)*. Carbon fibers obtained at high temperatures of 2400-3000°C have a tensile modulus as high as 830 GPa *(33)*, which is much higher than for PAN-based carbon fibers. The carbon yield of the pitch is very high, typically 75-85%.

In contrast to PAN-based carbon fibers, mesophase-pitch-based carbon fibers display a variety of microstructures *(32)*, as shown in Figure 1.9. The most preferred

microstructures developed by pitch are radial and flat layer, which are the most common microstructures observed in commercial pitch-based carbon fibers. Pitch-based carbon fibers are also able to develop a highly graphitic structure, which leads to high thermal and electrical conductivity values. The thermal conductivity of some grades of pitch-based carbon fibers can reach 1000 W m^{-1} K^{-1}, approximately three times higher than copper *(7, 12, 34)*.

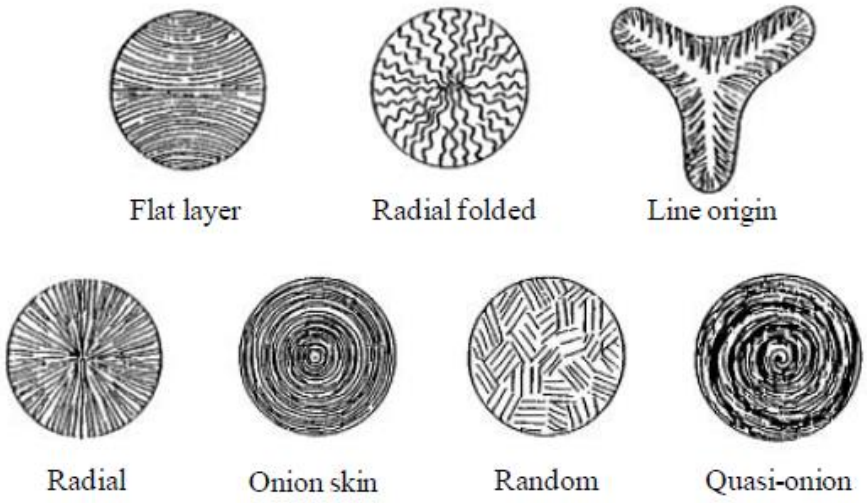

Figure 1.9 Different microstructure of pitch-based carbon fibers *(32)*.

1.2.3 Cellulose

Cellulose is a glucose-based, linear, natural polymer connected by β-1-4 linkages, as shown in Figure 1.10. Cellulose dose not melt, but can be dissolved in solvents to enable wet-spinning. Natural cellulose fibers, such as cotton and flax, have not been favored for carbonization because of their discontinuous structure and low degree of orientation. Instead, regenerated cellulose fibers are used to make carbon fibers, such as

textile-grade rayon and viscose rayon *(35, 36)*. However, these rayon-based carbon fibers have low mechanical properties and low carbon yield, so less than 1% of the global carbon fiber production is rayon-based *(13)*.

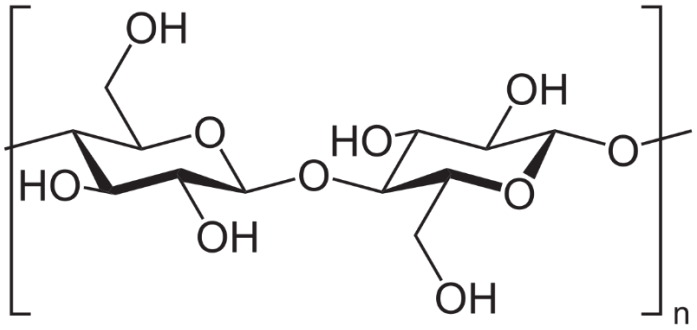

Figure 1.10 Chemical structure of cellulose

Rayon-based fibers are produced via wet-spinning process. To prepare the spinning solution, cellulose is dissolved in a basic solution, such as sodium hydroxide, and is then treated with CS_2 to form cellulose xanthate *(37)*. The solution is extruded through a spinneret followed by coagulation in a sulfuric acid solution *(5)*. The rayon fibers are stabilized in air at temperatures as high as 400ºC. The rayon precursor starts to degrade at 240 ºC, leading to the major loss of solid content and molecular orientation. Carbonization is performed in an inert atmosphere under similar condition to those of PAN or pitch. In this step, tension is very important to generate molecular orientation, which is lost during pyrolysis. The resulting rayon-based carbon fibers can achieve a tensile strength of 1.2 GPa and a modulus of 100 GPa *(38)*.

Carbon fibers also have been produced from Lyocell fibers, which are spun from cellulose solutions using N-methylmorpholine-N-oxide (NMMO) as the solvent *(39)*. The

Lyocell precursor fibers have a more circular cross-sectional shape and less defects compared with rayon-based fibers. The resulting carbon fibers display a strength and modulus as high as 1.1 GPa and 100 GPa, respectively *(40)*.

As mentioned in 1.2.1, the vast majority of high-performance commercial carbon fibers are currently produced from the synthetic precursor PAN via wet-spinning. The cost of PAN can contribute up to 50% of the manufactured cost of CFs *(41)*. In current commercial processes, PAN copolymers are typically used to optimize processing conditions to maximize the mechanical properties of the end-product *(42)*. However, the high cost of precursor materials and the energy of the conversion process are the principal contributors to the high cost of carbon fibers. Also, the nitrile group in acrylonitrile generates toxic by-products (viz, hydrogen cyanide) during heat-treatment *(18)*. Therefore, the search continues to replace such precursors either fully or partially by the use of environment-friendly alternatives. Among naturally occurring biomass, lignin is regarded as a potential carbon fiber precursor, due to its low cost and carbon-forming chemical structure.

1.3 Overview of lignin and lignin-based carbon fibers

Lignin is one of the world's most abundant renewable biopolymers, with 25%−30% of land biomass consisting (on a dry basis) of lignin, exceeded only by cellulose. In addition, it is the only abundant biopolymer with aromaticity. More than 50 million tons/year are available worldwide as a mostly non-commercialized by-product *(43)*. In recent years, with the development of modern methods of separation and chemical analysis, numerous of studies have been performed on the characterization and

applications of lignin. Several recent literature studies are summarized in our recent review paper *(11)*.

1.3.1 Chemical structure of lignin

Lignin is a complex, amorphous, and random polymer with aromatic rings. Phenylpropane monomers, displayed in Figure 1.11, constitute the main backbone of lignin, which is randomly linked by carbon-carbon and ether bonds. Depending on species of plant from which lignin originates, the composition of phenylpropane monomers is different. P-coumaryl alcohol is found predominately in grass (p-hydroxyphenyl, or "H"). Softwoods primarily consist of coniferyl alcohol (guaiacyl, or "G"), while hardwoods have a mix of both coniferyl and sinapyl alcohol (syringyl, of "S") *(44)*. These monomers are enzymatically polymerized in a natural way with a final product possessing a random network structure, presented in Figure 1.12. β-O-4 is the predominant linkage in all types of lignins. In softwood type, about 50% of the linkages are β-O-4 types, whereas in hardwood lignin these contributed up to 60% *(44, 45)*. Condensed lignin linkages are the 5-5, β-5, β-1, and β-β linkages. Note that lignin contains a significant portion of carbon and functionalized aromatic rings, which makes lignin an abundant source of biomass possessing aromaticity. The phenolic hydroxyl groups and the methoxyl groups are functional groups, which are the most reactive sites in lignin *(46)*. The number of these sites is very important during thermal stabilization to form a three-dimensional matrix network.

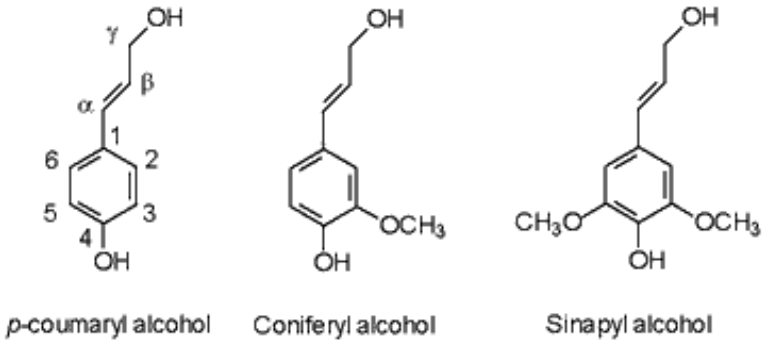

Figure 1.11 Chemical structures of the phenylpropanoid alcohols used to construct the lignin polymer. The proportions of these three phenylpropanoid alcohols differ between lignins of different plant species *(47).*

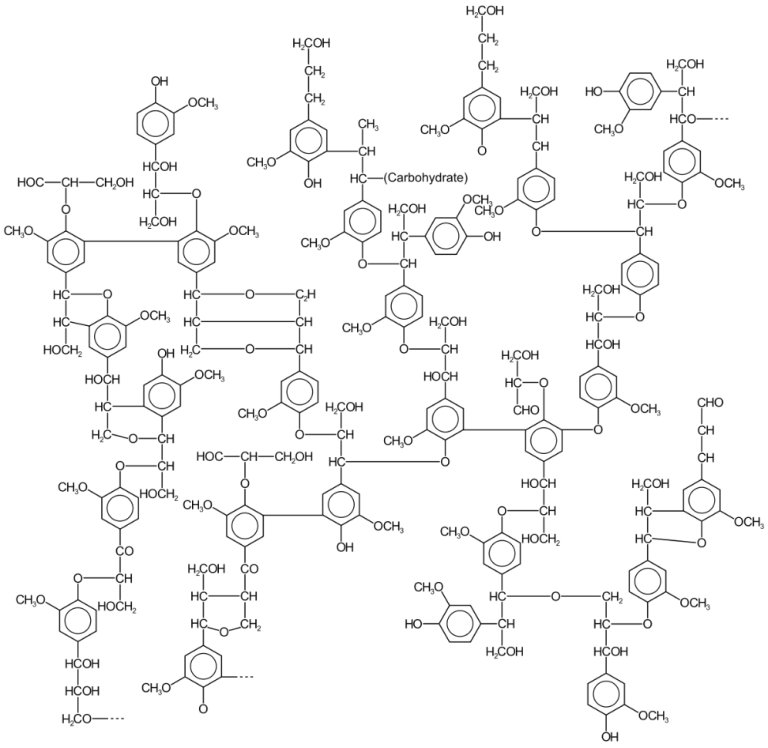

Figure 1.12 Chemical structure of lignin.

1.3.2 Separation of lignin from biomass

The cross-linked form of lignin within wood must be broken down to separate it from the cellulosic fibers. This requires drastic chemical breakdown of the chemical linkages and is accomplished by chemical pulping, and are generally divided into three categories: organosolv, alkaline, and acidic pulping processes.

Organosolv pulping

The organosolv pulping process utilizes an organic solvent to dissolve lignin and hemicellulose away from the cellulose in the biomass. Many organic solvents have been investigated, including alcohols, organic acids, and ketones *(48)*. Lignin obtained from organosolv pulping processes has a higher purity since there is no addition of inorganic moieties and sulfur during the process. Short-chained alcohols, such as methanol and ethanol, have been reported for pulping biomass. For example, the Organocell process is a two-stage pulping method using methanol as the solvent to break down lignin *(49)*. Wood chips are digested in methanol/water solution at 195ºC, and the cellulose remains as a insoluble fibrous known as "pulp", while lignin is collected from the pulping liquid. Ethanol is utilized in the Alcell process, which was developed in the 1980's *(50)*. The lignin is depolymerized and collected from the pulping liquor, and cellulose is left over. Formic acid is another pulping reagent studied in many publications *(51, 52)*. The lignin is broken down and dissolved in solution in the presence of formic acid at temperatures between 140 to 220ºC. Acetic acid has also been investigated as a pulping reagent in combination with additional mineral acids or other organic compounds *(53, 54)*. The

lignin obtained from these pulping processes has low sulfur content and generally a low molecular weight. However, today organosolv pulping processes are not commercially available due to their high cost.

Soda and kraft pulping

Soda pulping is one of the forms of alkaline pulping utilizing an aqueous solution of sodium hydroxide as the pulping reagent. The soda process is not as harsh as other processes, and is more suitable to treat lower quantities of lignin in grass and crops *(55)*. Kraft pulping, a type of soda pulping, is the most dominant commercial process in the world due to the superior qualities of the pulp that is produced *(46)*. During the kraft process, white liquor consisting of an aqueous solution of sodium hydroxide and sodium sulfide is added to wood chips at temperature up to ~175ºC. Cleavage occurs at the linkages that hold the phenylpropane units together, mainly β-O-4 bonds, which leads to the generation of free phenolic hydroxyl groups in the resulting kraft lignin *(56)*. After the pulping, cellulose is separated from waste liquor that contains most of the lignin and a large portion of the hemicellulose. This mixture is also called black liquor. The cellulosic pulp is further treated by bleaching, washing, and drying to form paper.

In black liquor, the lignin and hemicellulose are partially degraded and dissolved. After evaporation, the concentrated black liquor (containing lignin, hemicellulose and other organic species) is fed to the recovery boiler. The organic matter is burned to produce heat that is used to produce steam. Rarely is a portion of black liquor sent to a lignin-recovery process.

Sulfite pulping

Sulfite pulping is an acid process with the presence of sulfurous acid (H_2SO_3). During the sulfite pulping, wood chips are digested in sulfurous acid at temperature between 120 and 180ºC for 1-5 hours *(57)*. The acidic cleavage of ether bonds results in dissolution of lignin and generation of sulfonates as shown below *(58)*:

$R\text{-}O\text{-}R' + H^+ \rightarrow R^+ + R'OH$

$R^+ + HSO_3^- \rightarrow R\text{-}SO_3H$

Thus, the sulfur content resulting is relatively high compared to the lignins generated from other pulping process due to the addition of sulfonic group. Because of the sulfonic group, these lignins are water soluble. Lignosulfonates can be recovered from the waste liquor by adding calcium hydroxide for precipitation *(59)*.

1.3.3 Lignin recovery

Recent processes have been developed to recover lignin from black liquor by acidification. In the LignoBoost process, the black liquor is acidified with carbon dioxide to precipitate the lignin, and the filtered lignin is re-dispersed with aqueous acid followed by filtration and washing *(60)*. The LignoForce process was developed by adding an oxidation step before acidification to improve filterability and lignin precipitation *(61)*. The oxidation step facilitates the filtration rates of lignin slurries from black liquor and also decreases the ash content of the final lignin product compared to un-oxidized process. The Sequential Liquid-Lignin Recovery and Purification (SLRP) process

recovers lignin from alkaline liquor using carbon dioxide to lower the pH of the black liquor to promote lignin precipitation *(62)*. The lignin precipitates as a solvated liquid phase at pH ~9.5, and then the lignin phase is sent to a sulfuric acid acidification reactor. The pH is reduced to ~2.5 when lignin precipitates as a solid.

1.3.4 Lignin purification

During kraft/sulfite pulping, sulfur and/or metals are introduced so that the lignins recovered from black liquor are relatively high in ash content compared to the lignins generated by organosolv pulping. Although such kraft lignins are suitable for low-value applications, such as clean-burning biofuels, high-purity lignin with low ash content is required for high-value applications, such as producing carbon fibers. Thus, the purification of lignin is essential to make kraft lignins and lignosulfonates more suitable as carbon fiber precursors.

The average ash content of lignins obtained from traditional recovery processes is above 1 wt%, mainly including sodium, potassium, calcium, and aluminum *(60, 62)*. In contrast, organosolv lignin has significantly lower ash content (about 0.1 wt%). The ash content of kraft lignin when recovered from traditional methods is too high for high-value applications. This is an important factor for the use of such biomass as carbon fiber precursor because the presence of impurities cause defects during carbonization and weaken the resulting carbon fibers. Zhang and Ogale reported significant improvement in tensile strength of Ace-SKL derived carbon fibers when the ash content was reduced from ~3% to 0.15% *(63)*.

Several studies have been reported to remove ash from lignin using filtration technology. Jönsson et al. *(64)* reported ultrafiltration methods to purify lignin starting with a hardwood kraft black liquor. The permeates, which contained lignin and a minor amount of hemicellulose, was further concentrated by nanofiltration. This method can result in lignin with a reported ash content of 0.31%. A similar study has been reported by the same research group using nanofiltration followed by ultrafiltration to concentrate lignin and hemicellulose from softwood black liquor *(65)*. Johansson also reported lignin purification using a diafiltration method *(66)*. The permeate was then acidified with sulfuric acid, and the lignin was collected via another filtration step. However, the ash contents of the lignin reported in this study range between 2 and 8%, which is high for high-value applications.

In a recent study, Klett and Thies *(1)* used aqueous hot acetic acid in a continuous process to purify and fractionate kraft lignin which has already been recovered by SLRP process, shown in Figure 1.13. In this process, two equilibrium liquid phases were formed, when kraft lignins were combined with hot aqueous acetic acid at the appropriate conditions. The metal salts were extracted to the solvent-rich phase, and the lignin-rich phase contained ultraclean lignin. This process reduced ash content of kraft lignins from 2-4% values typical for kraft lignins to <0.1%. No other technology is currently available to obtain an "ultrapure" lignin from bulk kraft lignins.

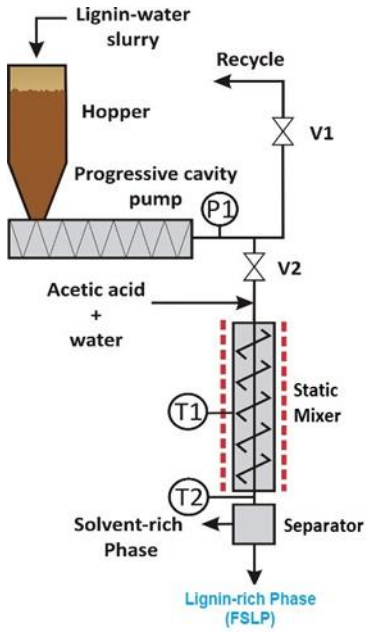

Figure 1.13 The continuous-flow version of the Aqueous Lignin Purification using Hot Acids (ALPHA) process. Adapted from reference *(1)*.

1.3.5 Lignin Fractionation

As noted above, lignin is a polydisperse mixture with wide range of molecular weight that depends on the pulping process and the degree of depolymerization. For high value applications, such as carbon fibers, controlled molecular weights are required. Therefore, the fractionation of lignin to controlled molecular weight ranges is yet another important operation towards the effective use of lignin as a precursor for producing carbon fibers. In prior studies *(68)*, fractionation was used to primarily remove the large molecular weight fractions from softwood lignins to enable melt-spinning of the remaining, relatively lower MW lignin fractions. However, as will be discussed later, melt-spun lignin fibers have not been reported to lead to superior carbon fibers.

Zhou et al. *(69)* reported lignin fractionation by sequential lignin precipitation by acidification. NaOH was added to corn stalk residues and the precipitation carried out by sequential acidification at different pHs. The molecular weight of precipitated lignin reduced as the pH increased.

In the study by Klett and Thies *(1)*, which utilized hot acetic acid for purification of lignin, it has also been reported that simultaneously fractionation of lignin could be achieved. In this process, the solvent mixture can make two liquid phases. The first phase is a lighter solvent-rich, which extracts metal salts and low molecular weight lignin species, whereas the second phase is a denser lignin-rich phase containing higher molecular weight lignin fractions. This unique extraction system that use a homogeneous solvent mixture to create two liquid phases can be used to simultaneously purify and fractionate lignin, and was used in the latter part of the current study.

1.3.6 Carbon fibers derived from lignin

Otani et al. *(70)* firstly reported producing carbon fibers from lignin (hardwood kraft, softwood kraft) via melt-spinning and dry-spinning in the 1960s. The carbon fibers obtained from hardwood kraft lignin by melt spinning had diameters of 20-30 μm and a strength of 785 MPa. The precursor fibers were also produced by dry-spinning of alkali lignin solution with added polyvinly alcohol to improve fiber integrity. A commercial carbon fiber derived from lignin was produced by Nippon Kayaku Co in Japan in the 1960s. The lignin fibers were dry spun from lignosulfnate, and the resulting carbon fibers had relatively low mechanical properties *(71)*. In 1974, Mansmann *(72)* developed a

method for co-spinning lignosulfonate and PEO by dry-spinning with rapid subsequent heat treatment, providing carbon fibers with strengths up to ~800 MPa.

New attempts were made in the 1990s, but these studies focused on making carbon fibers by melt-spinning. Like PAN, most native lignins do not melt – they simply start decomposing when heated above 200-250 °C *(73)*. Therefore, a wide range of modification techniques have been applied to lignin so that it can be spun into precursor fibers (which are then converted into carbon fibers). Sudo et al. *(74)* described lignin preparation using high-pressure steam treatment of wood, with subsequent extraction with organic solvent or alkali. The resulting lignin precursor was melt-spun into fibers and converted into carbon fibers with tensile strength and modulus (TS/TM) of 660 MPa and 40.7 GPa, respectively. Sudo et al. *(75)* then reported the use of phenolysis process to treat lignin. Carbon fibers produced from the phenolyzed lignin presented tensile strength about 450 MPa, which is lower than that of the hydrogenated lignin.

Uraki et al. *(76)* reported organolsov lignin-derived carbon fiber with strengths up to 355 MPa. The organolsov lignin was obtained from an aqueous acetic acid pulping method to facilitate melt-spinning due to a limited acetylation during the process. Kadla et al. *(77)* investigated carbon fibers derived three lignins: an organosolv hardwood lignin (Alcell lignin), a hardwood kraft lignin, and softwood kraft lignin (Indulin AT). The hardwood lignin could be melt-spun into fibers, while the softwood lignin could not since it had low thermal stability and therefore cross-linked during spinning. Alcell lignin with Tg of 68ºC was melt-spun between 138-165ºC, and the hardwood kraft lignin with a Tg of 83ºC was spun at 195-228ºC, providing carbon fibers with strength of 338 MPa and

422 MPa, respectively. Baker et al. *(78)* improved Alcell lignin by the use of thermal pretreatment to increase Tg, which reduced the thermal oxidation time and increased the strength of the resulting carbon fibers up to 710 MPa.

In another study, Baker and coworkers *(79)* turned their attention towards an organic purified hardwood kraft lignin (OP86) that was melt-spinnable. The resulting fibers had diameters as low as 10 μm. However, a heating rate as slow as 0.01ºC/min during thermal stabilization was required to avoid fiber fusion, and the carbon yield was relatively low for this type of lignin precursor. The resulting carbon fiber possessed a tensile strength of 520 MPa. In continuing work, Baker applied thermal pretreatment to adjust the Tg and melt-flow properties of the OP86 lignin, which resulted in a narrower molecular distribution. The heat pretreatment strategy was an effective method to accelerate the thermal oxidation. This method improved carbon fiber properties, and the best carbon fibers had an average tensile strength of 1.07 GPa. Modulus value was not measured *(72)*.

High Tg lignins were also investigated by adding plasticizers such as PEO, PP and PET to facilitate melt flow. Kadla et al. *(80)* reported the use of PEO to plasticize kraft hardwood lignins with high softening temperatures. The amount of PEO added to lignin was 3-5 wt% in order to improve spinning performance and prevent fiber fusion during thermal stabilization. The highest tensile property of carbon fibers derived from lignin-3% PEO blend reached 448 MPa. Further to this, Kubo et al. *(81)* also reported a similar study with PET and PP as carriers to improve spinning performance and thermal properties. Although it was found that the addition of synthetic thermoplastic polymers

into the blend improved melt-spinning, no improvement was observed in the mechanical properties of the resulting carbon fibers. Softwood kraft lignin could not be converted into a fusible precursor even with the addition of PEO because of the high percentage of guaiacyl groups.

Qin et al. *(82)* reported carbon fibers obtained from pyrolysis lignin via melt-spinning. However, large voids were formed in the precursor fibers, resulting in low tensile strength of 370 MPa. Nordstrom et al. *(68)* investigated both softwood and hardwood kraft lignin recovered by the LignoBoost process and further treated by ultrafiltration to reduce polydispersity. It was found that the permeate lignin could be melt-spun into fibers, while the non-permeate lignin could not. The authors provided information about using low Tg permeate lignin to plasticize high Tg lignin and to improve fiber spinability. Norberg et al. continued to use softwood kraft lignin permeate to produce carbon fiber *(83)*. Because the guaiacyl groups in softwood lignin crosslink more easily, the thermal stabilization could be completed with a rapid heating rate (15ºC/min), which is much faster compared to hardwood kraft lignin precursors. The authors reported carbon fiber diameters of 30 μm and strengths of 377 MPa. The large diameter and low tensile strength of carbon fibers indicated a poor drawdown ratio and a lack of process control during fiber spinning.

As seen above, there are significant challenges to generating lignin-based carbon fibers via melt-spinning with the strength and modulus desired for even moderately high-performance composites (i.e., values of at least 2 and 200 GPa, respectively, as displayed by inexpensive PAN-based carbon fiber) *(84)*. In particular, the T_g of the lignin must be

low enough so that it can be spun without solvents at temperatures below decomposition – but Tg must also be high enough for the lignin to undergo rapid stabilization. To get around this conundrum, dry-spinning of partially acetylated softwood kraft lignin fibers was reported by Zhang and Ogale *(63, 85)*. Partial acetylation (vs. complete) allowed solubility of lignin in acetone. The as-spun fibers possessed crenulated cross-sectional shape because of the out-diffusion of solvent. Note that the crenulated surface provides up to 30% larger surface area for carbon fiber and matrix bonding when making composites. The dry-spun lignin fibers were stabilized and carbonized under tension to maintain molecular orientation. The carbon fibers obtained from this process displayed tensile strength and modulus of 1.05±0.10 GPa and 52±2 GPa, respectively, which is among the highest reported in literature.

As discussed above, the vast majority of lignin-based carbon fibers display a low strength below 1.0 GPa, significantly less than values of 3 GPa obtain from PAN. To further improve mechanical properties, a lignin/PAN polymer-blending approach has been used. While this approach does not eliminate the use of PAN, it reduces the content of PAN. Husman reported PAN/lignin precursor fibers with different lignin content (up to 45%) by wet spinning *(86)*. However, the resulting precursor fibers with lignin content higher than 20% had micron-sized voids, resulting from lignin leaching during spinning, causing macro-voids in the resulting CFs. To remedy this, higher molecular weight PANs were investigated, but the lignin leaching problem still existed. In another study *(87)*, lignin sulfonate (LS)/PAN blend was wet-spun into precursor fibers for low-cost CFs in which PAN serves as the framework and LS is used as an extender. However, a

microporous structure was obtained in the precursor fibers, and the properties of CFs were not reported. Recently, Liu et al. *(88)* reported void-free CFs from lignin/PAN blends using a gel-spinning technique. The low coagulation temperature (-50°C) significantly reduced the counter-diffusion rate, with reduced lignin leaching. The tensile strength and modulus of resulting CFs were 1.72 ± 0.2 GPa and 230 ± 7 GPa, respectively. The advantage of gel-spinning is that it minimizes lignin out-diffusion and makes void-free CFs from lignin/PAN blends. However, compared to conventional wet-spinning using a PAN solution, this process requires a concentrated spinning solution and very low coagulation temperatures, which increase the complexity of the process.

The introduction of PAN into lignin poses similar environmental concerns similar to those posed by pure PAN-based CFs. Therefore, recent research focus returned to lignins derived from alternative biomasses. For example, a corn-stover lignin fractionated with methanol and then acetylated yielded carbon fiber with strength and modulus of 0.45 and 62 GPa, respectively *(89)*. However, stabilization rates were slow and the final fibers were large (~40 μm). Blends of tulip poplar/switchgrass lignins (50/50) extracted from biomass via organosolv fractionation were melt-spun and converted to carbon fiber (TS/TM = 0.52/38 GPa), with the stabilization rates being improved by the addition of switchgrass lignin *(90)*. In related work, a phenolic bio-oil recovered from hardwood pyrolysis was catalytically polymerized to produce a melt-spinnable precursor that led to better properties for lignin-based carbon fibers (TS/TM = 0.85/85 GPa) *(91)*.

The tensile properties of different lignin-based carbon fibers that were discussed above are summarized in Table 1.2. All types of lignin-based carbon fibers have relatively low mechanical properties as compared with those of PAN or mesophase-pitch-based carbon fibers. The melt-spun lignin fibers are inherently difficult to thermo-oxidatively stabilize because of their low degree of thermal reactivity. The precursor fibers partially fuse during stabilization and carbonization steps, leading to surface defects on resulting carbon fibers. Moreover, the mechanical property of lignin-derived carbon fibers is low due to the intrinsic structural heterogeneity, the impurity levels, and the methods of isolation employed. First, lignins recovered from kraft pulping and biofuel industry usually contain considerable amounts of both organic and inorganic impurities. For carbon-fiber applications, these impurities have to be removed, which otherwise would cause defects within the resulting carbon fibers. Oganosolv lignin has higher purity compared to kraft lignin and lignosulfonates due to lignin recovery without an addition of inorganic moieties and sulfur. Second, lignin is a highly branched biopolymer containing molecules with a broad molecular weight distribution. Due to the random branched structure and lack of molecular homogeneity, the resulting fibers display lower strength and modulus compared to PAN-based carbon fibers. Therefore, research studies on lignin purification, fractionation, and modification are of interest.

Table 1.2 A summary of the tensile properties of carbon fibers produced from different lignin precursors in prior studies

Lignin type	Diameter (μm)	Tensile strength (MPa)	Modulus (GPa)	Reference
Various types of lignin	-	150-800	-	Otani,1969 *(70)*
Steam-exploded hardwood	8±3	660±230	40.7±6.3	Sudo, 1992 *(74)*
Organosolv hardwood	14±1	355±53	39±13	Uraki, 1995 *(76)*
Kraft hardwood	46±8	422±80	40±11	Kadla, 2002 *(80)*
Kraft hardwood/PEO	34±4	448±70	51±13	Kadla, 2005 *(81)*
Organic-purified hardwood	10±1	520±182	28.6±3.2	Baker, 2011 *(79)*
Organic-purified hardwood	-	1070	-	Baker, 2013 *(72)*
Pyrolysis-based	49±2	370±38	36±1	Kadla, 2012 *(82)*
Kraft hardwood and softwood	36-78	233-377	25-33	Nordstrom, 2013 *(68)*
Acetylated softwood kraft	5.9±0.2	1040±100	52±2	Ogale, 2014 *(63)*
Repolymerized pyrolytic	29-50	860±160	85±37	Bai, 2016 *(91)*
Organosolv switchgrass	25.8±2.2	370±74	35±3	Rials, 2016 *(92)*
Organosolv yellow polar	17.1±1.6	544±96	36.5±2.8	Rials, 2016 *(92)*
Corn stover	39.1±5.4	454±98	62±14	Bai, 2018 *(89)*
Lignin/PAN blend (30% lignin) gel-spun	11±1	1720±200	230±7	Kumar, 2015 *(88)*
Lignin/PAN blend (25% lignin) wet-spun	-	2250	217	Husman, 2014 *(86)*

1.4 Objectives

The development of lignin-based carbon fibers with improved mechanical performance is highly desirable. As evidenced by the studies referenced in Section 1.3 above, blending lignin with PAN is an approach to integrate the advantages of good mechanical properties of PAN with the cost advantage of lignin. Another possible approach is to develop lignin precursors with very low ash content to reduce defects and high molecular weight to facilitate molecular orientation during the spinning,

stabilization, and carbonization steps. Such improvements could in principle lead to carbon fibers with enhanced strength and modulus.

Therefore, this study investigated different lignin-based precursors to make carbon fibers with enhanced mechanical properties, mainly focused on lignin/PAN blends (L/P blends) and lignin precursor with high purity and controlled molecular weight (MW). Aqueous Lignin Purification using Hot Acids (ALPHA), recently developed by Thies and co-workers *(1)* was utilized to produce fractionated-solvated lignin precursors (FSLPs), which contain low ash content and controlled MW. The overall goal of this study was to study the process and properties of FSLPs and lignin/PAN blends-based carbon fibers via solution spinning. The specific objectives of the study were to: (i) study the rheological properties of L/P blends to establish suitable wet-spinning conditions, establish thermal stabilization and carbonization conditions for L/P precursor fibers, investigate the effect of lignin content on the microstructure and mechanical properties; (ii) study high purity FSLPs created via the ALPHA process, establish dry-spinning conditions, and develop suitable thermal stabilization and carbonization conditions to enhance the performance of the resulting FSLP-based carbon fibers; (iii) investigate the processing structural and property relationships between the lignin and the resulting carbon fibers.

Chapter 2 focuses on develop L/P blends with various lignin contents for the purpose of making carbon fibers via wet-spinning. The effect of lignin composition on the viscoelastic behavior of L/P blend solutions was reported. Porous cross-sectional morphology was observed in L/P precursor fibers due to lignin leaching with the solvent. Therefore, the out-diffusion of lignin from the fibers to coagulant was quantified and

reduced by adding lignin in the coagulant bath in order to lower the concentration gradient between spinning solution and coagulant. The method of controlling lignin content in coagulant provided a simple and low-cost process to produce void-free L/P fibers. The effect of the addition of lignin on L/P based carbon fiber microstructure was studied using Raman spectroscopy and X-ray diffraction. The results have been published *(93)*.

In Chapter 3, a study on producing carbon fibers from fractionated-solvated lignin precursors (FSLPs) via dry-spinning is discussed. The process of fractionation and purification to produce FSLPs with increased molecular weight and low ash content was developed and has been reported by the Thies group *(1, 94)*. Dry-spinning was performed on FSLPs of different MW and of very low ash content. The role of spinning conditions on dry-spun lignin fibers, spinnability, microstructure and mechanical characterization of the lignin fibers was discussed. Stabilization was performed under tension. Weight load and the percentage of extension during stabilization was discussed. Also, the morphology of the resulting carbon fibers were compared.

Chapter 4 addresses the structural and property changes of FSLPs during the various processing steps, including spinning and thermal treatment. The microstructure of lignin fibers and the resulting carbon fibers was studied by FT-IR and X-ray diffraction. Various carbonization temperatures were used, ranging between 1000 and 2100°C. A detailed study of the effect of heat treatment on structure was investigated using Raman spectroscopy, X-ray diffraction and TEM. Both electrical and tensile properties after each thermal treatment have been reported. Also, the molecular weight effect on the

microstructure of resulting carbon fibers was studied. The results of this study indicate that both the ash content and molecular weight of the lignin precursor can play an important role in improving the performance of lignin-based carbon fibers. The results presented in Chapter 3 and 4 have been published *(94)*.

Finally, Chapter 5 summarizes the conclusions drawn from the research and provides recommendations for future work.

CHAPTER TWO

CARBON FIBERS DERIVED FROM WET-SPINNING OF LIGNIN/POLYACRYLONITRILE BLENDS: EFFECT OF LIGNIN COMPOSITION IN BLENDS

2.1 Introduction

Bio-derived precursors are of increasing interest in the production of CFs not only as an environmentally friendly material but also to reduce the reliance on synthetically derived PAN precursor, used primarily in current commercial CFs *(5, 7, 32, 95)*. As mentioned in Chapter one, lignin plays an important role as a potential precursor for various carbon products, including producing CFs *(11, 72, 78)*. The estimated cost of lignin precursor for CF manufacture is conservatively three times lower than textile grade PAN. Since lignin is substantially oxidized, the thermal oxidation of lignin fibers requires shorter duration compared to that for PAN fibers, which further reduce energy consumption during conversion process *(41, 72)*. However, mechanical properties of lignin-based CFs obtained to date are significantly lower than those of PAN-based CFs.

To further improve mechanical properties, lignin/PAN polymer blending approach has been used to combine the good mechanical property of PAN, and the sustainability of lignin *(11, 72, 86-88, 96)*. PAN fibers are typically processed by wet-spinning, while lignin fibers are processed by melt-spinning. Lignin recovered from the pulping process does not have a long, and linear molecular architecture. Therefore, lignin does not have adequate extensional viscosity to be converted into fibers by wet-spinning. Thus, the precursor fibers have been produced from polymer blends.

Industrial feasibility of wet-spun lignin/PAN fibers were investigated by Zoltek and Weyerhaeuser *(86)*. Although carbon fibers up to 25 wt% lignin content were successfully produced with targeted tensile properties, lignin leaching (2-3%) occurred during precursor spinning, creating production problems. Lignin leaching will cause macro-voids in lignin/PAN fibers with increasing lignin content. Voids in lignin/PAN fibers were also reported in more studies, which was described in Chapter 1 section 1.3.5. Gel-spinning technique was reported to make void-free CFs from lignin/PAN blends *(88)*. However, compared to conventional wet-spinning using a PAN solution, this process requires concentrated spinning solution, and very low coagulation temperatures, which increase the complexity of the process (and also the process cost). The objectives of experiments presented in this chapter were to (i) systematically investigate processing of precursor fibers from common grades of lignin/PAN blends, and obtain void-free lignin/PAN fibers; (ii) study the effect of lignin on the microstructure, and mechanical properties of lignin/PAN blends based carbon fibers. It is noted that the results of this chapter were published in our recent paper (93).

2.2 Experimental

2.2.1 Materials

Polyacrilonitrile homopolymer with a molecular weight of 233,000 g/mol, and a glass transition temperature (Tg) of 125 °C was obtained from Sigma-Aldrich (Milwaukee, WI, USA) and used throughout this study. Softwood kraft lignin (SKL, Indulin AT, Mead-Westwaco, North Charleston, SC, USA), a low-cost commercially available lignin was used in its as-received ("whole") state to retain the cost-competitive

advantage of lignin, i.e., it was not modified in any manner. It contained about 3 wt % ash content, and had a Mw about 6500 g/mol as measured by Size-exclusion chromatography. The solvent used was dimethyl sulfoxide (DMSO), obtained from Sigma-Aldrich Co.

Lignin and PAN were dissolved in DMSO at 60 °C to prepare solutions containing 20 wt % of solids, and 80 wt % of solvent. The mass ratios of lignin to PAN within the solid blends were 25:75, 35:65, 45:55, and 50:50 (L25/P75, L35/P65, L45/P55, and L50/P50). PAN solution was prepared containing 16 wt % in DMSO.

2.2.2 FTIR

Fourier transform infrared spectroscopy (Nexus 870 FT-IR ESP, Nicolet) was used to determine the interaction between lignin and PAN in the spinning solution. All samples were analyzed using KBr transmittance technique, and scanned in a range between 400 and 4000 cm^{-1} wavenumbers.

2.2.3 Rheology and spinning

PAN and lignin/PAN solutions were tested for their rheological behavior using an AR2000 rheometer with a cone-and-plate fixture at low shear rates (0.1-50 s^{-1}), and ACER capillary rheometer at high shear rates (100-10,000 s^{-1}). The cone of diameter 20 mm has angle of 2º 0’4”, and the tip is truncated to a depth of 49 μm. The capillary of diameter 1 mm has an L/D of 25. All testing was conducted under ambient conditions at ~25ºC. The viscosity values for each solution were fitted to a modified Carreau model. (Eq 2.1) where $\eta(\dot{\gamma})$ is the shear viscosity, $\dot{\gamma}$ is the shear rate, λ is the time constant, η_0 is the zero shear

viscosity and n corresponds to the power law index *(97, 98)*. For polymer solutions, the solvent viscosity is usually used for the η_∞, but can be ignored for concentrated solutions such as those used in the present study. In cone-and-plate rheometer, the primary normal stress difference N1 can be calculated from normal force.

$$\frac{\eta(\dot{\gamma})}{\eta_0} = [1 + (\lambda\dot{\gamma})^2]^{(n-1)/2} \quad (2.1)$$

PAN and L/P fibers were wet-spun from blend solutions into fibers using a 200 hole, 60 μm diameter spinneret at room temperature. The coagulant bath consisted of 65 wt% DMSO/35 wt% distilled-deionized water. This was followed by washing of the precursor fibers in water bath at room temperature. Two different concentrations, 0.1 and 0.2 wt%, of lignin were added into coagulant bath to control out-diffusion. After wet-spinning, solid fibers were post-stretched with a max draw ratio of three in a water bath at 80°C.

2.2.4 Lignin out-diffusion measurement

To quantify the out diffusion of lignin, L35/P65 solution was spun into 65% DMSO/35% water coagulant, but one containing different lignin contents (0, 0.1%, and 0.2%). About 5 mL coagulant samples were withdrawn from the bath (total volume ≈ 5000 mL) for UV-vis spectroscopy analysis after different spinning time periods, ranging up to 900s. Cumulative concentration of lignin in the coagulant was measured as a function of spinning time. Varian Cary 50 Series UV-Vis spectrometer was used to measure absorbance of lignin in DMSO/water coagulant. 65wt% DMSO/35wt% water coagulant was used as baseline solvent. Lignin was dissolved in baseline solvent to make standard

calibration solutions with different concentrations (0.00175%, 0.0035%, 0.005%, 0.0075% and 0.01%). All samples were diluted with baseline solvent to lower absorbance values.

Based on previous studies *(99)*, lignin concentrations were measured using ultraviolet-(UV) visible spectroscopy given that the absorbance spectrum of softwood kraft lignin solution in DMSO exhibits a sharp peak at a wavelength of 283 nm. The absorbance spectra of lignin standard calibration solutions in the DMSO/water, displayed in Figure 2.1, confirmed the peak at a wavelength of 283 nm. A plot of absorbance at this wavelength versus lignin concentration yielded a "calibration" relationship, shown in Figure 2.1.

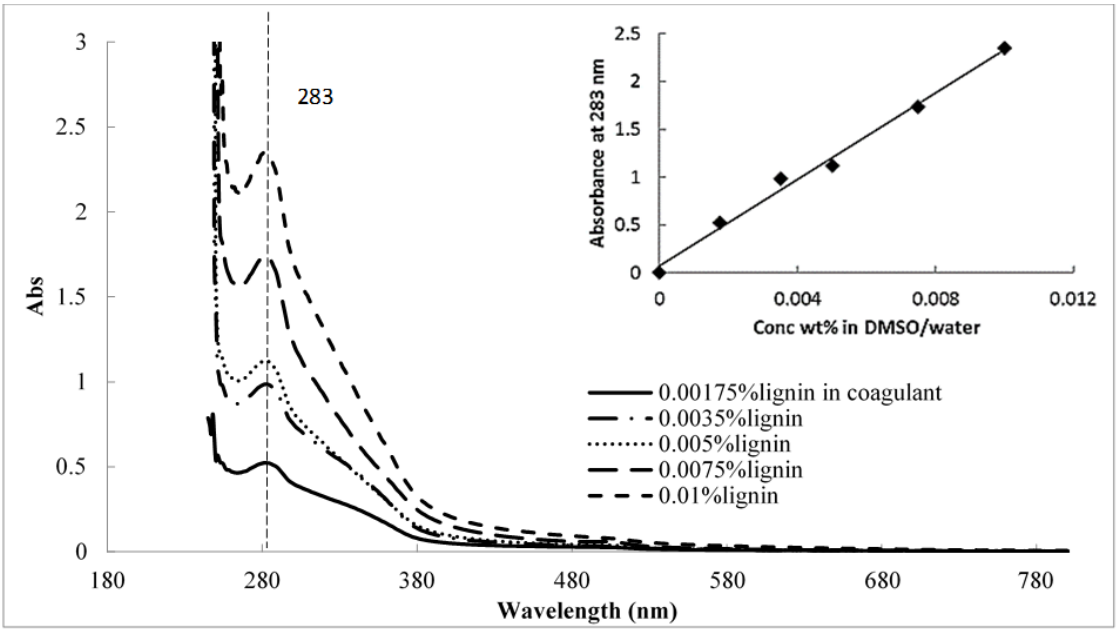

Figure 2.1 UV-Visible absorbance spectra of various lignin content in DMSO-water coagulant. Inserted graph is the calibration curve.

2.2.5 Stabilization and carbonization

A 5-10 cm long of precursor fiber bundle was cut, and prepared before thermal stabilization. The precursor fiber bundles (both PAN fibers, and lignin/PAN blend fibers) were stabilized in an ATS oxidation oven in air environment using a heating rate of 1°C/min up to 300°C, and held there for 1 hour. Fiber tows were stabilized under tension (approximately 0.07 g·denier^{-1}), shown in Figure 2.2 (a). Thermally stabilized fibers were carbonized in a helium environment using an HP 50 furnace. Fibers were suspended in a custom-designed graphite rack, shown in Figure 2.2 (b) with an applied tension of about 0.05 g·denier^{-1}, heated to 1200°C at a rate of 7°C/min, and held for 1 hour.

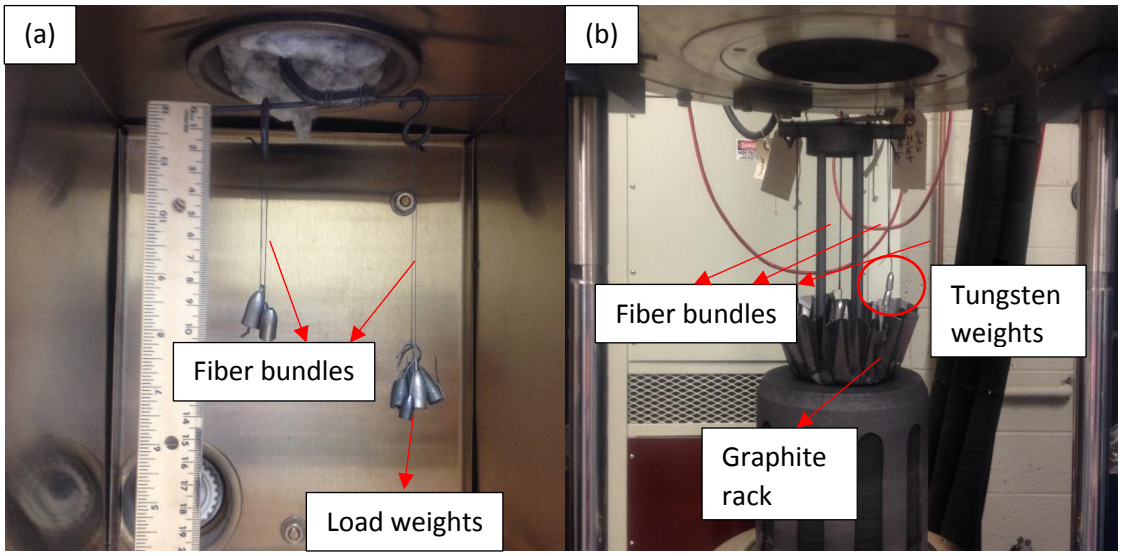

Figure 2.2 (a) Stabilization and (b) Carbonization of lignin/PAM fiber bundles under tension.

2.2.6 Characterization of fibers

Morphological analysis of fibers was conducted by scanning electron microscopy (SEM) with a Hitachi 4800 SEM unit. The samples were prepared by mounting a fiber bundle between two adjacent pieces of double-sided carbon tape. The fiber samples were held in liquid nitrogen for 1-2 min, then quickly removed, and fractured by bending two carbon tapes towards each other. The carbon tape and the samples were adhered to stainless still sample stabs in vertical direction. The as-spun fibers were coated with platinum using a sputter coater for 1 min to prevent charging in the SEM. From SEM micrographs, the length and diameter measurements were carried out using Quartz PCI software (version 8). At least 10 micrographs at different magnification were captured for each group of samples.

Raman spectra of CFs were obtained using a 785 μm laser in a Raman microscope system (Renishaw). Carbon fibers were mounted on a glass slide, and fixed with scotch tapes at both ends. Raman spectra using an objective lens of 50× magnification at 25 mW laser power with exposure time of 10 s. WiRE 3.4 software was used to analyze the spectra with Gaussian-Lorentzian curve fitting to determine the I_D/I_G ratio. At least five replicates per type of fibers were measured.

Wide-angle X-ray diffraction (WAXD) studies were conducted using a Bruker D8 Venture Dual Source diffractometer with CuKα radiation ($\lambda = 0.15406$ nm). The unit was equipped with an IμS microfocus source at, a Photon 100 CMOS detector, and Apex3 software to generate integrated azimuthal (2θ) profiles. Samples were in the form of fiber bundles that were glued with fast cure acrylate glue; one sample from each group was

sprinkled with NIST-grade silicon standard powder for accurate location of 2θ position. The scan time was 120s per run. The baseline correction and peak fitting were processed on WiRE 3.4 software. The d-spacing of (002) planes was calculated using the standard Bragg's law (Eq 2.2):

$$d_{002}=\lambda/2\sin\theta \quad (2.2)$$

where λ is the wavelength of X-ray (0.154 nm), and θ is the angle of incidence of the X-ray beam.

An MTI single filament tensile testing unit was used to measure the tensile properties of single fibers mounted paper tabs with a gage length of 25 mm following ASTM test method D-3379-75. Compliance correction was performed to eliminate system compliance from testing equipment and sample preparation. Compliance correction for modulus was performed on PAN based and L50P50 based CFs using shorter, and longer gage lengths of 10 and 35 mm (ASTM D-3379-5). Twenty samples per type of fibers were prepared and tested.

2.3 Results and Discussion

2.3.1 Effect of lignin on viscoelastic behavior of lignin/PAN blends

Figure 2.3 displays the steady shear viscosity as a function of shear rates at room temperature for PAN and L/P spinning solutions obtained from two different sets of experiments conducted independently on cone-plate (low shear) and capillary (high shear) instruments. All L/P-DMSO solutions had a nominal solid content of 20 wt%, whereas the lignin fraction within the L/P solid blend was varied from 0.25 to 0.5. The viscosity of L/P

solutions decreases throughout the entire measured range as lignin content increases. All solutions displayed an approach to Newtonian plateau at shear rates less than 0.5 s^{-1}. However, at higher shear rates, such as those encountered in the spinnerets during wet-spinning, a shear thinning behavior was observed for all concentrations of lignin, including the highest one (50 wt% lignin).

The modified Carreau model was used to fit the viscosity data and the model parameters are shown in Table 2.1. Note that while lignin has highly branched polymeric structure, which is distinct from linear-chain PAN polymer, L/P blend solutions exhibit power law index, and shear thinning behavior similar to that of PAN. The composition independence of ***n*** implies that lignin and PAN form single-phase solution in DMSO. Also, zero shear viscosity η_0 is shown to decrease with the incorporation of lignin, which has a tighter molecular structure as well as much lower molecular weight as compared with PAN. For concentrated polymer solutions, the viscosity scales with molecular weight as $\eta \sim M^3$*(100)*. Thus, lignin may be considered as a diluent for PAN given that the viscosities of L/P blends decrease with increasing concentration of lignin.

Because the wet-spinning process involves not only high shear rates within the spinneret, but also extensional flows during drawdown (in the coagulation bath), the elastic response of solutions can indicate the spinability of the blend solutions. The dependence of N1 on blend composition is displayed in Figure 2.4. Generally, the presence of lignin in solution reduces normal stress exhibited by the blend. Thus, the presence of lignin not only reduces shear viscosity, but also the normal stress, indicating a negative effect on viscoelastic behavior. These fundamental rheological studies confirm the need for a higher

solid content (as compared with pure PAN) in the blend solutions during the spinning process. For a semi-concentrated polymer solution, the viscosity scales with concentration as $\eta \sim C^5$ *(101)*. Therefore, a higher solid content in the blend solutions can compensate viscosity reduction caused by the presence of lignin.

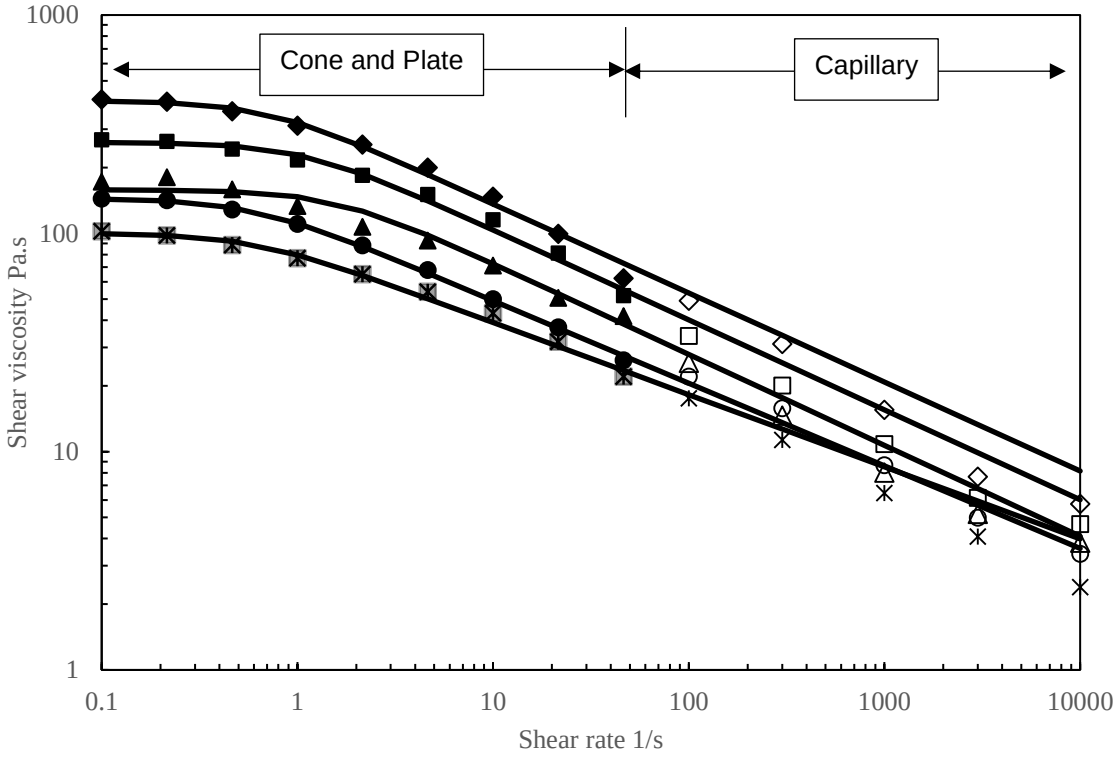

Figure 2.3 Viscosity vs Shear rate results of 20 wt% PAN and L/P solutions at room temperature (~25^{0}C) (♦ PAN20%, ■L25/P75, ▲L35/P65, ●L45/P55, *L50/P50) Open symbols represent data obtained from capillary rheometer whereas solid symbols are data from cone-and-plate rheometer.

Table 2.1 Carreau model fitting parameters of 20 wt% PAN and L/P solutions.

	PAN	L25/P75	L35/P65	L45/P55	L50/P50
n	0.60±0.01	0.58±0.01	0.62±0.05	0.65±0.03	0.66±0.01
λ	1.50±0.09	1.06±0.17	1.24±0.84	1.68±0.05	1.92±0.27
η_0	409.4±6.9	260.8±0.02	168.0±13.7	136.3±11.1	108.9±12.6

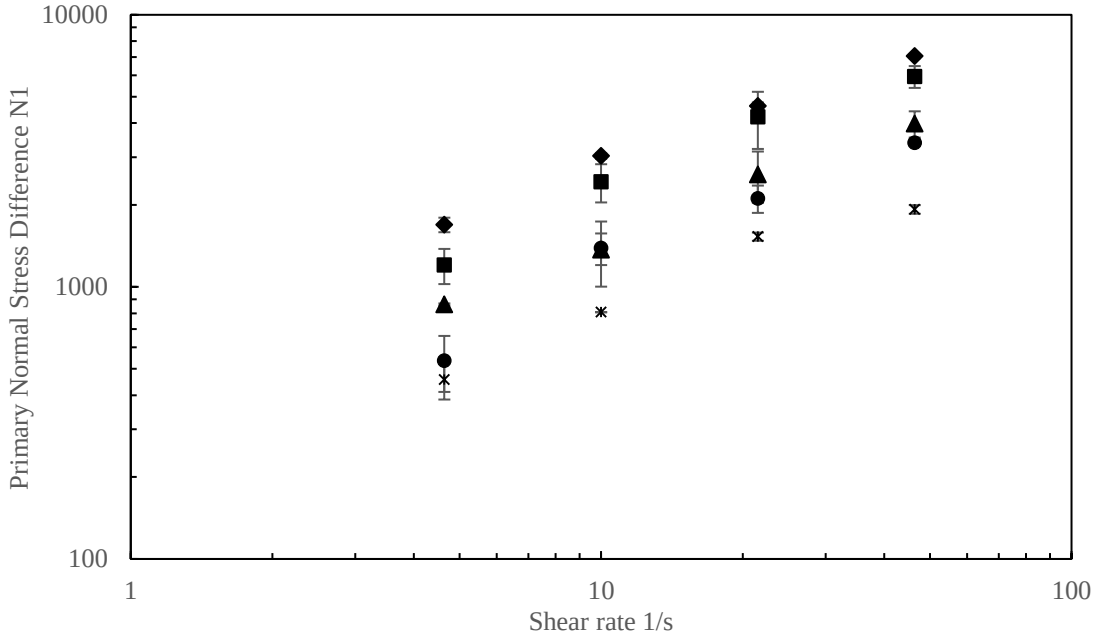

Figure 2.4 N1 versus shear rate of 20 wt% PAN and L/P solutions (at ~25^{0}C) (♦ PAN, ■L25/P75, ▲L35/P65, ●L45/P55, *L50/P50).

2.3.2 FTIR analysis

To identify the interaction of lignin and PAN in the spinning solutions, FTIR analysis was conducted for solutions of pure PAN as well as lignin-PAN blends in DMSO. The IR spectra for solutions were corrected relative to the spectrum for pure DMSO obtained independently. FT-IR spectra of PAN and lignin-PAN solutions for different lignin/PAN blend ratios are illustrated in Figure 2.5. The peak located at ~2240

cm^{-1} is associated with the -C≡N bond in PAN structure *(102)*. The broad peak located near 3500 cm^{-1} is the characteristic stretching vibration absorption peak of hydroxyl group. The peak at 1514 cm^{-1} corresponds to the skeletal vibration of aromatic ring structure in lignin *(87, 96)*. As the lignin blend ratio was varied, no new absorption peak was observed, and the characteristic peak positions of PAN and lignin in the polymer blends remained unchanged. This suggests that no major chemical reaction or crosslinking occurred between lignin and PAN in the spinning solution, and also confirms that lignin can be considered as a diluent during the wet-spinning.

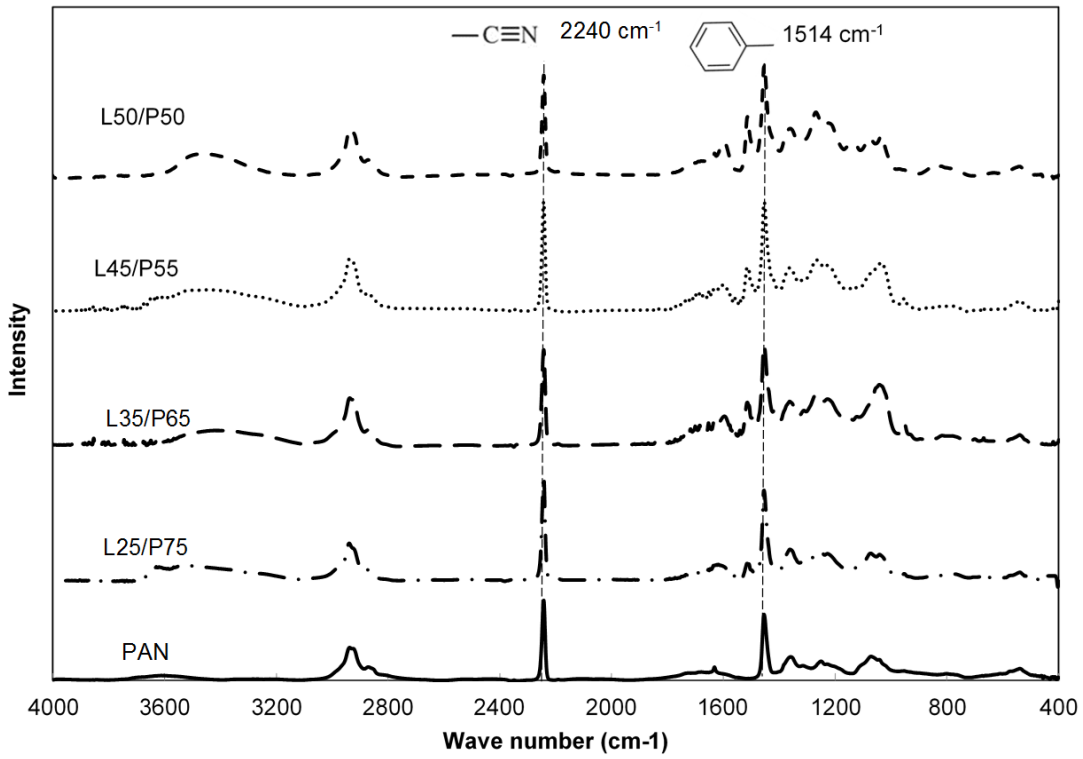

Figure 2.5 FT-IR spectra of PAN and L/P blend solutions corrected relative to the spectrum of pure DMSO.

2.3.3 Wet-spinning

All wet-spinning experiments were conducted at room temperature (~25ºC). The total amount of PAN in solution for successful fiber spinning was 16 wt%. Larger PAN concentrations (up to 20 wt%) were attempted, but were difficult to extruded from the fine diameter spinneret due to the pressure drop exceeding 90 psi. Fiber spinning trials for three different L/P ratios (25/75, 35/65, and 45/55 ratios) were attempted at 16 wt%, but were not successful. This is consistent with viscosity, and normal stress results reported above from shear rheology. Thus, the solid content for L/P spinning solutions was increased to 20 wt%, which resulted in successful wet-spinning of the L/P blend fibers. This observation is again consistent with the rheological results that suggested the use of higher solid contents to compensate for the reduced viscoelastic properties of L/P blend solutions (as compared to that of pure PAN solutions). A linear take-up velocity of 80 cm/min was employed during the spinning of the fibers. Figure 2.6 displays continuously wet-spun L/P precursor fibers with various lignin contents. There are approximately 200 filaments within a tow. The draw-down ratio (DDR) was controlled between 2 and 4 during wet-spinning. The resulting L/P fibers shown in Figure 2.7 (a) had an average diameter of 22±1 μm. Next, the fibers were post-stretched in a distilled-deionized water bath at ~80°C. The effective length of the post-stretching bath was 80 cm. The draw-down ratio used during the post-stretching step was approximately 4. After post-stretching, the diameter of L/P fibers was reduced to 9.5±0.2 μm, shown in Figure 2.7 (b).

Figure 2.6 As-spun L/P fibers with different lignin contents.

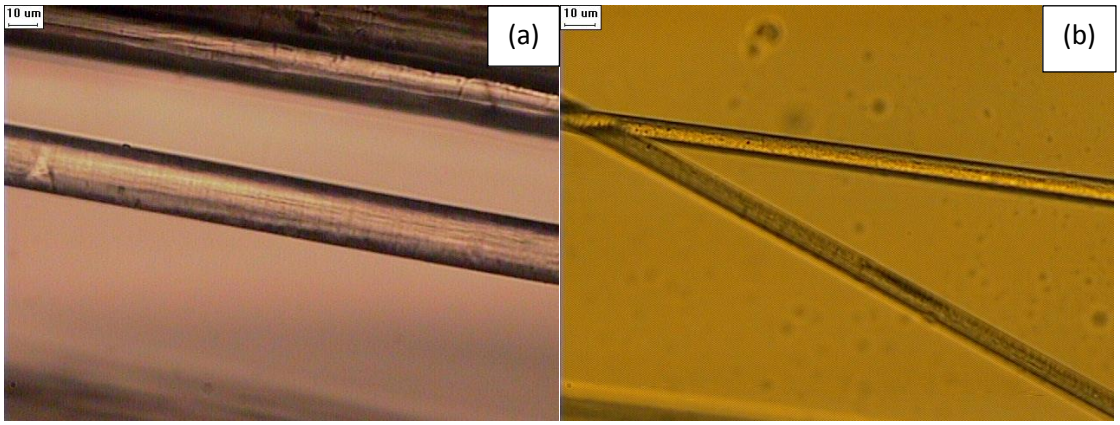

Figure 2.7 As-spun fibers of L/P blends (a) before post-stretching (b) after post-stretching.

2.3.4 Effect of lignin out-diffusion during wet-Spinning

During the wet-spinning process, as the spinning solution gets extruded from the spinneret capillaries into the coagulant bath, solid fibers are formed by the out-diffusion of the solvent (DMSO) into the coagulant. Figure 2.8 (a)-(c) display representative SEM micrographs of the cross-section of as-spun L/P fibers produced from 20 wt% solid content for various L/P ratios in the spinning solution. A porous structure was observed throughout the fiber cross-section. With an increase of lignin content from 25 to 45 wt%, the number and size of macro voids increased, and the solid fiber skin weakened gradually. The void-

formation phenomenon is consistent with that reported by Husman *(86)* in L/P fibers with lignin content above 20 wt%, who subsequently used PAN polymers with molecular weights 5-40% greater than the standard grade were used to increase solution viscosity. Although the macro-voids were reduced, these were not eliminated. Baker et al. *(72)* reported that the lignin may be separating from PAN during coagulation, resulting in the lignin leaching with the solvent. Figure 2.9 displayed the coagulant retrieved after wet-spinning of L35/P65 solution. As the spinning time increased, the lignin concentration in the coagulant also increased, which confirmed the lignin out-diffusion from fibers into coagulant, leaving pores in the fibers. As the lignin content in L/P blend increased from 25 to 45 wt% the lignin leaching became more severe, resulting in increased macro-voids illustrated in Figure 2.8 (c), which is undesired.

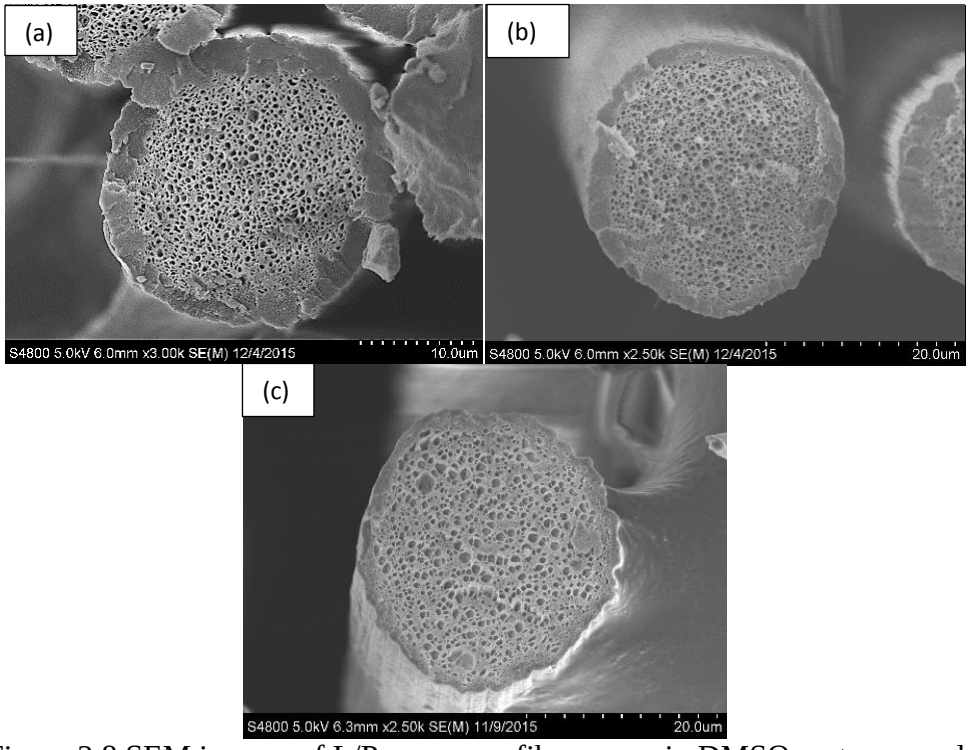

Figure 2.8 SEM images of L/P precursor fibers spun in DMSO-water coagulant (a) L25/P75 (b) L35/P65 (c) L45/P55.

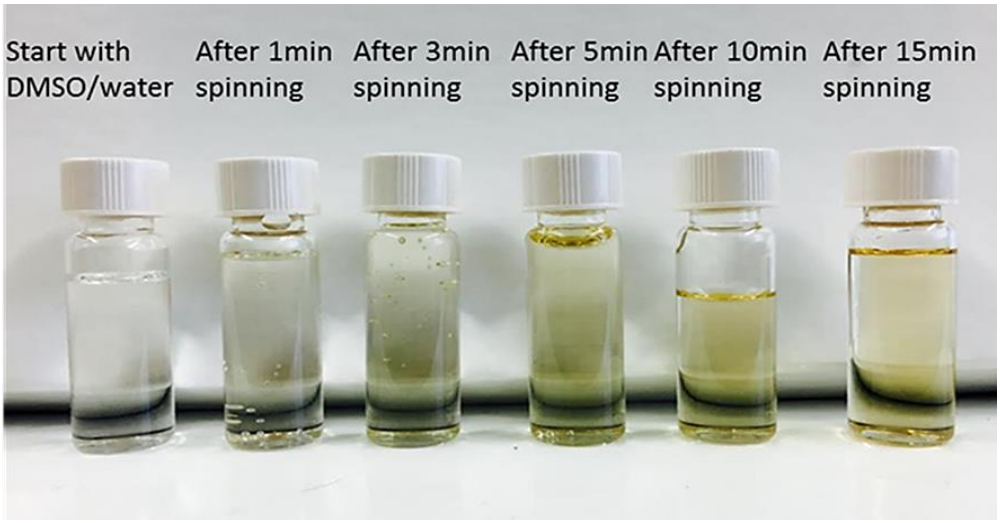

Figure 2.9 The coagulant retrieved after wet-spinning of L35P65 blend during different spinning periods.

The out-diffusion of lignin can potentially be reduced by two ways: (i) lower coagulation temperature, and (ii) reduce lignin concentration gradient between spinning dopes and coagulant. Liu et al. *(88)* have reported a gel-spinning technique using methanol coagulant bath at -50ºC, which effectively reduced the counter-diffusion rate and lignin leaching, as described in Chapter 1. The resulting carbon fibers displayed void-free cross section. However, this process requires concentrated solution dope and a low coagulation temperature, which makes it more complicated, and potentially more expensive than regular wet-spinning process. So, a method of controlling the coagulant composition to balance counter-diffusion rate of lignin during wet-spinning was explored. Increasing lignin composition in coagulant bath was approved to be an effective way to reduce concentration gradient and balance the out-diffusion.

To quantify the out diffusion of lignin, L35/P65 solution was spun into 65% DMSO/35% water coagulant, but one containing different lignin contents (0, 0.1%, and 0.2%). Cumulative concentration of lignin in the coagulant was measured as a function of spinning time using UV-Vis spectroscopy. All samples withdrawn from the coagulant bath were diluted with baseline solvent to lower absorbance values at 283 nm to ≤ 2.0 (for a pathlength of 10 mm). From this measurement, the lignin concentration was calculated by Beer-Lambert Law (Eq 2.3):

$$\%lignin_{coagulant} = \frac{Abs_{283}}{\varepsilon_{283} l} \tag{2.3}$$

where Abs_{283} is the absorbance of lignin coagulants at a wavelength of 283 nm, ε_{283} is the extinction coefficient for lignin standard at 283 nm, which can be calculated from the slope of calibration curve shown in Figure 1 and l is the pathlength (10mm). Figure 2.10 shows the real-time lignin concentration in coagulant during the wet spinning. The percentage of lignin loss was calculated by Equation 2.4:

$$\%lignin_{loss} = \frac{\Delta\%lignin_{coagulant} \times m_{coagulant}}{Q \times t \times 0.2} \tag{2.4}$$

where $m_{coagulant}$ is the mass of coagulant, Q is the mass flow rate of spinning solution in the wet spinning, and t is spinning time.

When the coagulant was devoid of any lignin, there was over 4% lignin that leached within 900s of spinning. Addition of 0.1% lignin reduced the lignin loss to 2.4%. Further, for 0.2% lignin concentration in the original coagulant, the lignin loss was further reduced to immeasurable level (below 0.5%). This observation confirms that the out-diffusion of lignin from fibers into coagulant was drastically reduced, and the method of

controlling lignin content in coagulant provided a simple, and low-cost process to produce void-free L/P fibers.

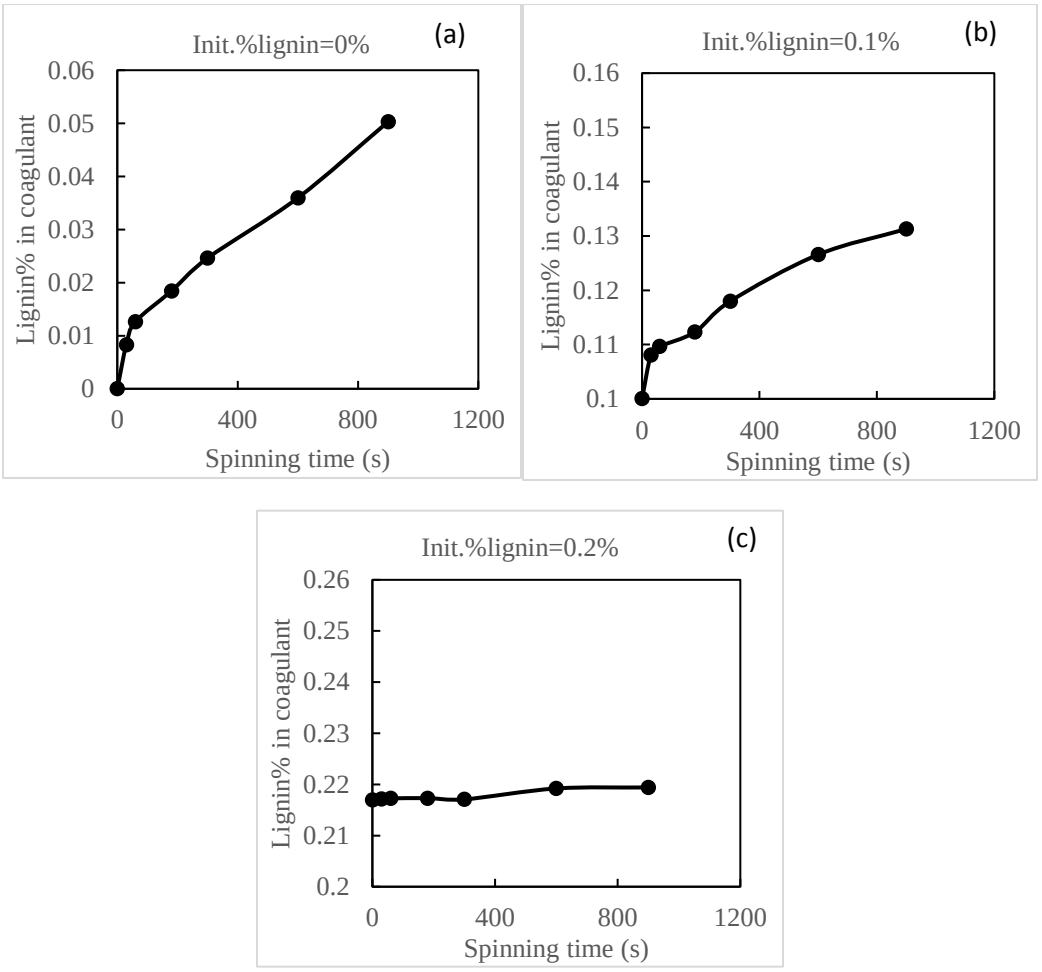

Figure 2.10 Cumulative concentration of lignin in coagulant during L35/P65 wet spinning: (a) Init.%lignin=0%, (b) Init.%lignin=0.1%, (c) Init.%=0.2%.

L/P fibers (L25/P75, L35/P65, L45/P55 and L50/P50) were spun using a coagulant with 0.2% added lignin, and the resulting L/P fibers are displayed in Figure 2.11. PAN fiber spun from DMSO/water coagulant is shown in Figure 2.11 (a). All the L/P fibers exhibit homogenous morphology, and show no voids in the cross sections,

independent of blend ratio. Macro-phase separation that occurred in previous studies was not found in the present results. No noticeable deterioration or change in the microstructure of L/P fibers was observed compared with that of pure PAN control fibers. However, L/P fibers displayed a nominally circular cross-sectional shape with crenulations, whereas PAN fibers displayed the characteristic smooth kidney-bean shape. This result indicates that lignin present in the blends could facilitate overall mass-transfer rate of the solvent, with a resulting increase in the specific surface area of the fibers. Note that L/P solid fibers display a smaller diameter (about 22 μm) as compared to the L/P porous fibers (about 27 μm) spun from DMSO/water coagulant. The observation about larger, porous fibers resulted from the fact that extrudates containing voids/bubble are difficult to stretch, and result in thicker fibers.

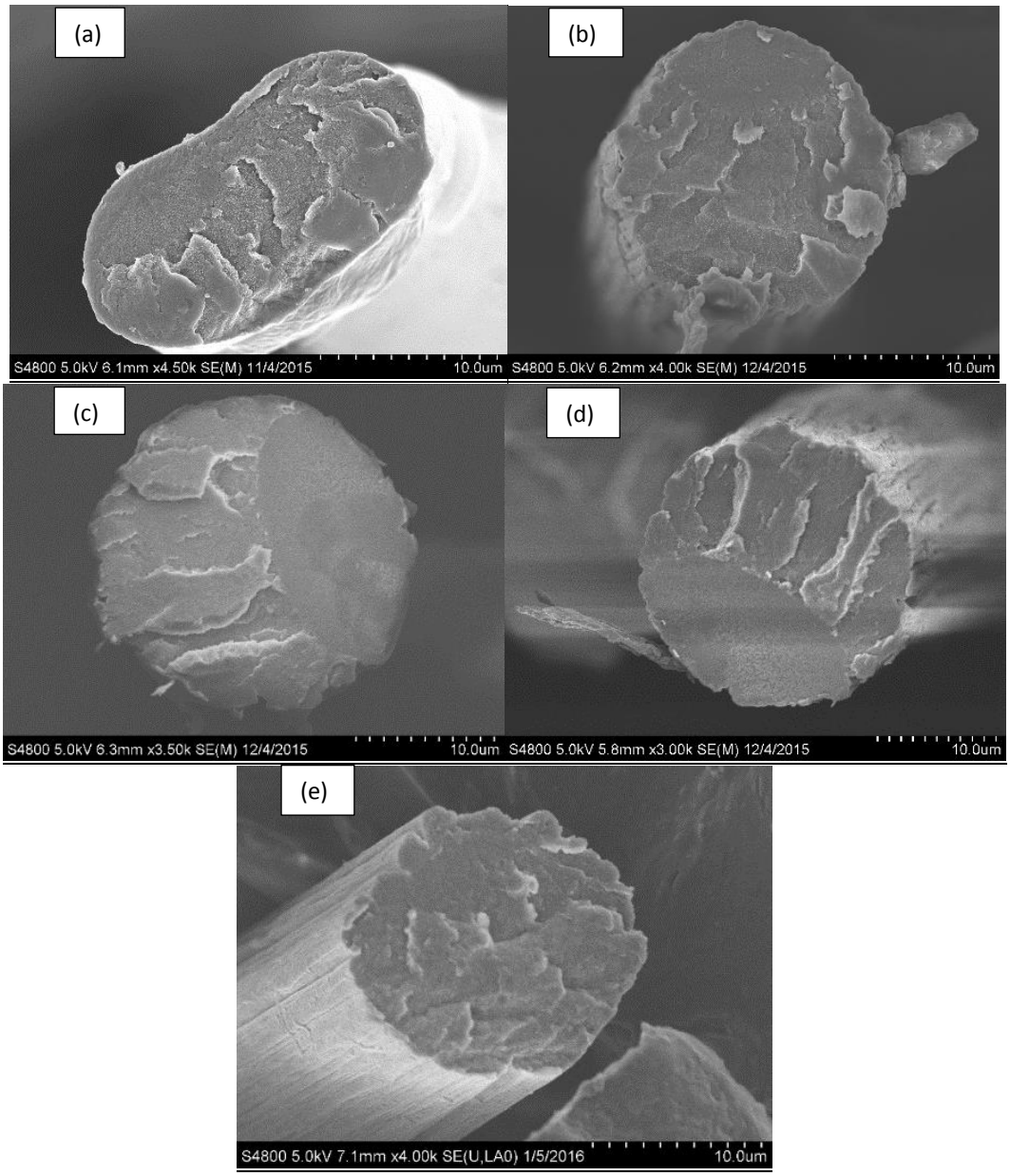

Figure 2.11 SEM images of pure PAN fiber and L/P fibers spun in DMSO- water coagulant with additional 0.2% lignin before post-stretching (a) PAN (b) L25/P75 (c) L35/P65 (d) L45/P55 (e) L50/P50.

2.3.5 Mechanical properties of lignin/PAN blend fibers

Figure 2.12 displays representative tensile testing curves of each set of L/P fiber samples. Figure 2.12 (a) shows the tensile property comparison of L35P65 precursor fibers with and without lignin diffusion control. The L/P fibers wet-spun through unmodified DMSO/water coagulant display a porous morphological structure, which leads to poor quality fibers showing average tensile strength of 67 MPa. However, the L/P fibers produced from out-diffusion controlled wet-spinning process present void-free structure, and display tensile strength about 250 MPa, which is almost 5 times higher than L/P porous fibers. As mentioned before, the morphology with voids in fibers is undesired, and such precursor fibers could not be successfully converted to high performance carbon fibers for structural applications.

Figure 2.12 (b) shows representative stress-strain curves of each set of L/P void-free precursor fibers as a function of lignin content. A similar trend in the stress–strain behavior is observed for all samples. The limit of linear proportionality was approximately 1%, and the yield point is very close to the proportionality limit for all L/P and PAN fibers. Also, strain hardening is seen for all samples owing to orientation and alignment of polymer chains in the direction of the load which increases the stress. Necking is not observed in these samples. The tensile properties of the PAN fibers in this study are consistent with those reported in the literature: 10-25% for the breaking strain, 0.1-0.7 GPa for strength, and 1-10 GPa for tensile modulus *(103-105)*.

Table 2.2 summarized the tensile properties of the fully post-stretched (DDR=4) PAN and L/P precursor fibers. PAN fibers (0% lignin content) show a higher tensile strength and modulus than L/P fibers due to better polymer chain packing and orientation. With an increase of lignin content from 25 to 50 wt%, the tensile strength of L/P fibers is reduced by only ~20%, meaning equal gravimetric lignin content (50%) could be incorporated into PAN to make fibers with limited performance reduction. Elongation at break of PAN is observed to be higher than L/P blend fibers, indicating that lignin molecules reduces the overall mobility of the PAN polymer chain, restrain their segmental motion, and reduces the elongation capabilities of the fibers by ~1%.

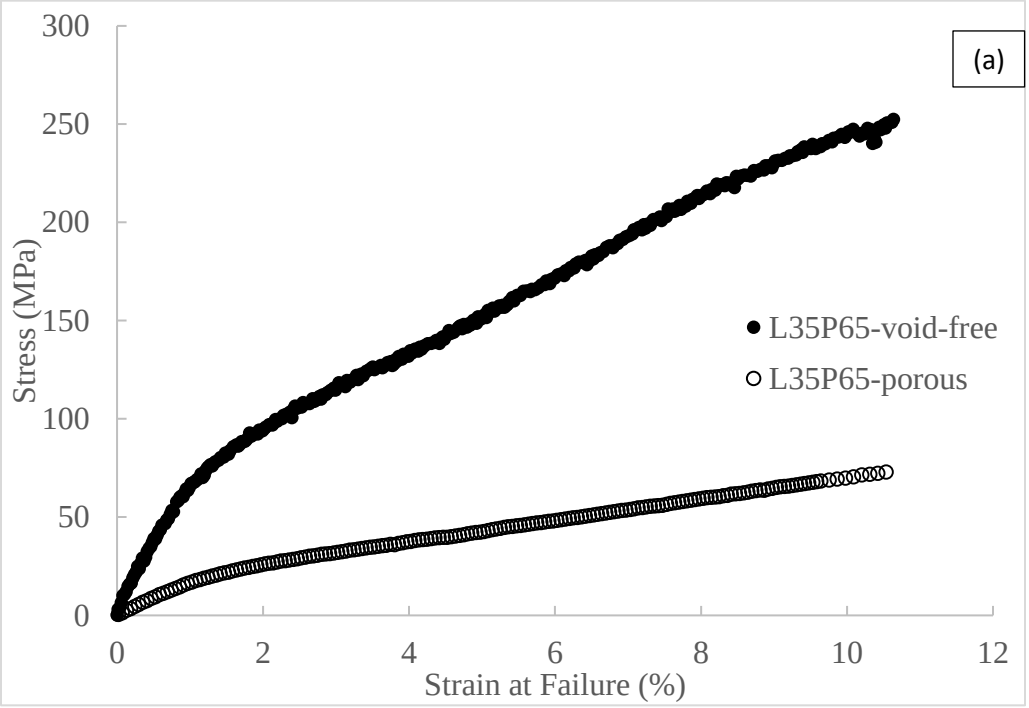

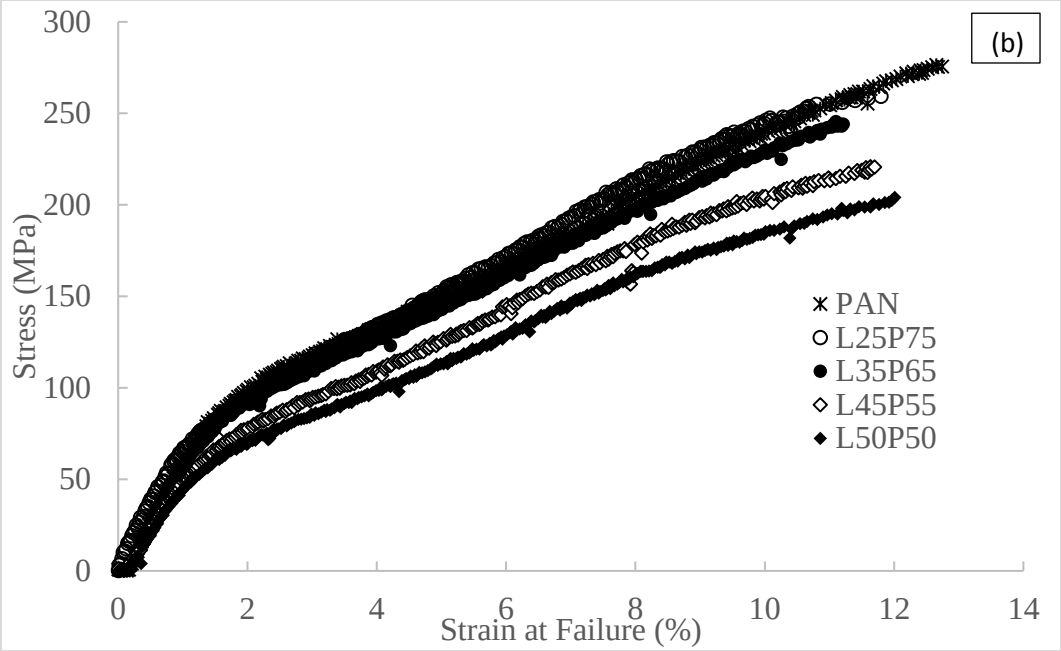

Figure 2.12 Representative tensile testing curves of each set of samples: (a) L35P65 fibers with and without diffusion control, (b) PAN and L/P void-free fibers.

Table 2.2 Tensile properties of pure PAN and lignin/PAN blend as-spun fibers.

	Diameter (μm)	Max stress (MPa)	Tensile Modulus (GPa)	Break Strain (%)
PAN	9.2±0.2	276±3	7.4±0.9	13.2±1.3
L25P75	9.3±0.4	260±8	6.1±0.3	11.9±0.8
L35P65	9.6±0.2	240±16	5.9±0.8	12.0±1.2
L45P55	9.5±0.2	215±18	5.1±0.5	12.2±0.7
L50P50	9.4±0.3	200±16	4.7±0.4	12.2±0.5

2.3.6 Effect of lignin on microstructure of carbon fibers

Microstructure of carbon fibers obtained from PAN and L/P precursor fibers is displayed in SEM micrographs of Figure 2.13. L/P CFs show no observable voids in the fiber cross-sections. Also, no fusion of CFs was observed, indicating the effective diffusion control of lignin, and proper heating rate were applied during each processing

steps to avoid defect formation, which would be detrimental for mechanical properties. PAN-based CFs display smooth kidney-bean shape. By comparison, the crenulated cross-sectional shape of L/P CFs was retained after heat treatment, which provides larger interfacial area as compared to smooth circular shaped fibers *(63)*.

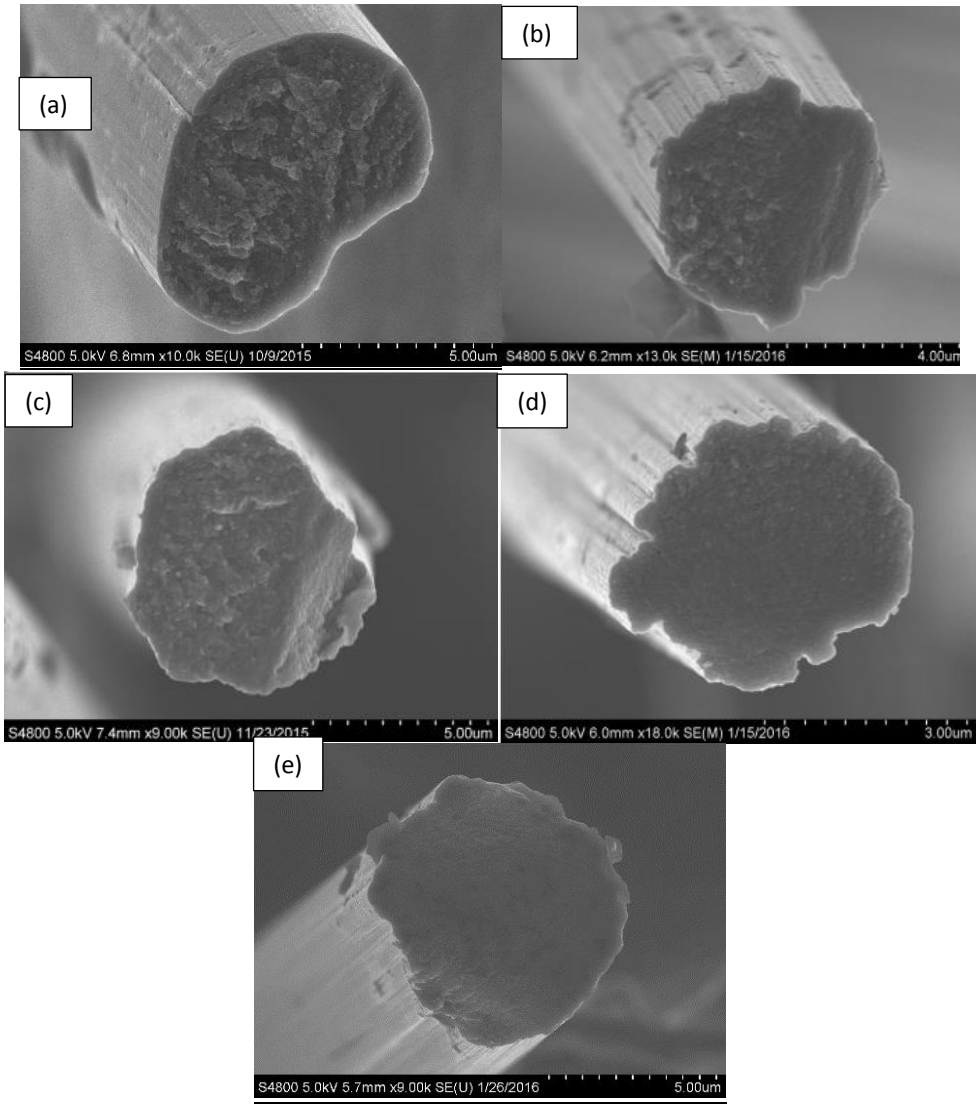

Figure 2.13 SEM images of PAN and L/P CFs (a) PAN (b) L25/P75 (c) L35/P65 (d) L45/P55 (e) L50/P50.

Raman spectra of CFs are displayed in Figure 2.14 (a). The Raman D-band (at ~1320 cm^{-1}) is attributed to structural disorder, and the G-band (at ~1590 cm^{-1}) is attributed to the graphitic structure. As shown in Figure 2.14 (b), integrated intensity ratio of D and G band (I_D/I_G) increases for a higher lignin content due to disordering of carbon structure resulting from lignin. Thus, a higher lignin content leads to a lower degree of graphitic crystallinity within the carbon fibers. WAXD results in the form of 2θ profiles are presented in Figure 2.15, with (0 0 2) peak from carbon, and (1 1 1) peak from silicon standard marked by circles. The NIST-grade silicon standard powder provides accurate location of 2θ peak position, viz. a sharp (1 1 1) peak at 28.4º. The PAN-based CFs displayed the (0 0 2) peak at 2θ ≈ 25.5º, with d_{002} spacing calculated at 0.349 nm. For L35P65 and L50P50 CFs, the peaks were broader, and less pronounced due to the increased lignin content (compared to pure PAN-based CFs). The (0 0 2) peaks for L35P65 and L50P50 CFs were detected at 25.0º and 24.8º, respectively. These 2θ values are even smaller than that for turbostratic carbon in pure PAN-based CFs, which indicates that L/P-based CFs possessed even lower degree of turbostratic carbon due to the higher lignin content. These WAXD results are consistent with those observed from Raman spectroscopy.

In a previous study *(88)*, it was shown that during stabilization, lignin/PAN leads to smaller crystal size as compared with pure PAN, indicating that the formation of cyclized ladder structure might be disturbed by the addition of lignin. Because lignin is a branched molecule, it played a role as "impurity" within the cyclized ladder structure of PAN

formed in stabilization. During carbonization, when the ladder structure is transformed into carbon layers, lignin hindered the formation of any graphitic crystalline structure. A lower graphitic crystallinity reduces lattice-dominated properties such as the modulus, but does not affect the tensile strength.

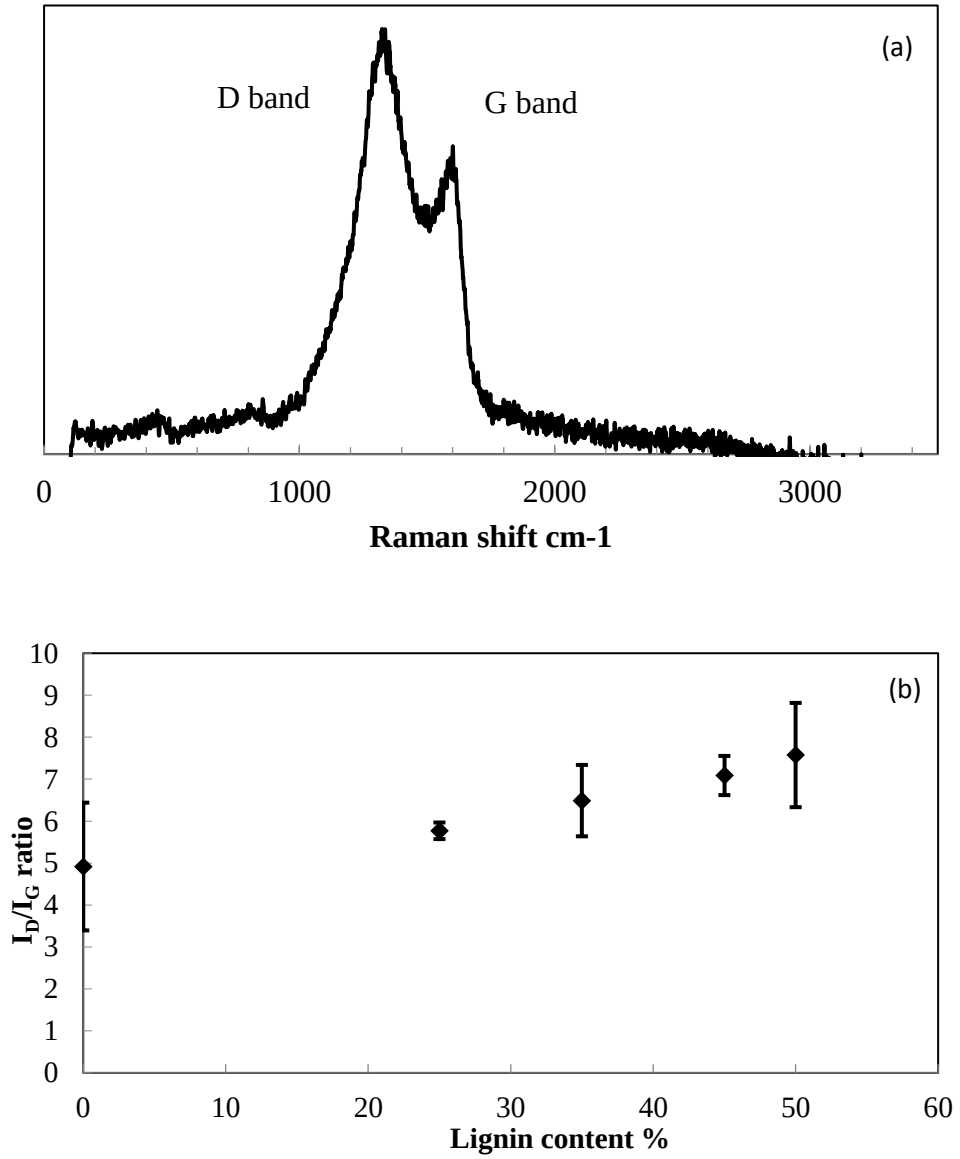

Figure 2.14 (a) Raman spectra of representative L/P CFs (b) Integrated I_D/I_G ratio for PAN and L/P CFs with different lignin content.

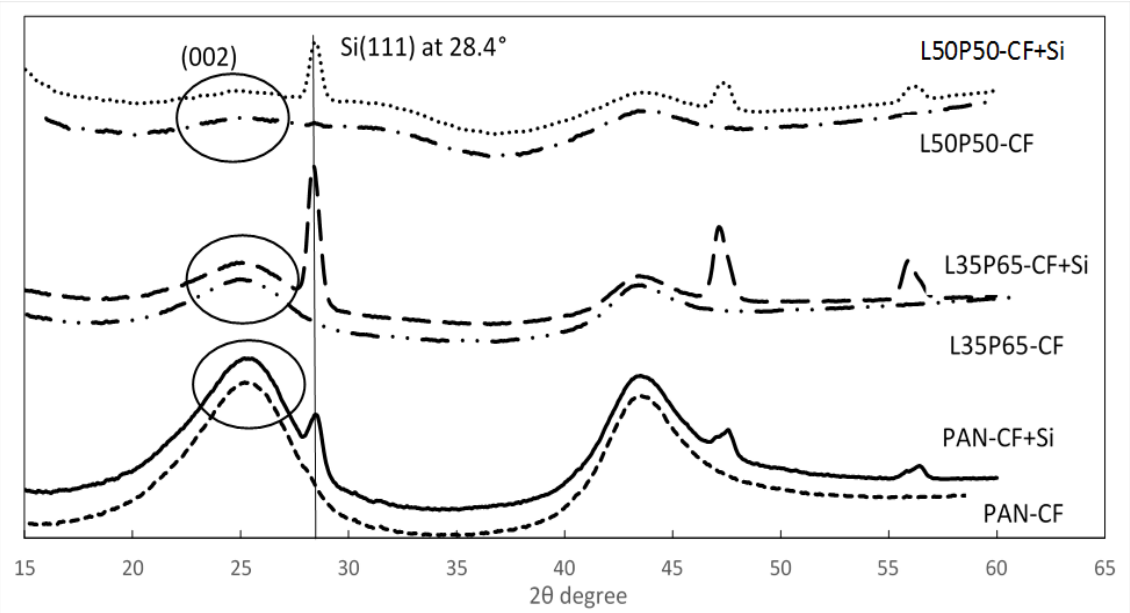

Figure 2.15 Integrated azimuthal (two-theta) profiles from wide-angle X-ray diffraction of PAN, L35P65 and L50P50 carbon fibers with and without silicon standard. Intensity values on the y-axis scale are in arbitrary units.

2.3.7 Mechanical properties of L/P-based carbon fibers

The tensile properties of CFs obtained from various combination of L/P are summarized in Table 2.3. The tensile strength significantly improved when voids were eliminated within CFs. The L35/P65 CFs with observable voids display a tensile strength of only 0.25±0.03 GPa. In contrast, the strength increased to 1.18±0.13 GPa when voids were eliminated in the fibers. Pure PAN-based CFs displays a tensile strength and modulus values of 1.38±0.12 GPa, and 155.2±7.3 GPa, respectively. Thus, under identical stabilization and carbonization conditions, L/P blend-based CFs possessed lower strength and modulus as compared to pure PAN-based CFs. With an increase of lignin content from 25 to 50 wt%, the tensile strength of resulting CFs is not significantly affected, meaning

equal gravimetric lignin content (50 wt%) can be incorporated into PAN without further decreasing the strength.

The compliance-corrected modulus of PAN-based CFs was measured at 187 GPa. The modulus of L/P CFs decreased with an increase of lignin content, because lignin disturbed formation of carbon layer plane. The compliance-corrected modulus of resulting L50/P50 CFs is 130 GPa. As expected, the modulus of these fibers is higher than that of pure lignin-based CFs (≈ 100 GPa) *(11)*, but lower than pure PAN-based CFs. The modulus of L/P blend-based CFs followed the simple rule-of-mixtures for composites, i.e., nominally 50% contribution from pure PAN-based CFs, and 50% from pure lignin-based CFs (187/2 + 52/2 ≈ 120 GPa). This indicates that the two components contributed proportionally to the tensile modulus. Thus, it is interesting to note that equi-component L/P fibers resulted in carbon fibers with tensile modulus higher than 100 GPa, establishing that the standard wet-spinning process, and 50 wt% lignin can be incorporated into a blended precursor to make carbon fibers with improved mechanical properties.

Table 2.3 Tensile properties of carbon fibers from different composition of PAN/lignin blends. Modulus values are reported without compliance correction.

	PAN CFs	L25/P75 CFs	L35/P65 CFs	L45/P55 CFs	L50/P50 CFs
Diameter, μm	7.0±0.3	7.0±0.2	6.9±0.4	6.9±0.4	7.0±0.3
Strength, GPa	1.38 ± 0.12^{a}	1.14 ± 0.53^{b}	1.18 ± 0.13^{b}	1.17 ± 0.10^{b}	1.20 ± 0.10^{b}
Modulus, GPa	155.2 ± 7.3^{c}	148.2 ± 5.8^{c}	124.2 ± 9.0^{cd}	113.1 ± 7.4^{d}	105.7 ± 3.1^{d}
Strain at failure %	0.9±0.1	0.7±0.1	1.1±0.2	1.0±0.1	1.1±0.1

Different superscripts denote statistical difference between groups at 95% confidence interval

2.4 Conclusions

In the initial phase of this study, lignin and PAN were blended to form precursor with lignin content as high as 50 wt%. Rheological measurements demonstrated that increasing lignin content in spinning solution reduced shear viscosity and normal stress, indicating a decrease of viscoelastic behavior. This was confirmed by Fourier transform infrared spectroscopy results that show no discernable chemical reaction or crosslinking between PAN and lignin in the solution, and also confirms that lignin can be considered as a diluent during the wet-spinning. Lignin/PAN fibers were spun via a standard wet-spinning process. The solid content for L/P spinning solutions was increased from 16 wt% to 20 wt% to compensate for the reduced viscoelastic properties of L/P blend solutions (as compared to that of pure PAN solutions). Although higher solid content blend solution was used to increase viscosity, the resulting precursor L/P fibers had micron-sized voids, resulting from lignin leaching during spinning, and it was confirmed by UV-vis that lignin concentration in the coagulant bath was increased as the wet-spinning continued. In order to eliminate the macro-voids within L/P fibers, out-diffusion of lignin during wet-spinning was investigated, and reduced by controlling the coagulant composition. It was confirmed by UV–vis that an insignificant amount of lignin leached out from fibers into coagulant when 0.2% initial lignin content was incorporated in the coagulant bath. Thus, void-free L/P CFs were produced via low-cost wet-spinning process. The absence of micron-sized voids, and micro-phase separation in the L/P precursor fibers indicated good compatibility between PAN and lignin. The tensile strength of L/P void-free fibers is approximately five times higher than porous fibers. The

equi-component L/P fibers (L50P50) display an average strength of 200 MPa, which is comparable to some PAN fiber properties in literature.

The L/P carbon fibers show no observable voids in cross-sections. Raman spectroscopy and WAXD results indicate that higher lignin content leads to a lower degree of graphical crystallinity. Lignin disturbed the formation of cyclized ladder structure of PAN during stabilization, disturbed the formation of carbon layers during carbonization, and reduced the tensile modulus of resulting carbon fibers. The carbon fibers obtained from modified wet spinning process displayed lower mechanical properties than those reported by Liu et al.*(88)* The relatively high ash content of ~2% in the as-received lignin generated defects within carbon fibers, which are deleterious for the tensile strength. By comparison, Liu et al. *(88)* have reported that the lignin used in L/P fibers was washed repeatedly to reduce ash content below 0.3%; also, a higher post-draw down ratio (about 13) was obtained in glycerol bath at 165ºC, which is almost four times higher than that obtained currently (about 3) in water bath at 80ºC. However, it should be noted that the fibers in this study were obtained from low-cost raw materials (ordinary PAN homopolymer and as-received lignin), and cost-effective processing steps. Thus, further improvement in CF properties is possible by using a better grade of PAN and purified lignin, albeit at increased costs.

Although mixing PAN with lignin improves the properties of resulting carbon fibers, the improvement of tensile strength is primarily contributed by PAN, and the introduction of PAN in blends poses same environmental concerns as those posed by PAN-based carbon fibers, viz. generation of HCN during thermal stabilization. Therefore, in

Chapter 3, an environmental-friendly, and cost-competitive lignin precursor with higher molecular weight, and low ash content was processed into carbon fibers to enhance the mechanical properties.

CHAPTER THREE

THE PROCESSING OF CARBON FIBERS FROM FRACTIONATED-SOLVATED LIGNIN PRECURSORS: EFFECT OF MOLECULAR WEIGHT

3.1 Introduction

As discussed in detail in Chapter 2, the wet-spun equi-component lignin/PAN (L/P) fibers with lignin content as high as 50 wt% were successfully produced, and converted to carbon fibers with tensile strength and compliance-corrected modulus of 1.20 ± 0.10 and 130 ± 3 GPa, respectively. In general, the mechanical properties of L/P-based carbon fibers exceed those of pure lignin-based carbon fibers *(11, 106, 107)*. However, the improvement of carbon fiber tensile strength is primarily contributed by PAN. Thus, no synergistic effects were found in the lignin/PAN blends, with the carbon fiber properties resulting primarily from the PAN component. Therefore, most recent research studies were focused on developing lignin precursor with chemical modification and fractionation to minimize the impurity content, and increase molecular weight (MW), in order to improve the resultant carbon fiber performance *(89-91, 108)*.

Most of the previous work discussed in Chapter 1 on melt-spun lignins, solvent fractionation has been used to isolate a lower molecular weight (and thus lower-Tg) portion of the lignin suitable for melt-spinning, followed by washing to remove contaminants (e.g., inorganics) from the lignin *(68, 89)*. However, the low MW lignin fraction and in particular its Tg, being well below the stabilization temperature, cause difficulties in stabilization and carbonization, and limit its utility in carbon fiber

production. For melt-spinning, the Tg of the lignin must be low enough so that it can be spun without solvents at temperatures below decomposition – but Tg must also be high enough for the lignin to undergo rapid stabilization. To get around this conundrum, Ogale and co-workers *(6, 63)* partially acetylated a softwood Kraft lignin so that it would dissolve in acetone, but also still have an acceptable rate of stabilization (total acetylation resulted in a lignin that could not be stabilized). The lignin–acetone solution could then be dry-spun (that is, the volatile solvent evaporates, leaving behind lignin fibers), eliminating the need for a low-Tg lignin.

This chapter mainly discusses the dry spinning process of a fractionated solvated lignin precursor, the following thermal stabilization and carbonization. A process recently developed by Thies and co-workers called Aqueous Lignin Purification with Hot Acid (ALPHA) *(1, 49, 109)*, simultaneously purifies and fractionates kraft lignin by molecular weight. The medium, higher and highest MW fractions of lignin, isolated via ALPHA, were directly dry-spun to obtain lignin (precursor) fibers. This was feasible because the higher MW portion is simultaneously purified and solvated, whereas the impurities and lower MW portion of the lignin are preferentially extracted into the solvent phase. This chapter investigates primarily the processing of carbon fibers derived from fractionated-solvated lignin precursor (FSLP). The specific objectives were to study (i) thermal properties of fractionated lignin precursors via ALPHA (ii) the role of (higher) molecular weights on the dry-spinning of precursor fibers, and the mechanical properties of the precursor fibers. (iii) the stabilization and carbonization of

precursor fibers under tension. The salient aspects of production of lignin fibers, and their carbonization were published in our recent paper *(94)*.

3.2 Experimental

3.2.1 Materials

The lignin-recovery process known as SLRP *(110, 111)* was used by the Thies group to isolate a softwood Kraft lignin from a black liquor having a solids content of 42 wt % and a Kappa number of 25. The lignin content was determined to be 99% via a simplified version of the Klason method *(112)*. The water content of the lignin, as determined by Karl–Fischer titration *(113)*, ranged from 30-45%, depending on ambient conditions in the lab. Mixtures of glacial acetic acid (ACS grade, 99.7% purity, VWR cat. no. MKV193-45) and distilled, deionized (DD) water with a resistivity >18.2 MΩ cm (Millipore Milli-Q Academic water purification system) were used as the solvent system for the ALPHA process. HPLC-grade (99.7+%) N,N-dimethylformamide (VWR cat. no. AA22915-K7) with the additive lithium bromide (VWR cat. no. 35705–14) was used as the mobile phase for GPC analysis.

3.2.2 Lignin fractionation and purification

This process was performed by the Thies group. A simplified schematic of the continuous-flow ALPHA process is shown in Figure 3.1. For a typical experimental run, a lignin–water slurry consisting of ~30-45% lignin in water is charged to the hopper and continuously delivered with the progressive cavity pump. The acetic acid–water solution of interest is delivered through the heated static mixer so that the slurry

and solution are intimately mixed at 90±5^{0}C. Within ~30 sec, the mixture of lignin, acetic acid, and water attains liquid–liquid equilibrium (LLE) and splits into two liquid phases. The solvent-rich phase contains most of the metal salts/impurities and the lower MW lignin, whereas the phase rich in lignin (solute) contains the purified, high MW lignin solvated with ~50% solvent – hence the term "fractionated–solvated lignin precursor" (FSLP).

The FSLP can be directly fed to a fiber-spinning device, but here it was dried for chemical analysis in a vacuum oven at ambient temperature and 29 in Hg vacuum for at least 24 h. Because it is highly hygroscopic, the dried lignin was then stored in a dessicator before use. Ash content was measured by weighing 3-4 gram dry lignin in a crucible and placing the crucible in a muffle furnace at 550±3°C for 20±4 hours. After cooling, the crucible was removed from the furnace and the residue (ash) mass was measured, for three duplicates. The lignin was analyzed for metals content by inductively coupled plasma–atomic emission spectroscopy (ICP-AES).

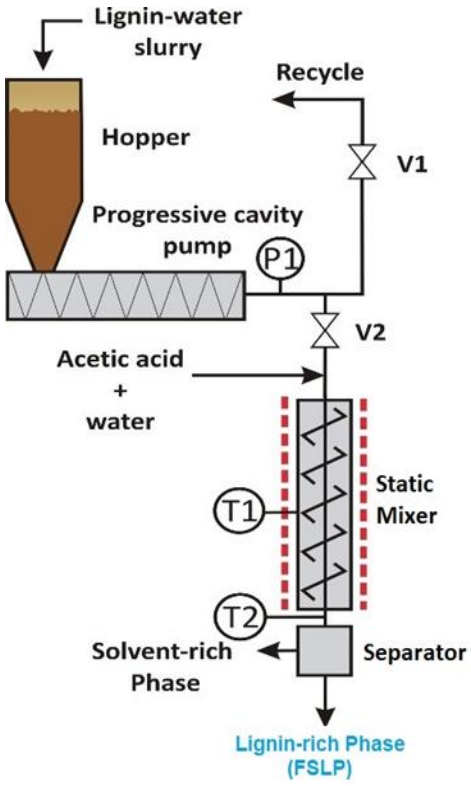

Figure 3.1 The continuous-flow version of the Aqueous Lignin Purification using Hot Acids (ALPHA) process (adapted from Refs 1).

3.2.3 GPC analysis of FSLPs

The molecular weight of the lignin fractions isolated in the polymer phase was determined by the Thies group using GPC (Alliance GPCV 2000). Two columns were used in series: a Waters Styragel® HT5 column (10 μm, 4.6 mm × 300 mm) followed by an Agilent PolarGel-L column (8 μm, 7.5 mm × 300 mm). The mobile phase consisted of 0.05 M lithium bromide in N,N-dimethylformamide (DMF) at a flow rate of 1 mL/min. Samples of the polymer phase recovered and dried as described above were dissolved in the mobile phase at a concentration of 1 mg/mL and filtered using a 0.2-μm nylon-

membrane syringe filter (VWR, part no 28145–487). Poly(ethylene glycol) (PEG) calibration standards were used for MW determination and were detected by refractive index using a Waters differential refractometer, while lignin samples were detected by UV–Vis with a Waters 2487 detector at 280 nm.

3.2.4 Thermal analysis of FSLPs

Thermogravimetry analysis (TGA) was conducted on Pyris 1 TGA (Perkin Elmer). All three FSLPs were devolatilized in vacuum oven at ~45°C for 48 hours. About 5-7 mg of lignin samples were loaded on platinum sample pan. The sample pan was heated in N_2 flow from room temperature to 900°C with a heating rate of 10°C/min, and cooled to room temperature at a rate of 20°C/min.

Differential scanning calorimetry (DSC) was performed on Pyris 1 DSC (Perkin Elmer Instrument). The baseline was created using an empty sample pan. The sample pan containing FSLP samples were heated to 250°C under N_2 at a heating rate of 15°C/min, and cooled to room temperature at a rate of 20°C/min. Second heating scan for each sample was used to determine the glass transition temperature.

3.2.5 Conversion of FSLPs into carbon fibers

For the purpose of dry-spinning, a solution was prepared from the dried polymer phase (i.e., the FSLP) by mixing it with a nominally equal amount of 85/15 acetic acid–water (AcOH/H2O) solution in a Paar reactor at 40-45°C for 30 min. This solution was then fed to a custom-designed spinning unit (AJA Inc., Greenville, SC) that consisted

of a steel barrel–plunger assembly. The spinning barrel has an inner diameter of 18mm. The solution was extruded at constant speed through a spinneret, which consisted of 18 holes that were 50 μm in diameter and 250 μm long. The barrel-spinneret assembly was held at elevated temperatures from 30 to 80 °C, which enabled evaporation of the solvent as the "dry" lignin fibers were taken up on a roll at speeds ranging from 20 to 30 m/min.

Next, these precursor fibers were thermo-oxidatively stabilized. Lignin fiber tows (2-3 cm long and weighing nominally 10-30 mg) were cut, and mounted within graphite end-tabs using fast-cure epoxy. The linear density of the fiber tow was calculated according to its length and weight. Fiber tows were inserted and hung in a preheated oven (Thermolyne 5000), illustrated in Figure 3.2. Weights were loaded at the bottom of fiber tows. The oven was preheated to 220°C for 30 mins. The fiber tow with load weights was inserted and hung in the oven where the local temperature in the oven was measured about 165°C. Then the temperature was raised up from 165 to 220 ºC at a rate of 20 °C/min, and then raised to 250 ºC at a rate of 10 °C/min, and held there for 1 h at 250 °C. This heating rate enabled the fiber tows to be post-stretched nominally ~400% before the oxidative crosslinking of lignin occurred, as shown in Figure 3.2 (b). After stabilization, the stabilized tows were mounted on graphite tabs to conduct carbonization under constant-length conditions (i.e., to prevent fiber shrinkage). As illustrated in Figure 3.3 (a), a piece of graphite sheet was folded and used as a frame. The ceramic adhesive paste (Alfa Aesar 43135-36) was applied on the edge surface of the graphite sheet, as shown in Figure 3.3 (b). The entire stabilized fiber

tow was placed on the graphite frame, and another small piece of graphite tab was cut and carefully placed at the edge of the fiber tow, as shown in Figure 3.3 (c). After two ends were glued with the ceramic paste, the rest parts were cut and removed, and the newly mounted sample was settled at room temperature for two hours, and then put into oxidation oven at 94°C for two hours for curing the adhesive. Carbonization was performed in a Thermolyne 21100 furnace by heating from room temperature to 1000 ºC at a rate of 7 ºC/min under a nitrogen flow of 0.1 L/min.

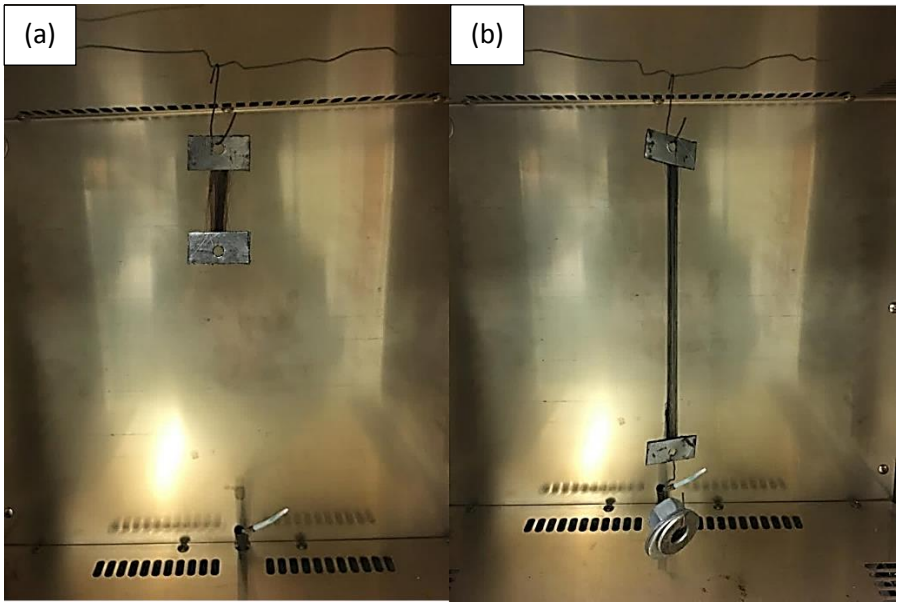

Figure 3.2 Stabilization of FSLP as-spun fiber tow (a) before tension was applied (b) fiber tow under tension and was extended.

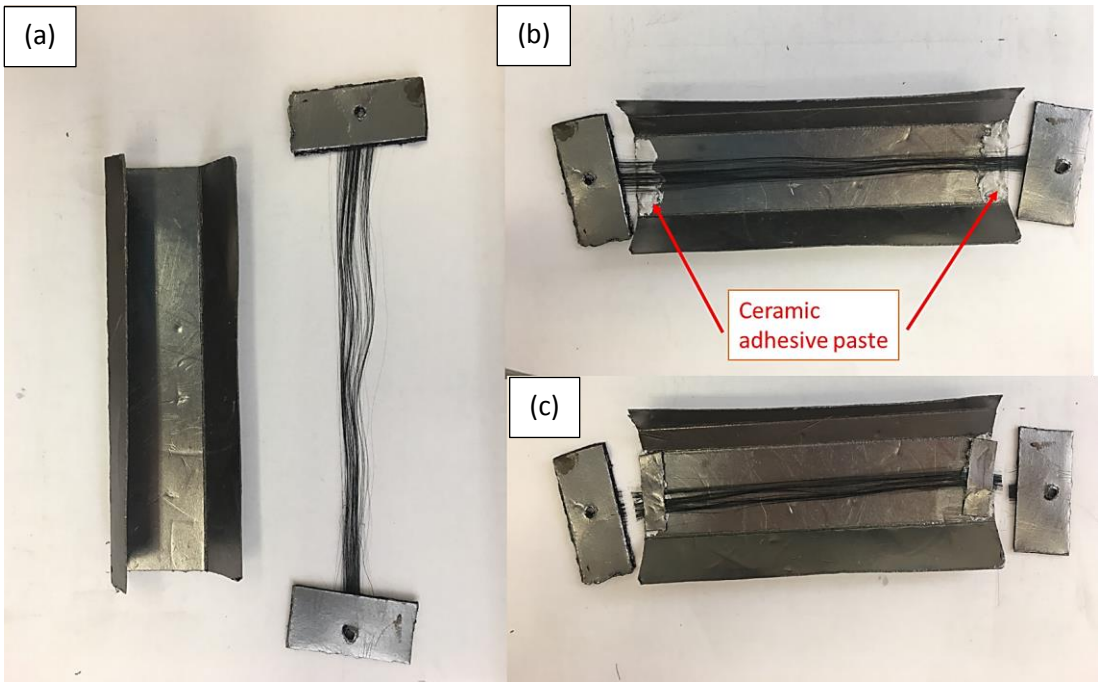

Figure 3.3 Mounting of stabilized fiber tows with ceramic adhesive paste for carbonization with constant fiber length.

3.2.6 Characterization of fibers

Morphological analysis of the precursor fibers was conducted by scanning electron microscopy (SEM) with a Hitachi 4800 SEM unit. The as-spun fibers were coated with platinum using a sputter coater for about 1 min. The sample preparation was described in section 2.2.6 in Chapter 2. The cross-sectional area of single fibers was measured using SEM micrographs and "Freehead shape measuring tool" in Quartz PCI software (version 8). Single filaments were mounted on paper tabs following ASTM test method D-3379-75. Accurate values for cross-sectional area, as measured by SEM, were used to calculate tensile modulus and strength of carbon fibers.

3.3 Results and Discussion

3.3.1 Lignin molecular weight and purity

ALPHA was operated to isolate increasingly higher-MW FSLPs in the solvated and cleaned lignin-rich phase by the Thies group. For the first ALPHA run, the bulk feed lignin was processed with a 30/70 AcOH/H2O solution at 90 °C. As seen in Figure 3.4, at these conditions only 10% of the lignin by weight was extracted into the relatively weak solvent phase, so 90% of the lignin separated out to form the lignin-rich phase (i.e., the FSLP) for subsequent conversion into carbon fibers. Note that this fraction is labeled in Figure 3.4 as being of medium MW, because it is only slightly higher in MW than the bulk feed lignin (which nominally is defined as being of "average/medium" molecular weight). With this FSLP, the idea was to produce a lignin that was much cleaner than the feed, but of similar molecular weight.

Next, the feed lignin was processed with a 56/44 AcOH/H2O solution; as seen in Figure 3.4, now 50% of the lignin was extracted into the solvent phase, and 50% of the lignin separated out to form the lignin-rich phase. Thus, this fraction is labeled as having a higher MW than the feed lignin. Finally, the feed lignin was contacted with a strong 67/33 AcOH/H2O solution; now, 90% of the feed lignin was extracted into the solvent phase, so that only 10% of the lignin formed the lignin-rich phase. This fraction is

labeled (see Figure 3.4) as having the highest MW of the three lignin-rich phases (i.e., FSLPs) that were isolated by ALPHA for conversion to carbon fibers. GPC chromatograms for the feed and for the medium, higher, and highest MW fractions are given in Figure 3.5 and indicate that ALPHA was successful in producing FSLPs of increasing MW.

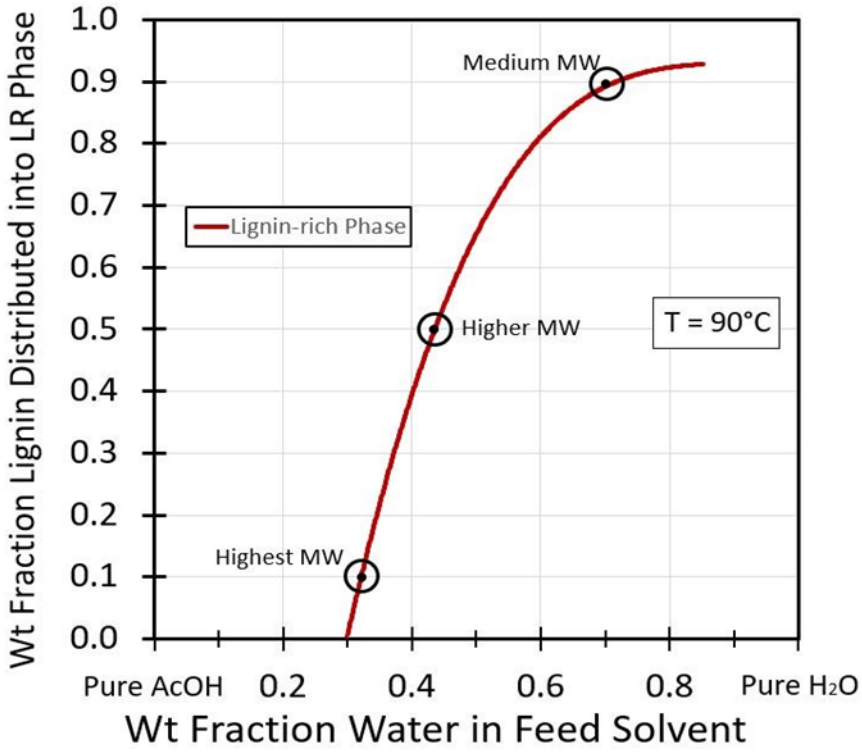

Figure 3.4 Equilibrium mass distribution of lignin into the lignin-rich (LR) phase for continuous-flow apparatus runs at 90 °C.

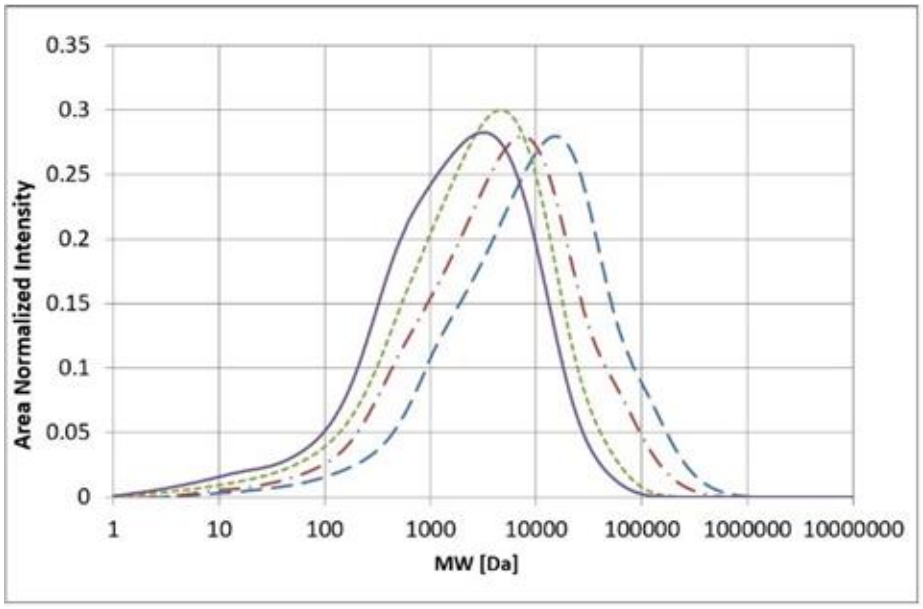

Figure 3.5 Molecular weight distributions of the lignin fractions (i.e., FSLPs) isolated via the ALPHA process: Feed SLRP (—), Med MW(- -), Higher MW(– •), Highest MW(– –).

The results of this ALPHA processing of a softwood Kraft lignin are summarized in Table 3.1. As expected, increasing AcOH/H2O ratio in the feed solvent enabled the isolation of FSLPs of increasing MW in the lignin-rich phase for conversion to carbon fibers. Furthermore, with ALPHA it is possible to reduce metals (and thus ash) impurities to levels significantly lower than ever reported for the purification of lignins. (The ash content of these FSLP lignins is almost two orders of magnitude cleaner than today's commercially available softwood Kraft lignins, and is also cleaner than today's best experimental organosolv lignins.) Finally, the metals in the lignin-rich phase are essentially at the same low levels (e.g., ~200 ppm Na) for all fractions, the effect of impurities as a variable was eliminated, which allows to focus exclusively on the effect of molecular weight (MW) differences.

Table 3.1 Lignin fractionation and purification via ALPHA*

Lignin Type	Yield [wt%]	AcOH/H_2O Ratio	Num. Avg. MW [Da]	Polydispersity Index (PDI)	Ash Content [wt%]	Na Content [ppm]
Feed lignin	100	N/A	5270±70	6.60±0.01	0.6±0.3	1400±50
Medium MW FSLP	90	30/70	7200±100	3.82±0.03	0.059±0.003	250±80
Higher MW FSLP	50	56/44	13800±150	4.44±0.03	0.069±0.005	210±50
Highest MW FSLP	10	67/33	28600±300	5.15±0.02	0.088±0.005	220±70

*All results are averages of duplicate samples.

3.3.2 Thermal analysis

The results from thermogravimetric analysis (TGA) of the three FSLPs are displayed in Figure 3.6. All three FSLPs with different MW show similar carbon yield around 40 wt% at 900°C. Lignin degradation occurs in three stages. In the first stage between 30-200°C, the initial weight loss between 30-100°C was about 3% which was mainly attributed to the loss of solvent and moisture within the samples. After the first weight loss, the degradation is slower between 100-200°C, and a plateau can be observed within this temperature range for all samples. The lignin degradation process mainly occurs in the second stage between 200-500°C, which is associated with primary lignin pyrolysis *(114)*. The pyrolytic degradation in this region involves the breakage of inter-unit linkages, which cause the release of monomeric phenols. Compared to higher and highest MW FSLPs, the medium MW FSLP (close to feed/bulk lignin) shows slightly larger weight loss in the temperature region, which

implies a lower thermal stability. At temperatures above 500°C, the degradation rate is slower and possibly related to the slow decomposition of non-carbonaceous elements. At 800°C, a carbonized polyaromatic structure is formed, and the remained weight percentage doesn't change for all three FSLPs. Overall, the FSLPs obtained from softwood have relatively high carbon yield compared to lignins obtained from herbaceous (carbon yield of 20-40 wt%) *(114)*. The increase of MW dose not significantly improve thermal stability, and the carbon yield for three FSLPs is not significantly different.

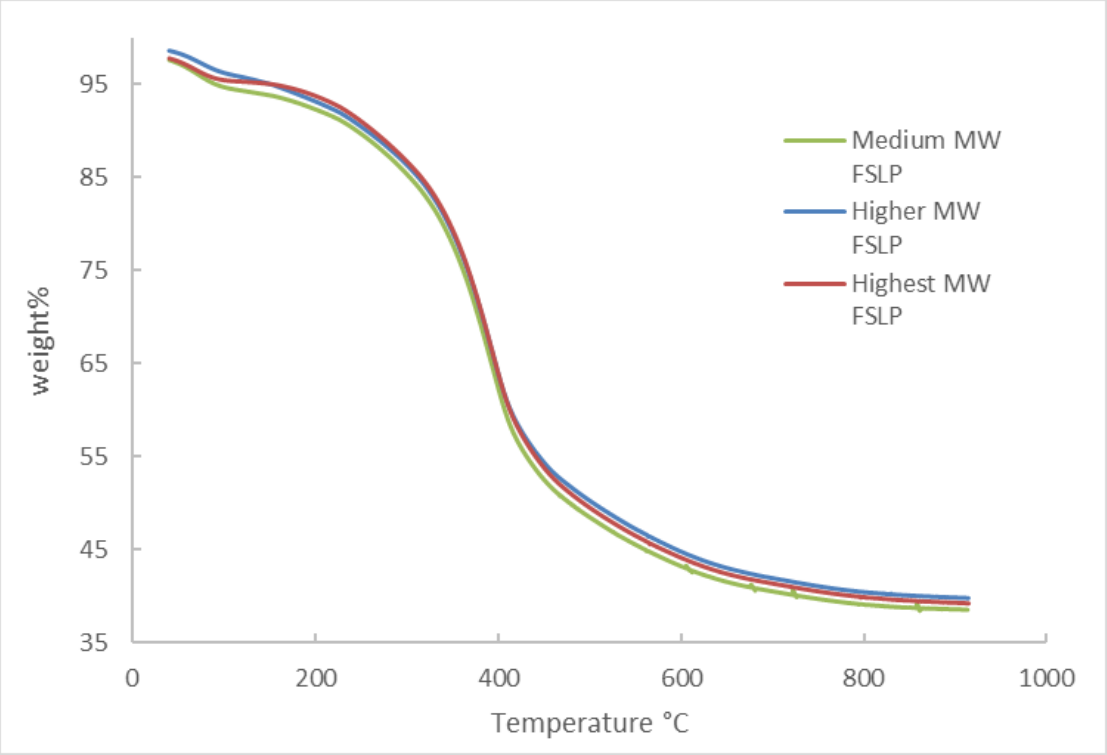

Figure 3.6 TGA thermograph of three different MW FSLPs in N_2 flow.

The DSC analysis of the three lignin fractions shows the glass transition temperature (Tg), which is presented in Figure 3.7. It appears that the lignin shows a broad transition range from 90 °C to150 °C. The glass transition temperature of the FSLPs was found within the typical range of softwood kraft lignin (110-160 °C), which is higher than hardwood kraft lignin (90-130 °C) due to the large content of guaiacyl units and a higher intensity of hydrogen bonds which corresponding to more rigid structure *(107)*. The highest MW FSLP shows a higher Tg value of 142°C than higher MW and medium MW FSLPs of 135°C and 112°C, respectively. ALPHA process effectively eliminates the low MW and low Tg species within the lignin precursor, leaving behind high MW portion. The increase in MW of FSLPs contributed to the increase of glass transition temperature. Thus, as mentioned in section 3.1, the high Tg values of lignin precursors lead to difficulties in melt-spinning. However, in our dry-spinning process, lignin was dissolved in solvent and dry-spun into fibers, so there is no need to have low MW and low Tg fractions.

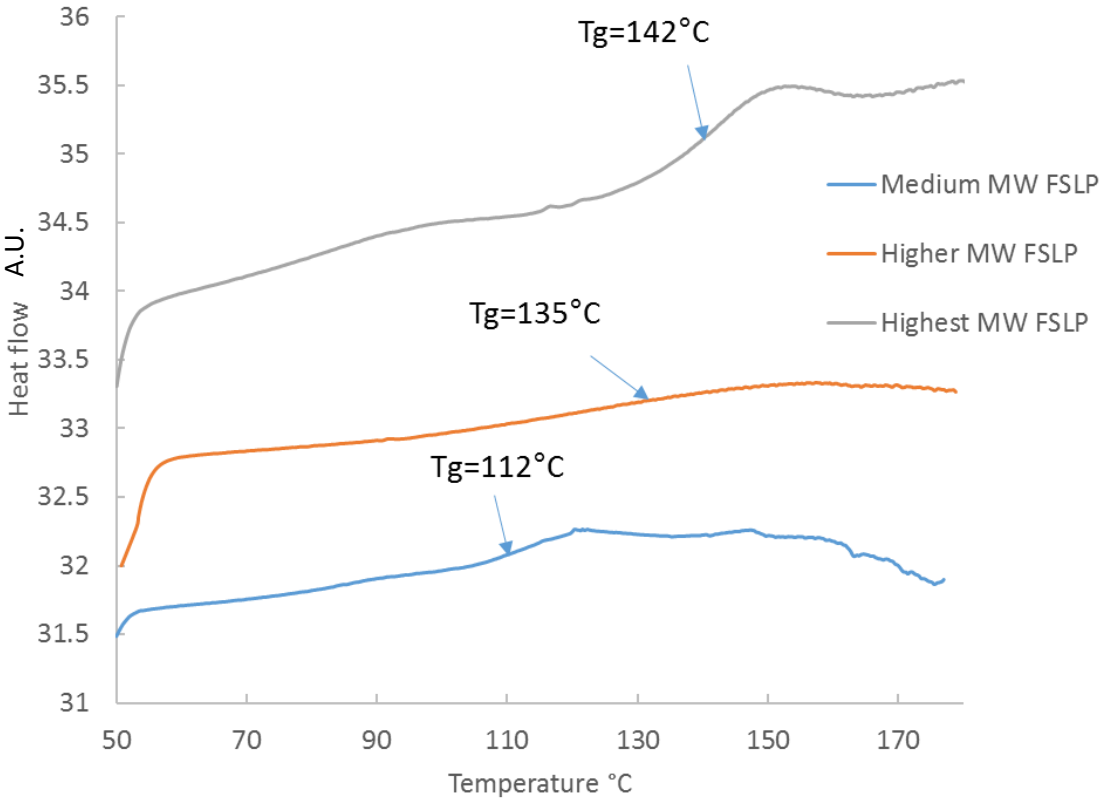

Figure 3.7 DSC thermograph of three different MW FSLPs in N2 flow.

3.3.3 Dry-spinning

During dry-spinning of a solution, the solvent must evaporate out of the extruded filament before the filament gets wound on a roll; otherwise, the moist filaments will stick together and prevent successful production of fibers. There are a number of variables that control spinability in dry-spinning process, including solution concentration, spinning temperature, filament solidification, etc. In all fiber spinning process, the most important solution properties are the polymer molecular weight and concentration, which can strongly affect solution viscosity and mass transfer rate. The

key engineering variables are temperature and pressure drop. In this study, three different MW FSLPs were dissolved in same solvent (acetic acid/water 85/15 wt) to form a concentrated spinning dope. High MW of lignin or high concentration of the solution can lead to higher viscosity. In order to keep constant viscosity values for all spinning solutions, it was necessary to decrease solid concentration in spinning dope for the highest MW FSLPs.

The effect of temperature on the viscosity of the concentrated solution can be described by the Andrade equation *(115)*:

$$\eta = A \exp\left(\frac{E_a}{RT}\right) \quad (3.1)$$

Where A is constant, E_a is activation energy. As describe in equation 3.1, the viscosity of the polymer solution is decreased with the increase of temperature. In addition, the viscosity of the lignin solution is also dependent on the shear rate due to the non-Newtonian behavior. As noted, it is important to establish a "spinnability window" in which the conditions are required to produce continuous lignin fibers with good quality.

Thus, initial dry-spinning experiments were performed using one MW grade lignin (higher MW FSLPs) to investigate effect of solution concentration and temperature on extrusion and drawn-down during dry-spinning. Viscosity values were estimated by pressure drop during spinning using equation 3.2.

$$\eta = \frac{\Delta P\, D}{4L\dot{\gamma}} \quad (3.2)$$

Where ΔP is the pressure drop, D is the diameter of spinneret hole, L is the length of spinneret hole, (L/D=5) and $\dot{\gamma}$ is the shear rate. During the dry spinning, the lignin solution was extruded through a spinneret containing 10 open holes with a constant flow rate. The wall shear rate was calculated from total flow rate Q using equation 3.3.

$$\dot{\gamma} = \frac{4Q}{10\pi R^3} \tag{3.3}$$

The experimental conditions, the pressure drop and calculated viscosity values are listed in Table 3.2. Firstly, 60 wt% solid content was used for all the spinning runs at temperature of 70±1°C, 80±5°C and 90±1°C. As the temperature increases, the estimated viscosity values decrease from 2.5 to 1.9 Pa·s. At 70 and 80°C, fibers could be continuously drawn down, and winded up on a take-up roll, but the drawn-down ration (DDR) is low, so that the as-spun fibers have large diameter. At 90°C, although solution could be extruded out of the spinneret, rapid evaporation of the solvent resulted in a very dry extrudate that could not be continuously drawn down (stretched), and no continuous as-spun fibers were produced at this temperature. Moreover, the spinning was extremely difficult, and the pressure drop within the spinneret was high (approached the alarm value of 3000 psi at 70°C), and only limited amount of fibers were collected. Representative SEM micrographs of lignin fibers produced at 70 and 80 °C are displayed in Figure 3.8. The as-spun fibers could not be drawn-down to fine fiber diameters below 25 μm, which is highly desired for making quality carbon fibers. In addition, note the significant extent of crenulation on the fiber surface, resulting from rapid out-diffusion of solvent that leaves a skin on the outside while the core is still wet.

As the core dries out, the skin collapses and results in the wavy/crenulated surface. The existence of doubly convex crenulation as well as occlusions are shown in Figure 3.8. The sharp crevices or occlusions (defects created where the two convex crenulations meet) lead to stress concentration when such fibers are subjected to tensile forces. As a result, such fibers were not further studied in following stabilization and carbonization steps. Therefore, lower spinning temperatures were investigated to reduce the out-diffusion rate of solvent.

Table 3.2 Dry-spinning conditions and estimated viscosity values during the process for higher-MW FSLPs.

Solid content (wt%)	T (°C)	ΔP (psi)	Viscosity (Pa·s)	Drawn-down ratio (DDR)	Spinnability
60	70±1	3000	2.5	2.8	Difficult
60	80±5	2500±10	2.3	4	Difficult
60	90±1	1670±20	2.1	Not continuous	No
55	40±3	>3000	2.9	Not continuous	No
53	45±5	745±11	1.9	6.7	Yes
53	40±3	1450±10	2.0	7.3	Yes
50	40±2	300±5	1.5	Insufficient solvent diffusion	No

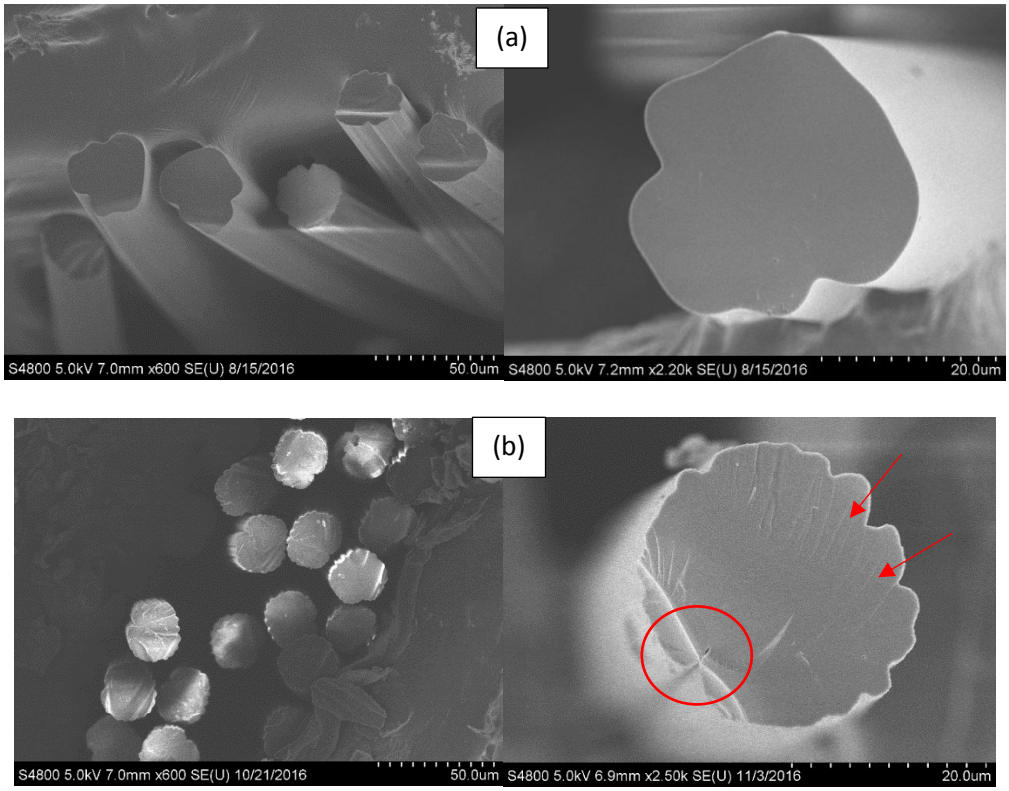

Figure 3.8 SEM micrographs of lignin fibers dry-spun from the higher-MW fractionated– solvated lignin precursor (FSLP) at (a) 70 ºC and (b) 80 ºC.

The solution concentration was reduced from 60 wt% to 50-55 wt% at lower spinning temperature range (40-50°C) in order to keep viscosity value around 2.0 Pa·s. The first spinning run was performed at 40±3°C using a 55 wt% spinning solution. However, the spinning was very difficult due to the extremely high pressure drop, and no continuous as-spun fibers were collected. The estimated viscosity was 2.9 Pa·s, which is too high for extrusion. Thus, a 53 wt% spinning solution was prepared. As shown in Table 3.2, after reducing solution concentration, the viscosity dropped from 2.9 to 2.0 Pa·s at same temperature, and the extrusion was much easier due to a lower pressure drop. The DDR was improved at 40 and 45 °C, and continuous fibers could be

collected on the take-up roll. The dry-spinning at 40-45°C using 53 wt% spinning solution displays better spinnability than it at 70-80°C using 60 wt% solution. Last, a more dilute solution at a lower lignin concentration of 50 wt% was prepared. The fibers can be easily extruded out of the spinneret, but insufficient out-diffusion of solvent was observed. The surface of as-spun fibers was still wet, so some coalescence of fibers was observed as the insufficient solvent out-diffusion could occur over the limited height of ~2 feet available in the present experimental set-up. Note, however, this problem can be solved if a longer/larger air chamber is available. Moreover, a solution viscosity that is too low can lead to broken filament during the drawn-down.

Within the range of conditions investigated with higher-MW FSLP, 40-45 °C was found to be the best temperature window where the spinning solution could flow easily and be drawn down. Therefore, for other two lignin fractions (medium-MW and highest-MW FSLP), similar experimental conditions were applied, shown in Table 3.3. Since medium-MW FSLP has lower MW than higher-MW FSLP, lignin concentration in the spinning solution was increased slightly to compensate for the reduced viscosity. Medium-MW FSLPs were dry-spun at 40ºC and 45°C, which led to good spinnability and large DDR. For highest-MW FSLP, a 50 wt% lignin solution was used to maintain viscosity around 2.0 Pa·s. Dry-spinning was performed at slightly lower temperature range between 30 and 38°C, giving the best spinnability. For a long-chain polymer solution, the viscosity scales with molecular weight (MW) as $\eta \sim MW^3$ (115). However, the FSLP spinning solutions did not follow the scaling law, and the viscosity of lignin solution increased proportionally as the MW increased. This indicates that,

unlike long chains within a polymer solution (that are entangled), the lignin molecules are not entangled, which also leads to difficulties in drawing down the fibers during dry-spinning.

In summary, a spinning temperature range between 30-45°C is found to be the best window. For each lignin fraction, the combination of temperature and solution concentration was tuned to keep apparent shear viscosity at 1.9-2.2 Pa·s with a steady shear rate about 1.6×10^5 to 2.5×10^5 1/s during continuous dry-spinning. Larger drawdown ratio was achieved, and fine as-spun fibers with diameter less than 25 μm were collected. Figure 3.9 displays the "spinnability window" for three MW FSLPs. The circled area represents the possible spinnability window in this current study. Also, it should be noted that the lignin fibers produced from these two windows present different cross-sectional shape, which will be further discussed in section 3.3.4.

Table 3.3 Dry-spinning conditions and measured viscosity values for medium and highest-MW FSLPs

Lignin fraction	Solid content (wt%)	T (°C)	ΔP (psi)	Viscosity (Pa·s)	Drawn-down ratio (DDR)	Spinnability
Medium MW FSLPs	55	40±1	1432±15	2.0	5.8	Yes
Medium MW FSLPs	55	45±5	741±5	1.9	5.8	Yes
Highest MW FSLPs	50	30±2	1489±10	2.2	6.8	Yes
Highest MW FSLPs	50	38±1	687±10	1.9	7.5	Yes

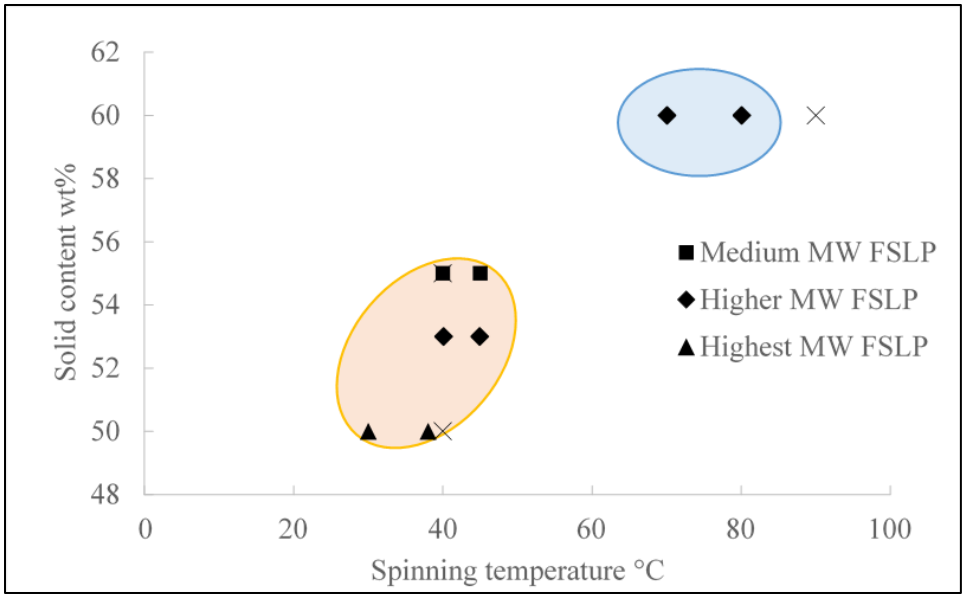

Figure 3.9 Possible spinnability window for different MW FSLPs studied in this current work.

3.3.4 Characterization of as-spun FSLP fibers

SEM micrographs of lignin fibers obtained from the three different MW FSLPs at low temperature range between 30-45 °C are displayed in Figure 3.10. The resulting fibers possess non-circular shape of dog bones. The ratio of major and minor axes of the cross sections (R) is used to determine the fiber circularity and listed in Table 3.4. It was found that the R value decreased with the increase of temperature, indicating that the circularity increases with temperature. The diffusion rate of solvent has found to have a significant impact on the cross-sectional shape of the precursor fibers. The spinning temperature is important because high temperatures increase out-diffusion of solvent and lead to the formation of rigid outer skin; however, low temperatures may lead to insufficient diffusion, coalescing of fibers or instability during drawn-down.

Lignin fibers dry-spun at 70-80°C shown in Figure 3.8 display a large number crenulations, indicating a rapid out-diffusion of solvent. The average number of crenulations on each fiber (C_N) are listed in Table 3.4. Overall, the circularity also increased with temperature, resulting in the R value closer to 1 at 70 and 80 ºC. At 30-45°C, note that a slower rate of solvent out-diffusion (as compared to that at 70-80 °C) leads to the exterior fiber surface being smoother with no crenulations. This phenomenon has also been observed in earlier study of dry-spun acetylated lignin fibers *(6)*, as well as others reported in the literature for wet-spun PAN fibers *(116)*. The average equivalent diameters of lignin fibers derived from the medium, higher, and highest MW fractions (FSLPs), as displayed in Table 3.5, were 21±1.0 μm, 18±0.7μm and 17±0.6 μm, respectively. Note that fibers spun from the medium-MW FLSP exhibited larger diameters than those spun from the higher and highest-MW FSLPs, because they could not be stretched as much during the drawdown step.

Table 3.4 Circularity characteristics of FSLP as-spun fibers with various concentrations and processing temperatures.

Lignin fraction	Solid content (wt%)	T (°C)	Ratio of major and minor axes of fiber cross-sections	Average number of crenulations per fiber	Cross-sectional shape
Highest MW	50	30	2.8±0.1	-	Dog bone
		38	2.6±0.1	-	Dog bone
Higher MW	53	45	2.6±0.1	-	Dog bone
	60	70	1.1±0.02	8.1±1.2	Crenulated
		80	1.1±0.05	17.6±2.3	Crenulated
Medium MW	55	40	2.5±0.2	-	Dog bone

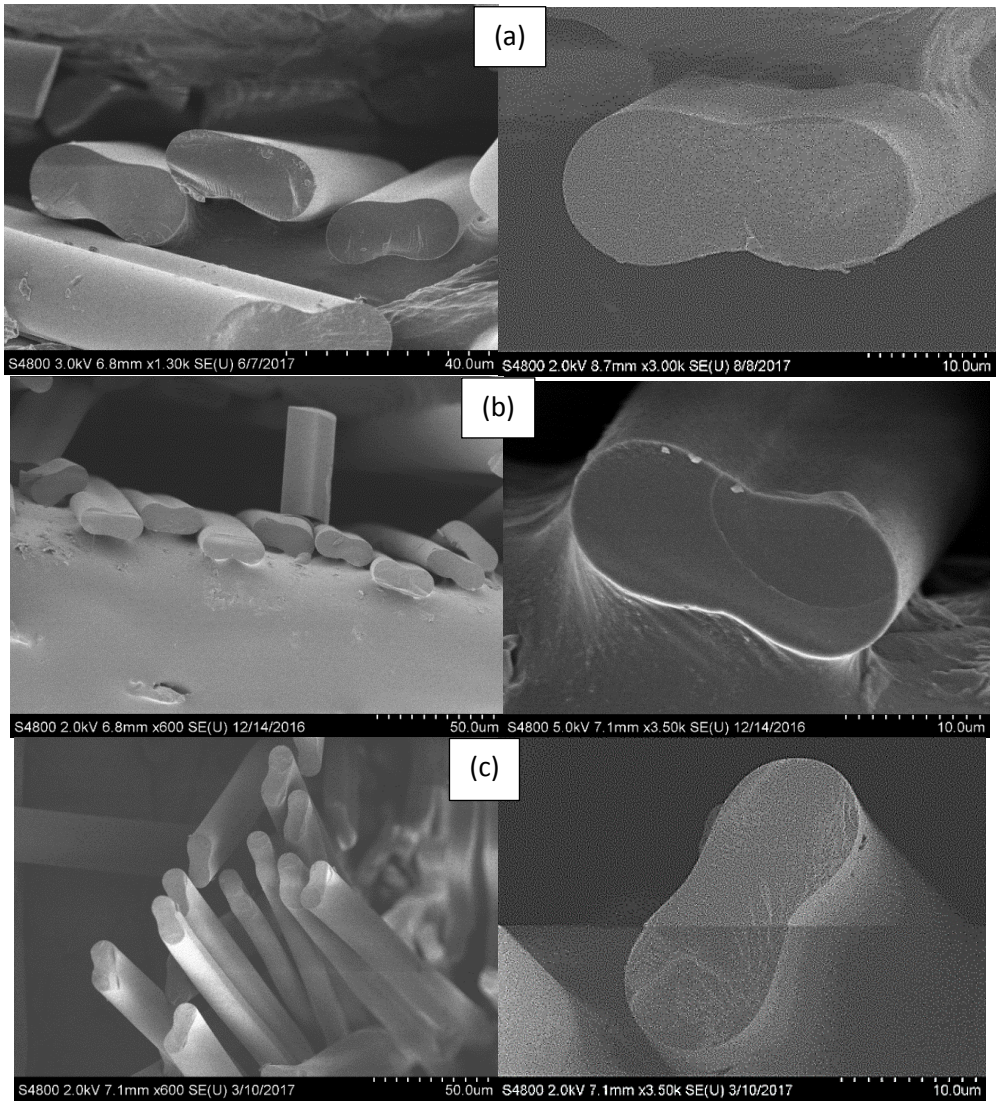

Figure 3.10 SEM micrographs of lignin fibers dry-spun from the (a) medium, (b) higher, and (c) highest-MW FSLPs in the low-temperature regime (30-40^{0}C).

Strain-stress curves of representative three MW FSLPs derived lignin fibers are displayed in Figure 3.11. All types of lignin fibers show a linear/elastic response to failure. Table 3.5 summarized the tensile testing results conducted on single filaments for each MW fraction of FSLPs. The lignin fibers dry-spun from medium MW FSLP (close in MW to the bulk feed lignin) show lowest strength of 35±5 MPa, whereas the tensile

strength of fibers dry-spun from higher and highest MW FSLPs are improved to 45±4 MPa, and 50±10 MPa, respectively. In addition, the modulus of lignin fibers also increased with the increase of MW. The modulus of the lignin fibers produced from the medium, higher and highest-MW FSLPs are 3.6±1.2 GPa, 3.9±0.3 GPa and 4.4±0.2 GPa, respectively. Thus, both strength and modulus are improved by using highest MW FSLPs. This is due to the better drawn down that could be achieved when using larger MW lignin precursor during the dry-spinning. Overall, highest-MW FSLPs as-spun fibers display better mechanical performance, and this result is encouraging since the final performance of carbon fibers greatly depends on the precursor fibers.

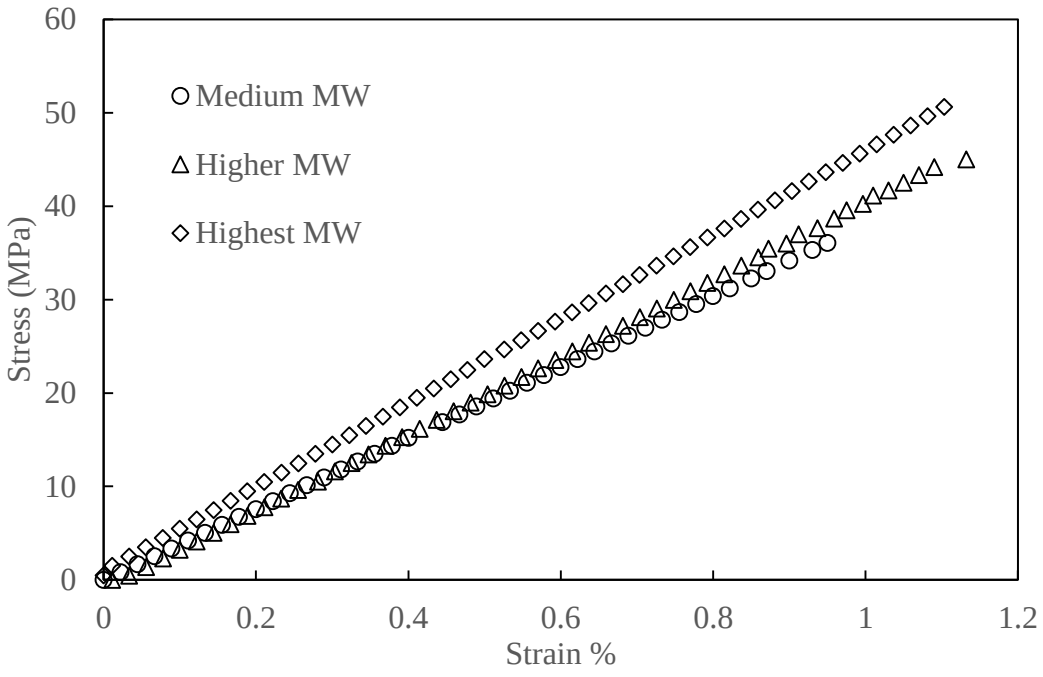

Figure 3.11 Representative stress-strain curves of medium, higher and highest MW FSLPs fiber spun at low temperature regime (30-45^{0}C).

Table 3.5 Tensile properties of lignin dry-spun fibers spun at low temperature regime (30-45^{0}C).

	Diameter (μm)	Max stress (MPa)	Tensile Modulus (GPa)	Break Strain (%)
Medium MW	21±1.0	35±5	3.6±1.2	0.9±0.2
Higher MW	18±0.7	45±4	3.9±0.3	1.1±0.2
Highest MW	17±0.6	50±10	4.4±0.2	1.1±0.3

3.3.5 Stabilization

In section 3.3.3, the best spinning temperatures were found between 30-45 ºC to achieve a good drawn-down, and prevent the occurrence of crevices on fiber surfaces. Therefore, all the as-spun lignin fibers from three MW FSLPs converted into carbon fibers were dry-spun in lower temperature regime between 30 and 45 ºC. A small amount of carbon fibers were also obtained from the lignin fibers dry-spun at 80 ºC.

The lignin fibers were stabilized at 250 ºC for a duration of only 1 hour. Because the source lignin was a softwood kraft lignin containing large amount of phenolic –OH group, which is known to undergo rapid crosslinking reactions, the lignin fibers have a high degree of reactivity that results in rapid thermal–oxidative stabilization. However, the rapid crosslinking limits the degree of fiber extension during the thermal stabilization. Stretching and crosslinking occurred at the same time during stabilization process, so to stretch lignin fibers and enhance the molecular orientation, high heating rate and enough tension needs to be applied to the fibers before the molecular cross-linking freeze the chain mobility within the precursor fibers. The fiber extension is defined as the percentage of the original fiber length.

Figure 3.12 shows the fiber stabilization temperature profile, and the fiber length change at different temperatures during one batch of stabilization. First, the oven was preheated to 220°C and held for 30 min, and then the fiber tow loaded with weights was hung in the oven. This process generally took 30s and the oven temperature dropped from 220°C to 165°C within the 30s. Once the sample loading was finished, the oven temperature went back to 220°C within about 3 min, and the max heating rate could reach approximately 20°C/min, which enabled instant stretching up to more than 450 % (percentage of original length) at 220°C. The lignin fibers undergo rapid crosslinking at 250°C, so that the extension was limited once the fibers were fully stabilized.

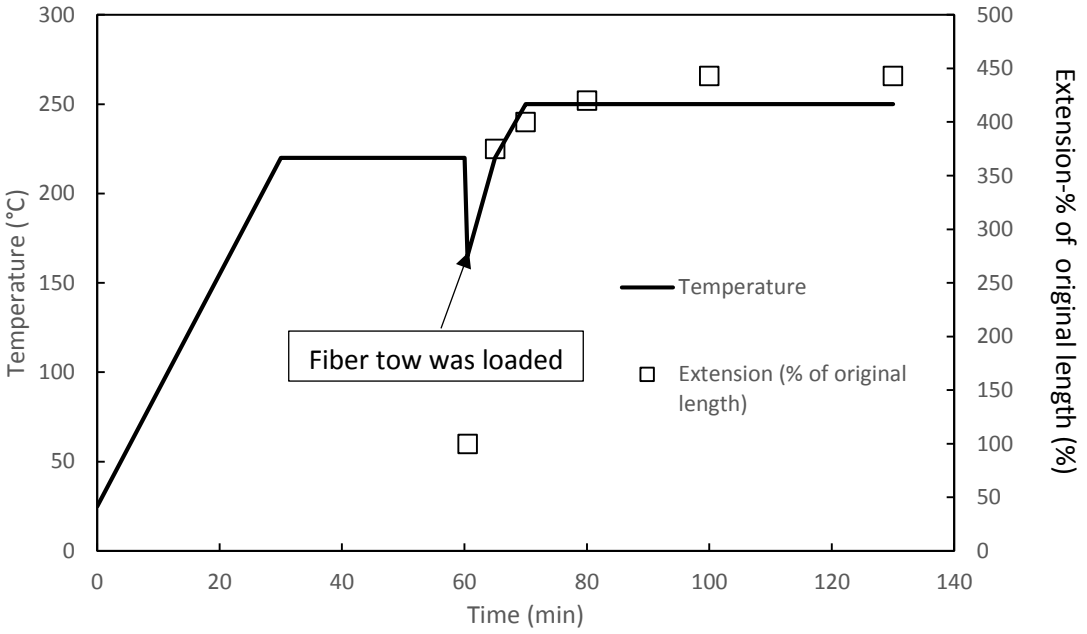

Figure 3.12 Fiber length change at different temperatures during one batch of stabilization.

Tension was applied to and the normalized load level (NLL) is defined in equation 3.4 *(6)*. In Figure 3.13, the fiber extension during stabilization is plotted against load level for different FSLPs. In the current study, a range of NLL between 3000-4500 g/(g/cm) circled in Figure 3.13 led to higher extents of stretching. The lignin fibers produced from medium-MW FSLP reach a maximum extension using load level around 3000 g/(g/cm), and then started to break when the NLL exceeded 3000 g/(g/cm). However, the fiber produced from higher and highest-MW FSLPs reached a maximum extension value when the NLL about 4000 g/(g/cm) is used. As expected, a larger load level results in larger fiber extension. Most of the fiber tows broke if using load level larger than 4500 g/(g/cm). When fiber tows broke, they lost the applied tension, and a negative extension (shrinkage) was observed.

$$NLL\ (cm) = \frac{Total\ weight\ load\ during\ stabilization\ (g)}{Linear\ density\ of\ fiber\ tow\ (\frac{g}{cm})} \tag{3.4}$$

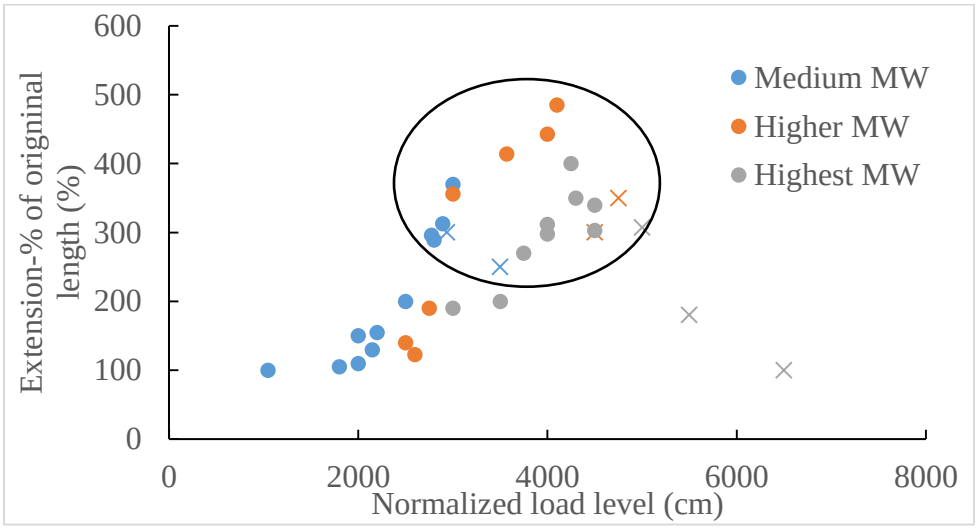

Figure 3.13 Extension during stabilization of FSLP fibers under different normalized load levels

3.3.6 Carbonization

Next, the stabilized fibers were successfully carbonized at 1000 °C. Carbonization was performed by fixing two ends of fiber tow to prevent shrinkage. Tension was applied during carbonization for some fiber tows, however, all of the fiber tows broke between 600-800 °C during carbonization. Note that below 800 °C, the carbonization is not completed, so when fibers break and lose applied tension, shrinkage can be observed, and certain level of orientation will be lost. Due to be limitation of this batch process, it is impossible to change load level during carbonization. Thus, the fibers were carbonized under constant length in this study. In continuous stabilization and carbonization process, the tension could be adjusted by using a series of take up rolls at different speeds. Applying tension during stabilization, and carbonization not only reduces fiber diameter, but also improves the orientation of the lignin molecules, therefore, it is very important in developing high strength and high modulus carbon fibers.

The cross sections of carbon fibers obtained from the three FSLPs are shown in Figure 3.14. Note that the dog-bone cross sections observed for precursor fibers are retained in carbon fibers. The resulting carbon fibers displayed a void-free microstructure with no fusion of fibers. If any surface fusion occurs on carbonized fibers, the fused regions serve as structural defects and deteriorate carbon fiber strength. The equivalent diameters of the resulting carbon fibers were nominally 6-7 μm, which is significantly smaller than those previously reported for carbon fibers spun from chemically unmodified softwood lignin *(83)*. The fine diameters obtained in this study are similar to those obtained for PAN-based commercial carbon fibers *(116)*.

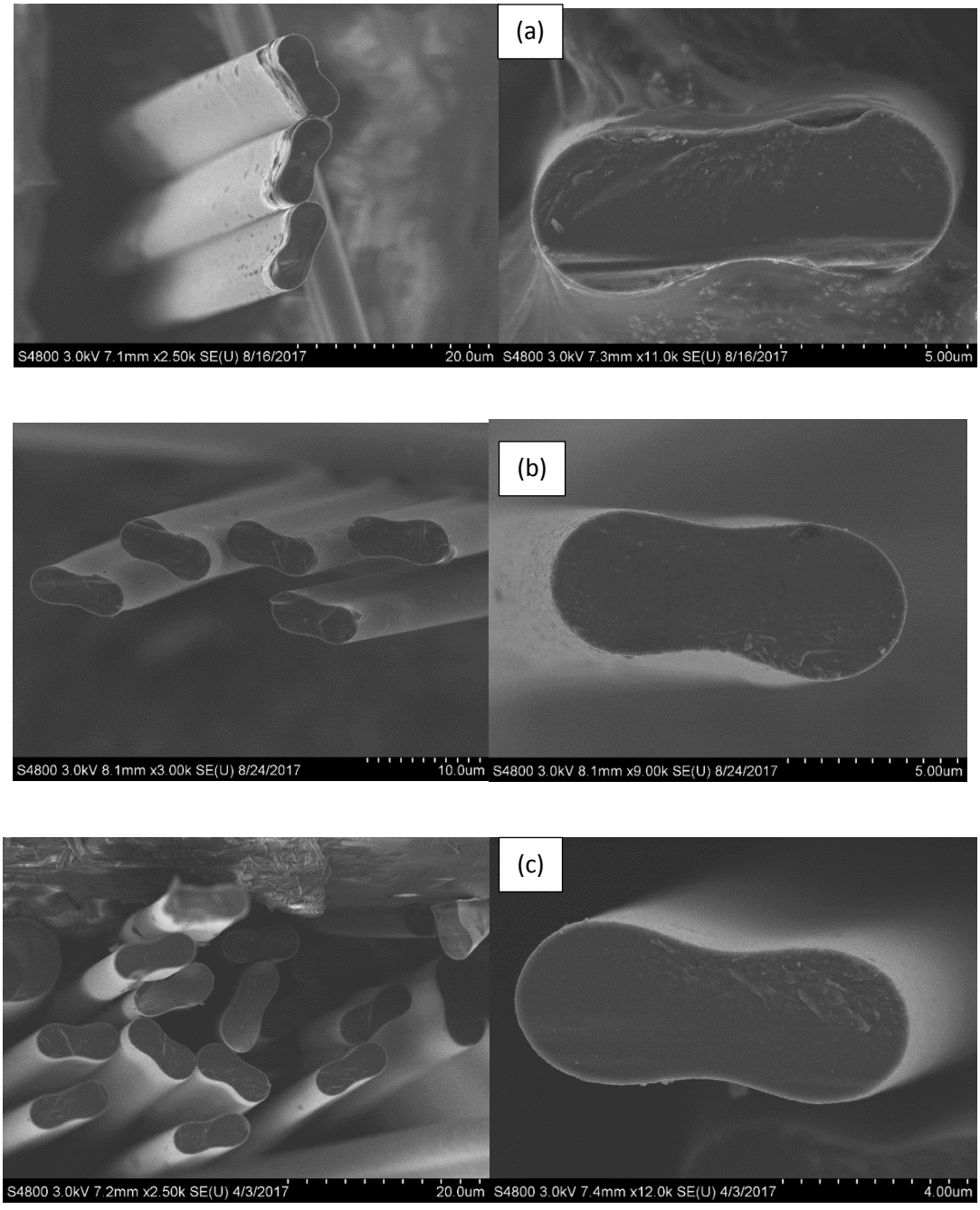

Figure 3.14 SEM micrographs of carbon fibers derived from the (a) medium, (b) higher, and (c) highest-MW FSLPs.

Figure 3.15 displays the SEM images of carbon fibers converted from the lignin fibers dry-spun at 80°C. The crenulated pattern from dry-spinning at elevated temperatures was preserved in the carbonized fibers. The average diameter of these types of carbon fibers is 15.8±0.7 μm, which is significantly larger than those fibers spun at lower temperatures. It is known that carbon fiber tensile strength increases with decreasing diameter. Therefore, it is expected that small-diameter carbon fibers (<6 μm) exhibit higher tensile strength values.

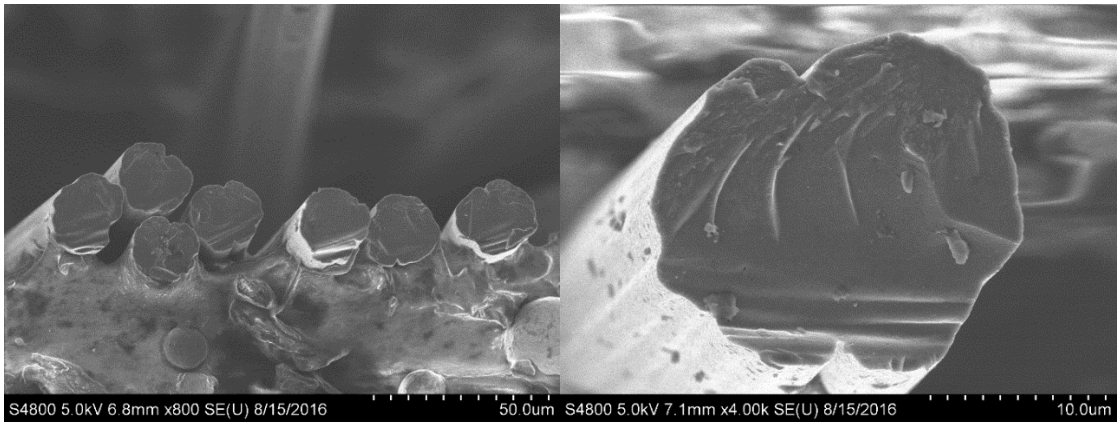

Figure 3.15 SEM micrographs of carbon fibers derived from the higher-MW FSLPs which were dry-spun at 80°C.

The lateral surface area of the CFs obtained from lignin fibers spun at 80°C is 26% higher than that of equivalent circular fibers (i.e., possessing equal cross-sectional area). For carbon fibers obtained from lignin fibers spun at 30-45°C, the relatively smoother surface found in precursor fiber was retained in the carbonized state, and the surface area is still 19% larger than that of equivalent circular fibers. The enhanced interfacial area increases fiber/matrix interfacial bonding in composite applications, and can help

improve the strength of resulting composites. A slower out-diffusion process can result in circular fibers, which would only increase the strength beyond that already achieved.

3.4 Conclusions

By taking advantage of the liquid–liquid equilibrium that forms between lignin and acetic acid/water solutions at elevated temperatures, very clean lignin fractions of higher molecular weight can be isolated within the solvated, lignin-rich phase, as the lower MW lignin and impurities are extracted into the co-existing solvent phase. These FSLPs were continuously produced via the ALPHA process. Compared to the different types of lignins that have been investigated for making carbon fibers, FSLPs possess promising characteristics, including high purity, high MW, high glass transition temperature and high thermal reactivity.

The dry-spinning conditions were extensively investigated using higher-MW FSLP, which is an intermediate MW grade in this study. The as-spun fibers dry-spun at elevated temperatures (70-80 °C) possess crenulated cross-sectional structure with some sharp crevices on the fiber surface. These occlusions are undesirable for subsequent processing of high strength carbon fibers. A temperature range between 30-45°C was found to be the best regime and was applied to other two types of FSLPs (medium and highest-MW FSLPs). All fibers produced at 30-45°C display non-circular dog-bone shape. Tensile testing results indicate that fibers obtained from highest MW FSLPs show higher tensile strength and modulus. This increase of tensile modulus is largely attributed to the high MW of lignin precursor, and the large drawn down ratio achieved

during dry-spinning. Results presented in this Chapter have been published in reference 94.

Tension was applied during thermal stabilization, and more than 400% fiber extension (% of original length) was achieved. Carbonization was performed with constant fiber length. The dog-bone cross section observed for precursor fibers is retained in carbon fibers, and displayed 19% larger lateral surface area than that of equivalent circular fibers. The structural and crystalline transition during the production of carbon fibers, and the mechanical properties will be further discussed in detail in Chapter 4.

CHAPTER FOUR

MICROSTRUCTURE AND PROPERTIES OF CARBON FIBERS PREPARED FROM FRACTIONATED LIGNIN PRECURSORS

4.1 Introduction

As discussed in Chapter 1, lignin is an abundant biopolymer with aromaticity and has drawn attention as an alternative precursor for producing low-cost carbon fibers *(11, 72)*. The production of carbon fibers is a complex process involving a series of steps. Most of prior studies on lignin-based carbon fibers have focused on the fiber forming step. Although different types of lignin precursors have been developed to produce carbon fibers, the highest tensile strength reported was only 1.05 GPa *(11, 63, 68, 89-91, 106)*. In current literature, lignin fibers were mainly carbonized at 900 to 1000 °C. Lignin fibers carbonized at higher temperatures (1000-2800 °C) have been reported only a few times in the past. In general, lignin is considered as non-graphitizable due to its highly cross-linked structure with heterogeneity.

Otani et al. *(117)* studied high temperature carbonization of lignin, and reported work on the structural changes occurring beyond 1700°C, and increased structural ordering was evidenced. Rodriguez et al. *(118)* investigated the structural changes occurring in kraft lignin at temperatures up to 2800°C. Johnson et al. *(119)* used TEM and X-ray diffraction to study the structure of lignin-based carbon fibers heated at 1500°C and 2000°C. The study revealed the existence of a heterogeneous fine structure of varied texture and many different continuous and discontinuous inclusions of a highly

graphitized nature. Therefore, for any new grade of lignin-based precursor, it is necessary to understand structure-property relationship of lignin-based fibers.

In Chapter 3, the dry-spinning process of a fractionated solvated lignin precursor (FSLP) and subsequent thermal stabilization and carbonization steps were discussed. A processable spinning window was established, the precursor fibers were stabilized under tension, and carbonized at 1000°C. In this chapter, the comprehensive microstructure and mechanical characterization of FSLP-based carbon fibers will be discussed with primary emphasis on (i) structural transition of lignin during the process (ii) the effect of MW on the crystalline microstructure and properties of FSLP-based carbon fibers, and (iii) the effect of thermal treatment on graphitic microstructure and properties of FSLP-based carbon fibers. Results on microstructure and tensile properties of carbon fibers were published in our recent paper *(94).*

4.2 Experimental

4.2.1 Carbon fiber production

The carbon fibers used in this study were produced from fractionated softwood kraft lignin precursor using an Aqueous Lignin Purification with Hot Acids (ALPHA) process developed by Thies and co-workers *(1, 94)*. Detailed information can be found in Chapter 3. In brief, a kraft lignin was recovered from a softwood black liquor from SLRP process, and three different MW fractions were isolated in lignin-rich phase during ALPHA process. Lignin fibers were spun from the three MW fractions via dry spinning method, and then subjected to oxidative stabilization at 250°C for 1 h. Finally, the

stabilized fibers were carbonized at 7 °C/min to 1000°C for 1 h. Portions of the batch carbon fibers carbonized at 1000°C were taken to further heat treatment at higher temperatures (1100°C, 1300°C, 1600°C and 2100°C) under helium environment in Astro furnace. Once the desired temperature was reached, the samples were maintained at this temperature for 1 h. Constant length was held for all samples during carbonization.

4.2.2 Structural characterization

Infrared spectra were collected by attenuated total reflective Fourier transform infrared (ATR-FTIR) spectroscopy (Nicolet iS50R FT-IR spectrometers, Thermo Scientific.) on a single reflection diamond ATR accessory (Type III A diamond). Each spectrum was averaged 64 scans at a resolution of 4 cm^{-1} between 4000-650 cm^{-1}. Morphological analysis of fibers was conducted by scanning electron microscopy (SEM) with a Hitachi 4800 SEM unit. The cross-sectional area of single fibers was measured using SEM micrographs and "Freehead shape measuring tool" in Quartz PCI software.

High-resolution transmission electron microscopy was carried out on a Hitachi 9500 TEM unit and operating at 300 kV. A fiber tow about 1 cm long were cut and placed vertically in a capsule and embedded within LR write resin (EMS 14381) and cured at ~60°C for 24 h, as shown in Figure 4.1. After the blocks were cured, they were microtomed as described below and illustrated in Figure 4.2. Firstly, the resin block was inserted into the specimen holder of the microtome and tightened in place. Then the diamond knife (DiATOME 35°) was inserted into the slot on the diamond knife holder. The diamond knife and holder were carefully adjusted to the correct position by raising

the holder or sliding the knife. The tip of the resin block needs to be placed close enough to the center of the diamond blade. When the stage was in place, the locking lever was lowered. The diamond knife was positioned such that the leading edge of the resin block appeared parallel to the knife edge. Then the tip of the resin block and the knife edge were wet by ethanol. Water was pipetted into the trough of the diamond knife, and the trough was slightly overfilled.

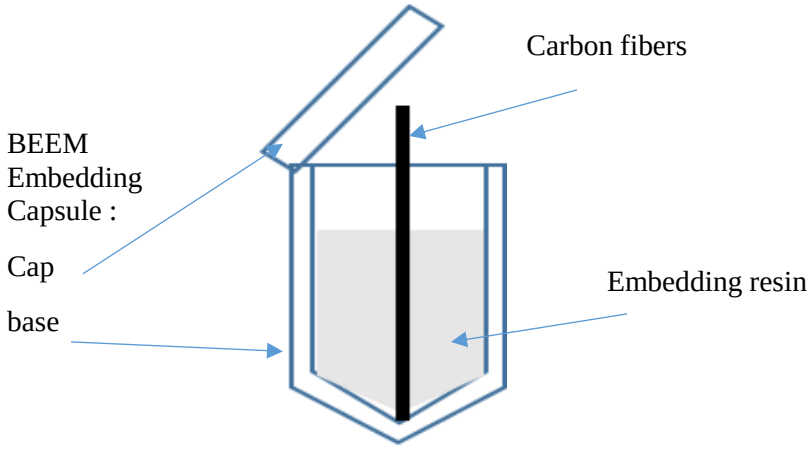

Figure 4.1 Embedding of carbon fibers for transverse sectioning.

During the initial cutting, coarse sectioning (circled in Figure 4.2) was used. Enter 0.5 µm (meaning the sample holder moves 0.5 µm per cutting towards the knife), and set speed of 10-25 mm/sec using speed knob. The initial cutting was finished once the carbon fiber bundle was exposed out. The trough of diamond knife must be cleaned using scotch tape and refill some water. During the fine cutting, ultra sectioning was used by entering 70 nm and setting speed of 10-25 mm/sec using speed knob.

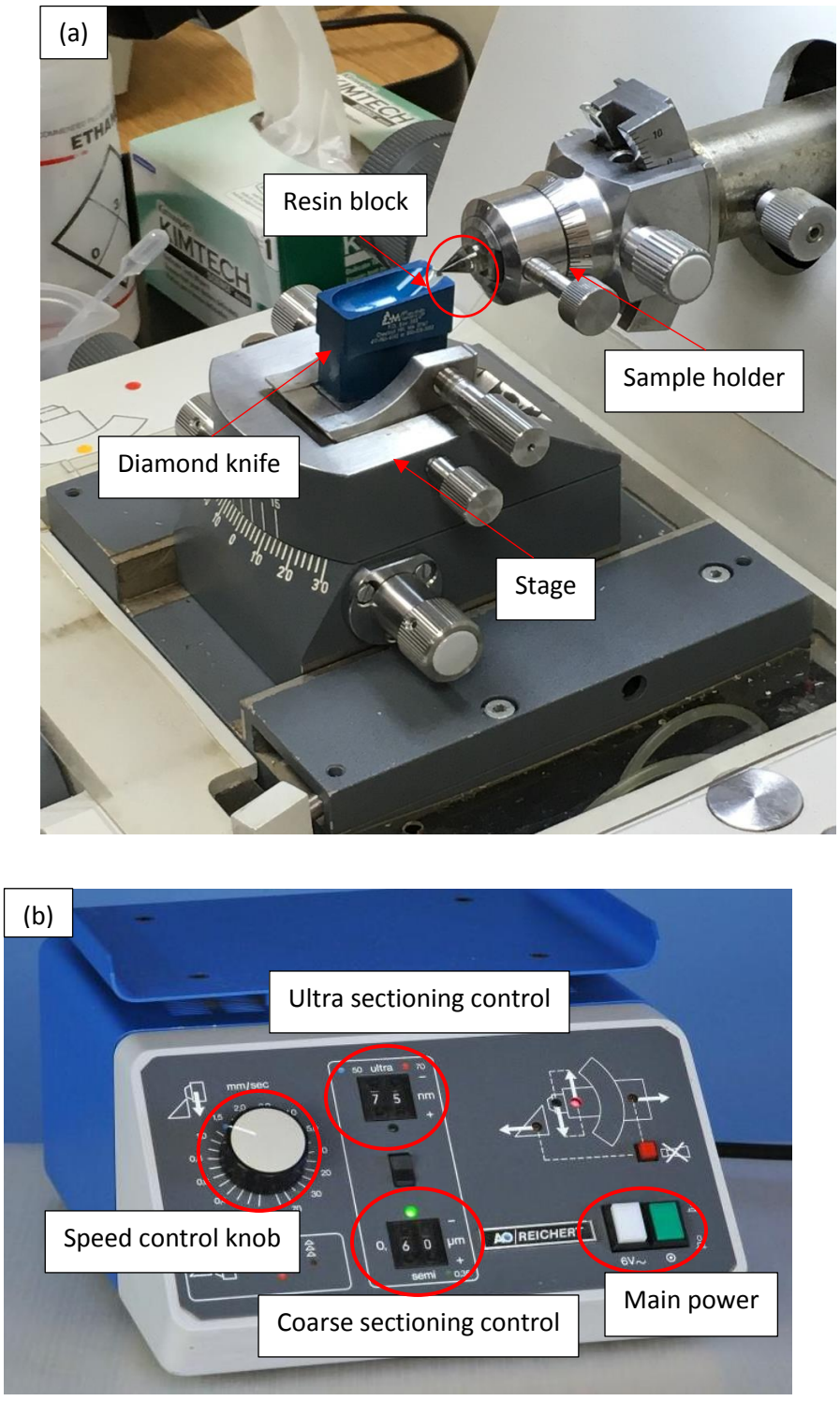

Figure 4.2 (a) Reichert-Jung Ultracut Microtome operation stage with resin block and diamond knife in position (b) Reichert-Jung Ultracut Microtome control box.

After some fine slices were obtained and collected enough in the trough of diamond knife, they were ready to be collected on TEM copper grid (Ted Pella Inc.), displayed in Figure 4.3. A fine-pointed tweezers were used to lift a copper grid by the rim. The copper grid was slowly moved down onto the slices (bright side down). After the fine slices adhered on the grid, the grid was lifted from the surface of the water and turned over to dry on a filter paper. The copper grids with sample slices collected on were stored in a grid box and dried for at least 20 hours. Often, during the microtoming process, the thin sample slices are likely to overlap when there are too many slices crowded together, and this is not preferred. To prevent overlapping, the thin slices must be well dispersed in water and too many slices should not be placed on one copper grid. Preparing more than three copper grids for a single fiber sample is recommended.

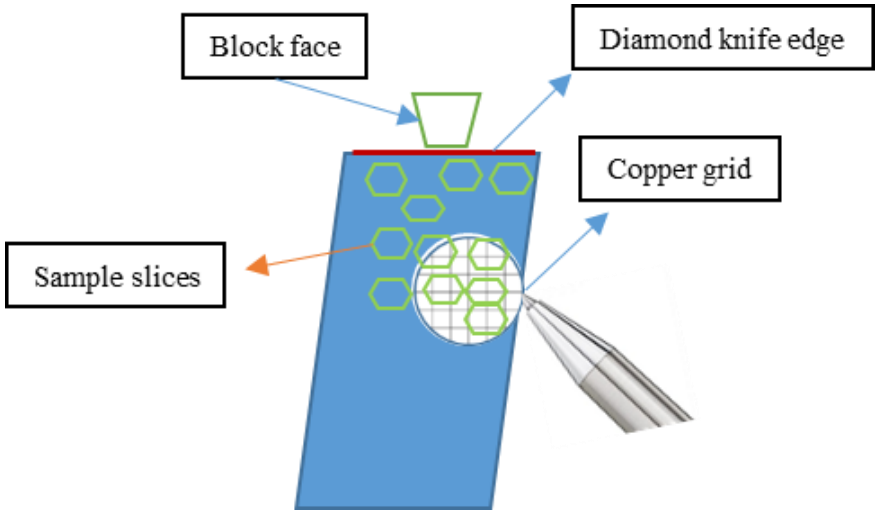

Figure 4.3 Collection of microtomed sample slices on copper grid.

Raman spectra of carbon fibers were obtained using a 785 μm laser in a Raman microscope system (Renishaw, West Dundee, IL). Carbon fibers were mounted on a glass slide and fixed with scotch tapes at both ends. Raman spectra using an objective lens of 50× magnification at 25 mW laser power with exposure time of 10 s. WiRE 3.4 software was used to analyze the spectra with Gaussian-Lorentzian curve fitting. Wide-angle X-ray diffraction (WAXD) analysis was conducted on bundles of fibers using a Bruker D8 Venture Dual Source diffractometer with CuKα radiation (λ = 0.15406 nm). The unit was equipped with an IμS microfocus source at, a Photon 100 CMOS detector, and Apex3 software to generate integrated azimuthal (2θ) profiles. The distance between the detector and the sample was 40 mm. Samples were glued with fast cure acrylate glue to form fiber bundles and mounted on a sample holder; one sample from each group was sprinkled with NIST-grade silicon standard powder (SRM 640d) for accurate location of 2θ position. The scan time was 120s per run. The interlayer spacing, d_{002}, and the crystallite height, L_c, which measured along the c axis were obtained from (0 0 2) peak. The interlayer spacing d_{002} is calculated using Bragg's law (Eq. 4.1):

$$\lambda = 2dsin\theta \tag{4.1}$$

Where λ corresponds to the wavelength of the X-ray beam, d is the distance between adjacent planes and θ is the angle of incidence of the X-ray beam. The crystallite stacking, L_c, can be calculated using the Scherrer Equation (Eq. 4.2) and Warren's broadening correction (Eq. 4.3):

$$L_c = \frac{K\lambda}{B\,cos\theta} \tag{4.2}$$

$$B^2 = B_M^2 - B_S^2 \quad (4.3)$$

Where K is 0.89 for the calculation of the thickness of crystallines along the c axis. B is the corrected full width at half maximum (FWHM) intensity of the spectrum peak, B_M is the measured FWHM, and B_S is the system broadening determined by the Silicon standard. According to the Maire and Mering model, degree of graphitization g%, could be calculated using the equation 4.4 below:

$$g\% = \frac{0.344 - d_{002}}{0.344 - 0.3354} \times 100 \quad (4.4)$$

The azimuthal scans of (0 0 2) peak were obtained by Datasequeenze 3.0, a graphical interface for analyzing data from 2D X-ray detectors. The plots were integrated from azimuthal angle (phi) between 0° to 180° to obtain two-theta plots.

4.2.3 Electrical and mechanical characterization

Electrical resistivity of single carbon fibers was measured using a two-probe method with a Megohmmeter (FLUKE-1503). Single carbon fibers were mounted on paper tabs with 10 mm gauge length and placed on parallel copper wires. SPI Flash Dry Silver Paint was used to reduce contact resistance between the carbon fiber and copper wire. At least five replicates were prepared and tested. A PHOENIX single filament testing unit (Measurements Technology Inc.) was used to measure the mechanical properties of the carbon fibers produced in this study. The single fibers were mounted on 25 mm paper tabs using fast cure epoxy glue. At least twenty fiber samples per fiber type were prepared and tested. A compliance correction method was used in conjunction with

three different gage lengths (10, 25, and 35 mm) to accurately measure the tensile modulus.

4.3 Results and Discussion

4.3.1 Structure transitions

Fourier Transform Infrared Spectroscopy (FTIR) spectra of highest MW FSLP fibers, stabilized fibers, and carbon fibers under different temperatures are displayed in Figure 4.4. The FSLP fibers exhibit all of the expected functional groups, viz. hydroxyl groups in the range of 3100-3500 cm^{-1}, the methyl and methylene groups at 2840-2950 cm^{-1}, aromatic methoxy groups at 2850 cm^{-1} as well as carbonyls at 1710 cm^{-1} , and aromatic rings in the range of 1510-1600 cm^{-1} and 900-1120 cm^{-1}. The absorption peaks at 1596 and 1510 cm^{-1} are "fingerprint region" typical for ATR-FTIR spectra and attributed to aromatic skeletal vibration. The peak at 1460 cm^{-1} represents aromatic skeletal vibration coupled by C-H deformation, same as the peak at 1420 cm^{-1}. The bands at the wavenumbers of 1270, 1120 and 1030 cm^{-1} display guaiacyl and syringyl units. The peak assignment in this work is consistent with other works of Norberg et al., Kubo et al., and Rials et al. *(83, 90, 120)*.

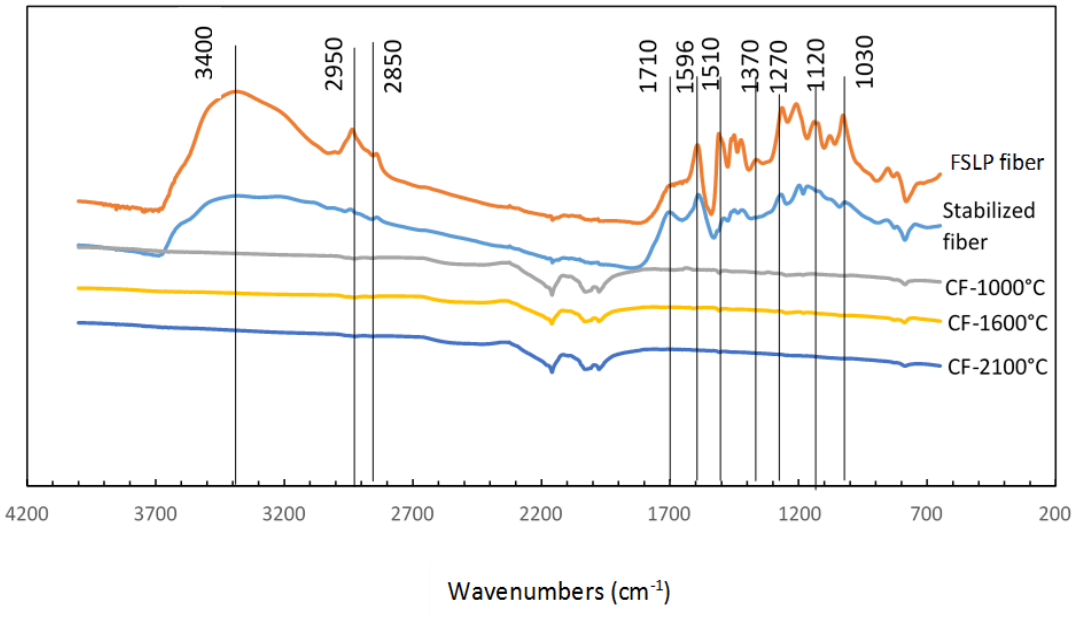

Figure 4.4 FTIR spectra of FSLP fibers, thermostabilized fibers and carbon fibers at different temperatures.

After thermal stabilization, the FTIR spectra displays an intensity reduction in the absorption peaks at 3400, 2950, and 2850 cm-1, which indicate a reduction of phenolic or alcoholic groups and removal of methyl groups as well. The intensity of peak at 1710 cm^{-1} representing C=O stretching increases in the stabilized fibers, whereas this peak only exists as a shoulder in FSLP fibers. This is an indicator to oxidized structure within the fibers due to rearrangement and oxidation reactions during stabilization. The decrease of absorption intensity peaks at 835, 1510, and 1600 cm^{-1}, corresponding to the substituted aromatic ring structure, is observed in Figure 4.4. This indicates the removal of aromatic substitutions. The oxidative stabilization leads to the formation of benzylic carbocation, and this has also been observed in other studies *(121)*. In IR spectrum region from 1500-1000 cm^{-1}, the intensity of signal decrease in each individual peak, which could be caused

by the formation of cross-linkages. Furthermore, demethylation was occurred during thermal stabilization indicated by the peak intensity reduction in IR spectra at 1370, 1420, and 2940 cm^{-1}. In general, the thermal stabilization process leads to a decrease in hydroxyl, methyl, and methoxyl groups due to the dehydration reactions, oxidation and cross linking. For the carbon fibers at 1000°C, and higher temperatures, all the IR bands disappeared, indicating that the aromatic bonded oxygen was depleted due to the disappearance of phenol, and carboxyl groups. This is consistent with other reported studies of kraft lignin *(122)*. As temperature increases, the fibers are fully carbonized and the turbostratic carbon structure is formed.

Figure 4.5 shows the XRD patterns of the FSLP fibers, stabilized fibers, and carbon fibers at 1000°C. A small amount of silicon powder was added on the samples as a reference standard to accurately measure 2-theta peaks. The NIST-grade crystalline silicon displays (1 1 1) peak at 28.4°, which was used as the reference peak. The FSLP fibers and stabilized fibers display broad peaks at 20.9° and 20.4°, respectively. Although lignin is considered to be an amorphous biopolymer, these peaks indicate the formation of ordered domains within the fibers *(123)*. After carbonization, the XRD spectrum shows well-defined peak at diffraction angles of 24.0° (0 0 2) and 43.3° (1 0 0)/(1 0 1), which indicates a newly formed carbon structure. Based on previous studies, *(124, 125)* the carbon structure is formed by lignin dehydration, decarbonylation, cleavage of side groups and the rearrangement of the network to form polyaromatic structure.

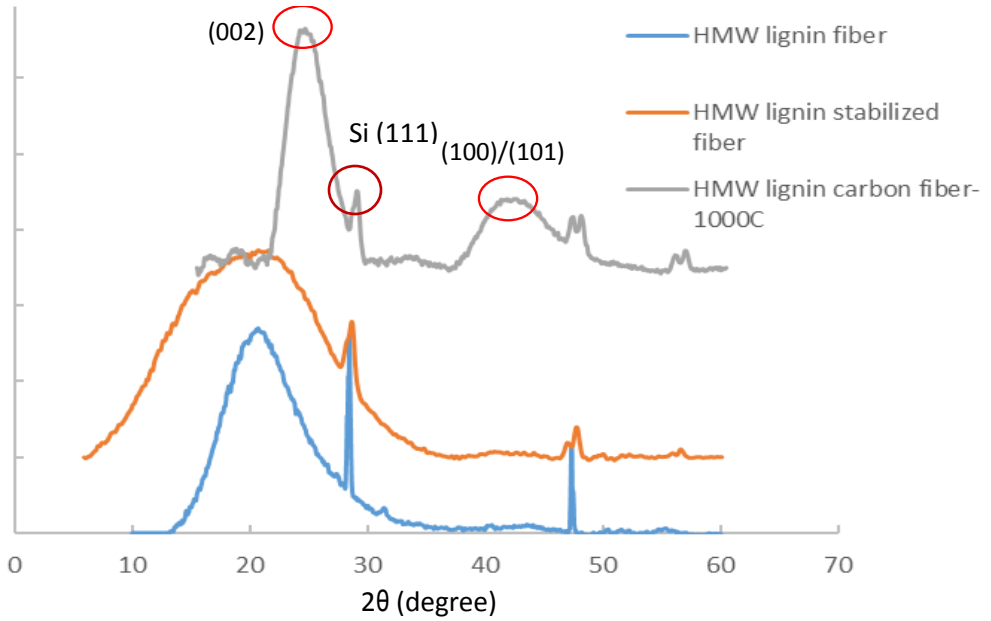

Figure 4.5 XRD profile of high MW FSLP fibers prior to and after stabilization and carbonization.

4.3.2 MW effect on crystal structure of FSLP-based carbon fibers

Raman spectroscopy was used to measure D- and G-bands to obtain disordered vs graphitic contents for lignin-based carbon fibers. Figure 4.6 illustrates the Raman spectra of medium, higher and highest MW FSLPs derived carbon fibers produced at 1000 °C. The Raman spectra are characterized by two predominant first order bands corresponding to D and G bands, which are centered at around 1310 cm^{-1} and 1587 cm^{-1}, respectively. The G band is attributed to the in-plane vibrations of sp^2-bonded carbon in graphitic crystalline. For less well-ordered carbon materials, another peak, known as D band, is attributed to structural vibrations of sp^2 bonds with structural imperfections *(126)*. For non-graphitic carbon fibers, the D band is a wide band, which is associated with the disordered structure of turbostratic carbon.

The ratio of areas for D- and G-peaks (I_D/I_G) for carbon fibers derived from the medium-MW FSLP (similar in MW to the bulk feed lignin) was 5.4. The I_D/I_G area ratio of lignin-derived carbon fibers has been reported in prior literatures studies *(127, 128)* to be 2-5, which is consistent with the values obtained in this study. The current value is similar to the ratio observed for PAN-derived fibers that contain turbostratic carbon, but much higher compared to 0.5-1.0 for carbon fibers derived from mesophase pitch, which are significantly more graphitic *(129)*. Thus, a low level of graphitic development is observed in lignin-based carbon fibers as inferred from a large I_D/I_G ratio. However, the ratio decreased to 4.4 for carbon fibers made from the higher-MW FSLP, and further to 3.6 for the highest-MW FSLP. Clearly, an increase in the MW of lignin fractions led to better carbon-layer formation in the resulting fibers.

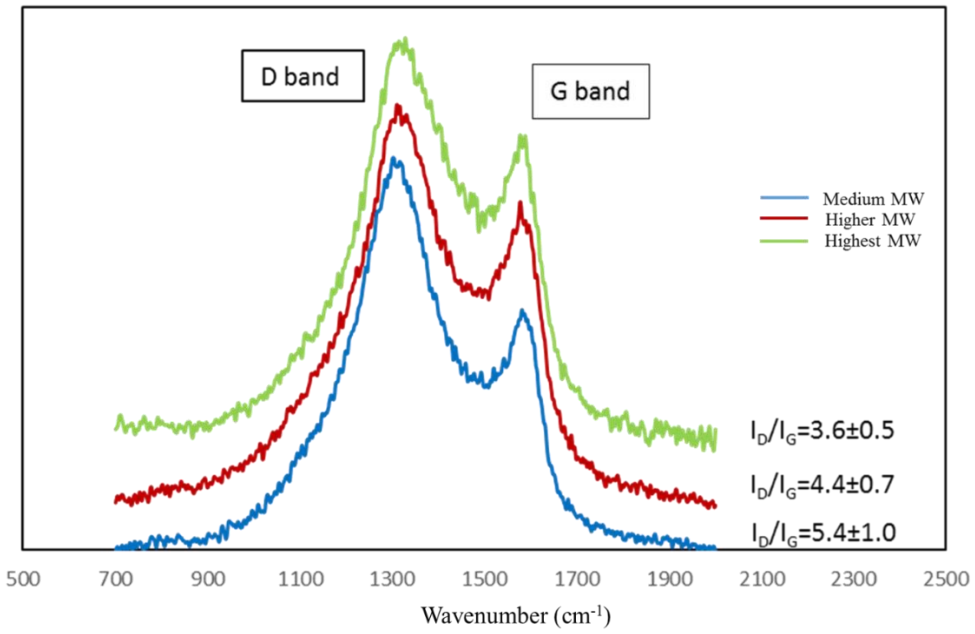

Figure 4.6 Raman spectra of carbon fibers derived from medium, higher, and highest-MW FSLPs at 1000°C. Intensity values on the y-axis scale are in arbitrary units.

For fibers carbonized at 2100°C, it was found that the increase in MW of FSLP also led to a better packed carbon structure. As displayed in Figure 4.7, both G and D bands become narrower at 2100°C than those observed at 1000°C. The ratio of areas I_D/I_G for medium-MW FSLP derived carbon fibers is 2.4, which is still much higher compared to the pitch-based carbon fibers. However, the I_D/I_G decreases to 2.2 and 1.9 for higher and highest MW FSLP-based carbon fibers, respectively. With the increase of MW, the G band increases in intensity while the I_D/I_G ratio decreases, which indicates that a better-packed carbon structure is formed. As a result, at both 1000 and 2100°C, the increase in MW of FSLP improves the formation of well-packed turbostratic carbon structure.

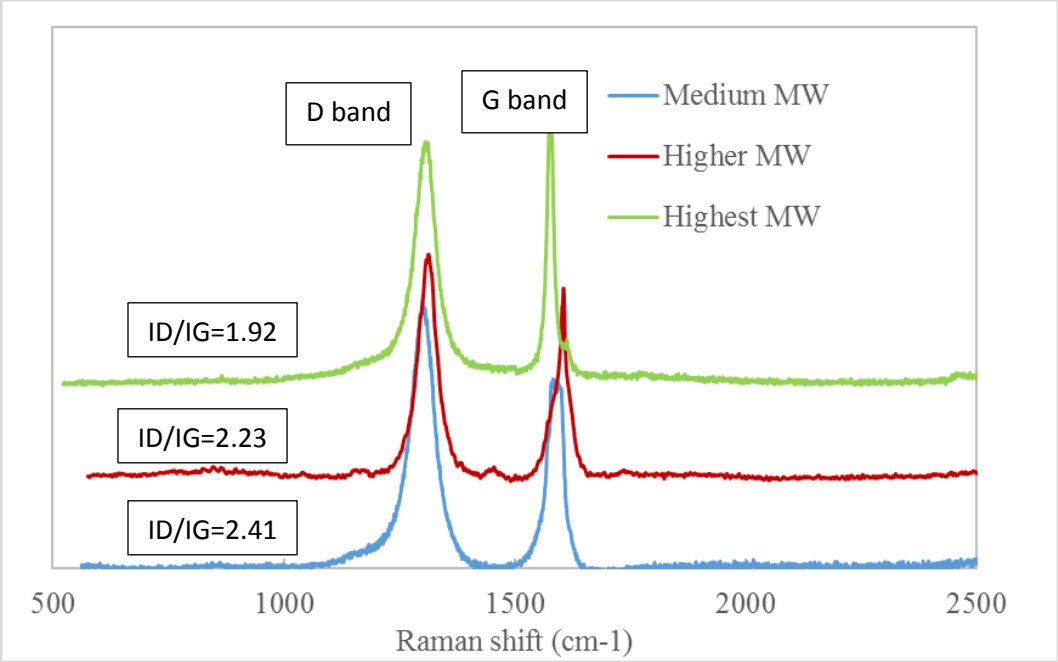

Figure 4.7 Raman spectra of carbon fibers derived from medium, higher, and highest-MW FSLPs at 2100°C. Intensity values on the y-axis scale are in arbitrary units.

A representative wide-angle X-ray diffraction 2-D pattern for FSLP-based carbon fibers is shown in Figure 4.8. NIST-grade silicon powder was added to one sample of each type as a calibration standard to provide accurate location of the (1 1 1) peak position, showing a ring marked on the image. The (0 0 2) peak displays an arc marked on the 2-D pattern. Figure 4.9 (a) displays wide-angle X-ray 2θ profiles for carbon fibers produced from the medium, higher, and highest-MW FSLPs at 1000°C. The sharp peaks marked in circle are the (1 1 1) peaks for silicon that appear at 28.4°. The integrated 2θ profile for the carbon fibers produced from the medium, higher, and highest-MW FSLPs displayed (0 0 2) peaks at 23.0°, 23.8° and 24.6°, respectively. The d_{002} spacings between layer planes, calculated using Bragg's law, were 0.386 nm, 0.374 nm, and 0.365 nm, respectively. A d_{002} spacing value of 0.387 nm, reported by Baker et al. *(106)* for melt-spun Organosolv lignin fibers carbonized also at 1000 °C, is consistent with that reported here for carbon fibers produced from medium-MW FSLPs. Overall, these inter-layer spacings are significantly higher than that for pure graphite (0.335 nm), indicating that these lignin-derived carbon fibers possess a low degree of graphitic crystallinity. However, the d_{002} spacing of the lignin-based carbon fibers consistently decreased with increasing MW of the FSLPs.

The orientation of the crystallites within the fiber was measured from the azimuthal scans on the (0 0 2) peak of the WAXD spectra. Figure 4.9 (b) shows the azimuthal scans of (0 0 2) peak of medium, higher and highest MW FSLPs derived carbon fibers. To compare the orientation, the full-width-at-half-maximum (FWHM) was measured for each set of samples. The smaller the FWHM, the more orientated are the crystallites

along the fiber axis. For medium MW FSLP derived carbon fibers, the FWHM is 120°, indicating a very low degree of orientation. Higher MW and highest MW FSLPs based carbon fiber samples developed a higher level of orientation with FWHM decreased to 112° and 113 °, respectively. All these WAXD results, in conjunction with Raman, confirm that a better packed carbon-layer structure was formed as the MW of the FSLPs increased.

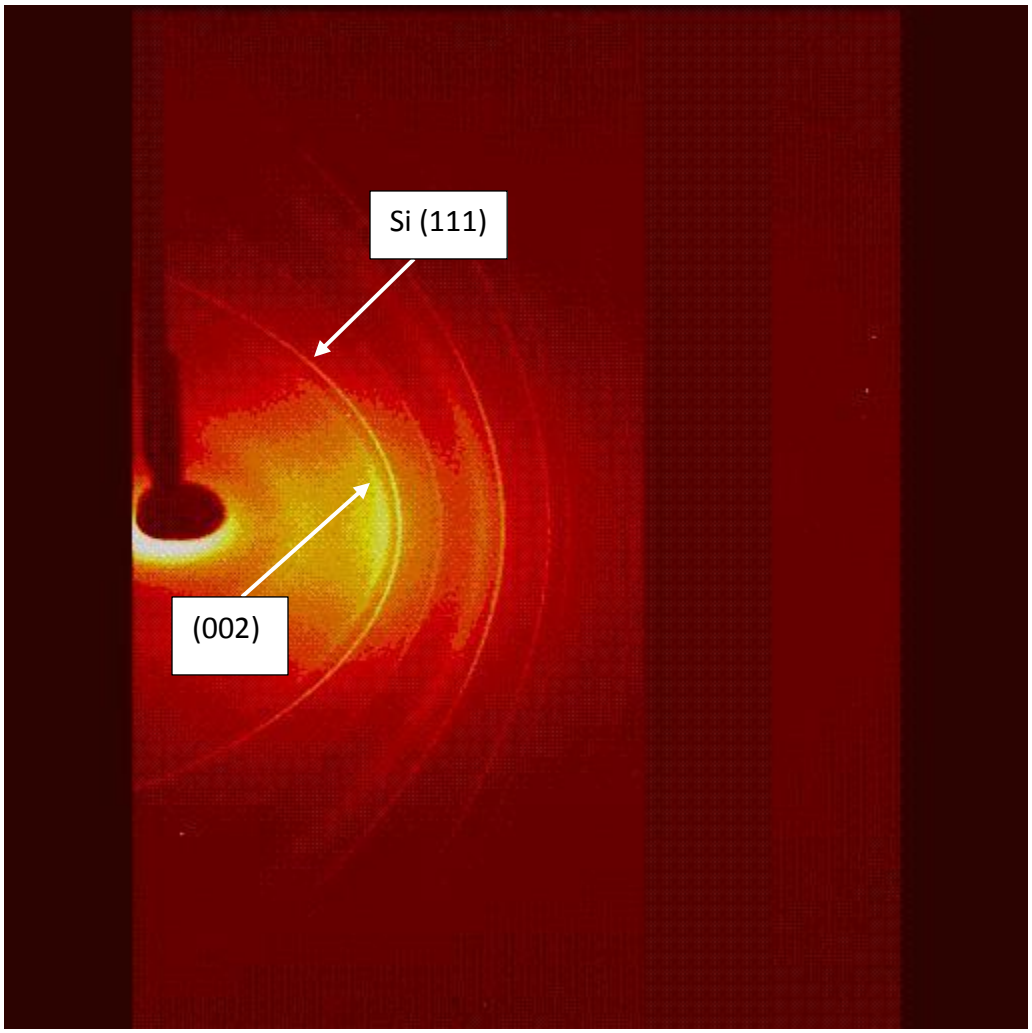

Figure 4.8 A representative 2D wide angle X-ray diffraction pattern of FSLP based carbon fibers.

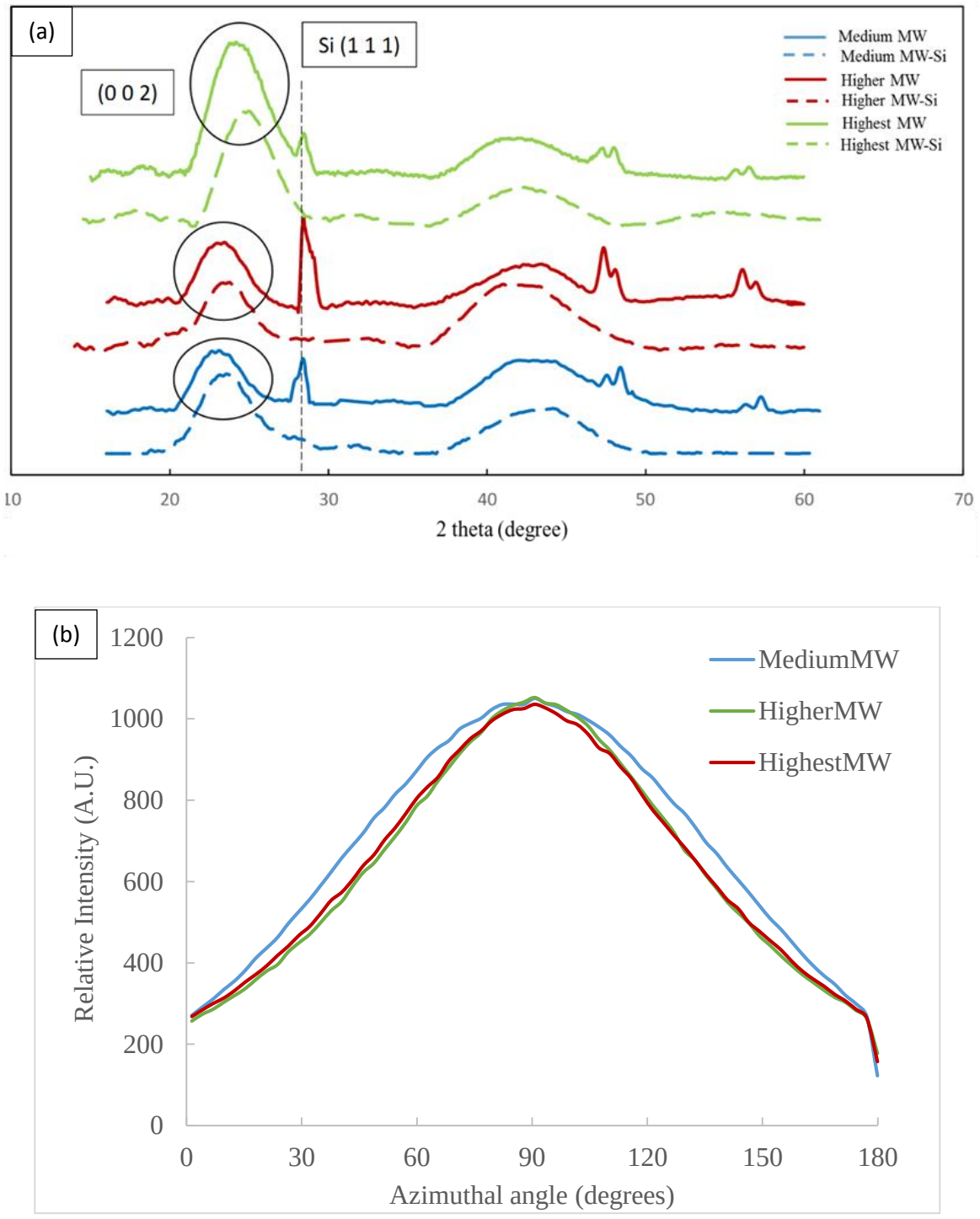

Figure 4.9 (a) Integrated azimuthal (2-theta) profiles (b) Azimuthal scans of the (002) peak from WAXD of carbon fibers derived from medium, higher, and highest-MW FSLPs at 1000°C. Intensity values on the y-axis scale are in arbitrary units.

4.3.3 Effect of carbonization temperature on crystal structure of FSLP-based carbon fibers

To evaluate the effect of carbonization temperature on crystalline structure of FSLP-based carbon fibers, only one type of carbon fiber: the highest MW FSLP-based carbon fibers were carbonized at different temperatures for further testing. Figure 4.10 illustrates the Raman spectra of the highest-MW FSLP derived carbon fibers prepared in the temperature range between 1000 and 2100 °C. The fibers carbonized at 1000°C and 1100°C present two broad, overlapping bands at ~1310 cm^{-1} (D band) and ~1585 cm^{-1} (G band), indicating a less well-organized carbon structure. The G' band is not pronounced in the spectra for these two types of carbon fibers. As the carbonization temperature increases to 1300°C and 1600°C, both D band and G band become narrower and their intensities increase. Also, G' band starts to show at 2610 cm^{-1}, becomes narrower, increasing in intensity, and slightly shifting to higher frequency with increasing temperature. The spectrum for carbon fibers at 2100 °C shows well-resolved D and G bands, and both bands further narrow. The G band increases in intensity with increasing temperature, whereas for the D band, the intensity decreases due to the structural ordering of carbon with rise in carbonization temperature.

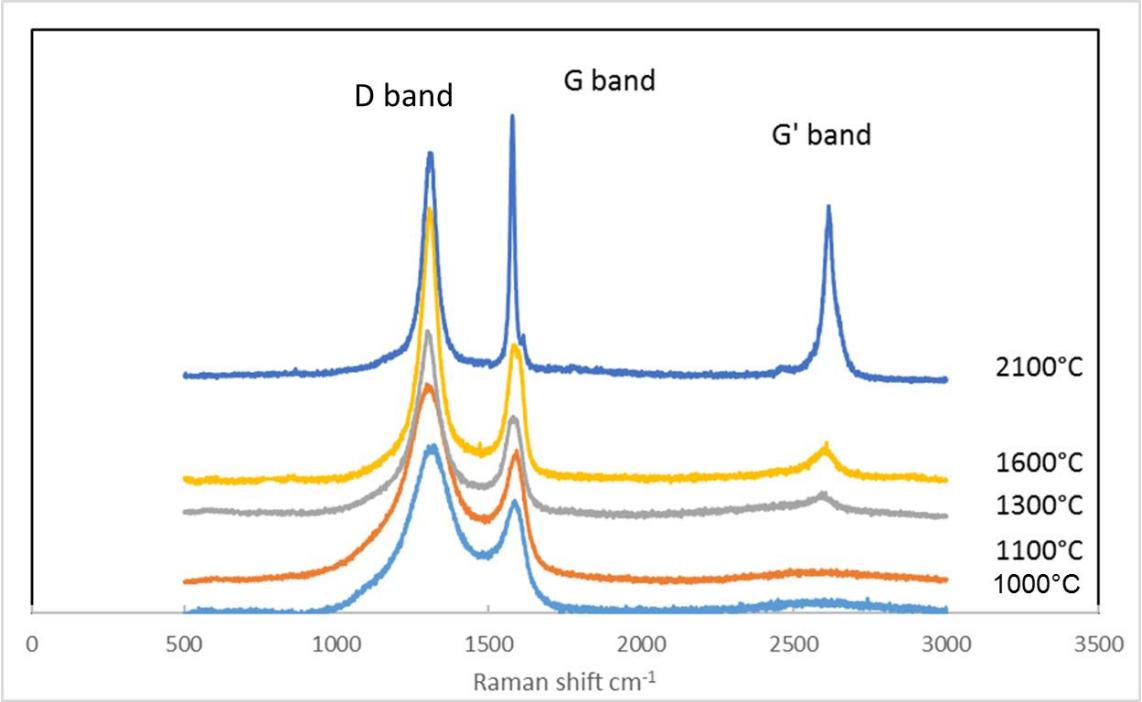

Figure 4.10 Raman spectra of highest-MW FSLP derived carbon fibers heat-treated at different temperatures between 1000°C to 2100°C.

The width of D and G bands was used as an indicator to estimate the degree of graphitic crystallinity. The full-width at half-maximum (FWHM) of D and G bands are listed in Table 4.1. The FWHM of D band decreases by a factor of ~4 over the entire carbonization temperature range, indicating an increase of order in the carbon fiber structure at higher carbonization temperatures. For the G band, the trend is the same, the FWHM of G band decreases from 96 to 40 cm^{-1}. The ratio of integrated area of the D and G bands, I_D/I_G is used to estimate the in-plane crystalline size, La, via the equation proposed by Tuinstra and Koenig *(130)* (Eq 4.5).

$$L_a = (2.4 \times 10^{-10} nm^{-3}) \times \lambda^4 \times \left(\frac{I_D}{I_G}\right)^{-1} \quad (4.5)$$

Where the λ is the wavelength of the laser, which is 785 nm in this study. This relationship is valid for more graphitic carbons. The I_D/I_G ratio becomes smaller with rising carbonization temperature, and this is consistent with that observed in PAN based carbon fibers *(131)*. The average L_a values for the carbon fibers are listed in Table 1. The average crystalline size L_a at 1000°C is 24.9 nm, which is consistent with the values of 2.3-55 nm reported in prior literature studies *(122, 132-134)*, while the average La increases to 46.2 nm at 2100°C. The crystalline size L_a increases with the increasing temperature, indicating that the graphitic-like structures grow by reorganizing more disordered structures within the carbon fibers as they are carbonized at higher temperatures. Although there is a significant improvement in the structural arrangement and ordering within the highest MW lignin based carbon fiber as the heat-treatment temperature increases, the carbon fibers still possess relatively low graphitic structure compared to mesophase-pitch based carbon fibers, i.e. I_D/I_G ratio of K1100 is 0.8, and L_a is ~120 nm *(135)*. This is consistent with the nonhomogeneous chemical structure of lignin which is not likely to form graphitic carbon layers.

Table 4.1 Raman spectroscopy results of highest MW FSLP-based carbon fibers.

Carbonization temperature (°C)	D FWHM (cm^{-1})	G FWHM (cm^{-1})	I_D/I_G	L_a (nm)
1000	203±16	96±1	3.61±0.52	24.9±3.1
1100	183±15	87±7	3.41±0.25	26.1±2.0
1300	158±38	83±5	3.24±0.16	27.5±1.3
1600	88±9	64±4	2.65±0.09	33.6±1.1
2100	59±2	40±7	1.92±0.07	46.2±1.6

Wide-angle X-ray diffraction was also used to evaluate carbon fiber structure in this study. Figure 4.11 shows the X-ray diffractogram for the fractionated lignin derived carbon fibers heat-treated at different temperatures. The silicon peaks located at 28.4°, 47.3° and 56.2° correspond to Si (1 1 1), Si (2 2 0) and Si (3 3 1) planes, respectively. As mentioned earlier in Section 4.3.2, the silicon peaks were used for accurate assignment of 2-theta peak position. The (0 0 2) peak, which corresponds to the stacking of graphitic layers, appeared at 24.2° for fibers carbonized at 1000°C, and shifts towards larger angles (26.2° at 2100 °C) with increasing temperature. The (0 0 2) peak is relatively broad and weak for those fibers carbonized at low temperatures, especially at 1000 °C and 1100 °C, indicating a lower degree of crystallinity and the presence of disordered carbon structure. With the increase of temperature, the (0 0 2) diffraction peak gained intensity and its width at half maximum decreased substantially, also being centered closer to the 2θ value of graphite (26.5°). The second peak at around 43° is due to the (1 0 0) planes.

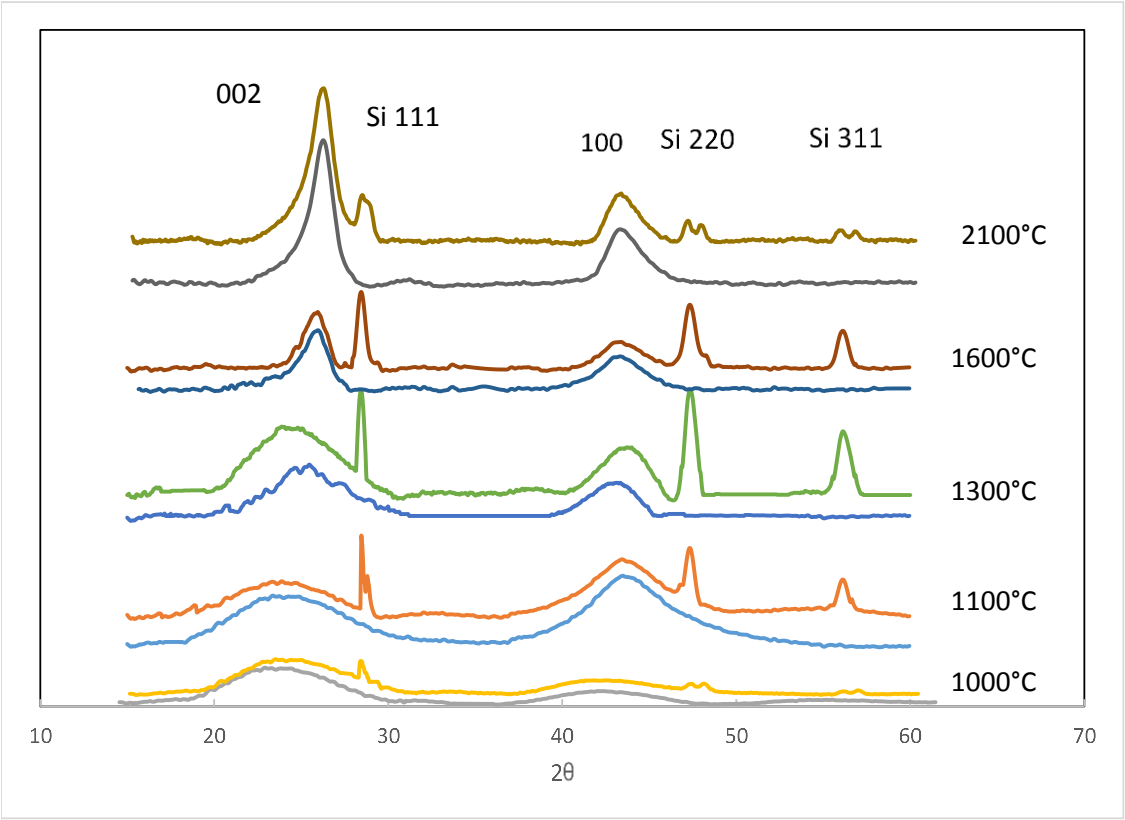

Figure 4.11 Integrated azimuthal (2-theta) profiles from WAXD of highest-MW FSLP derived carbon fibers heated at different temperatures between 1000°C to 2100°C.

Bragg's law (Eq 4.1) was used to calculate the d_{002} spacing (the distance between the layer planes) from the (0 0 2) peak, and the Scherrer equation (Eq 4.2) was for crystalline thickness L_c from the FWHM of (0 0 2) coupled with instrumental broadening correction (Eq 4.3). The results obtained are listed in Table 4.2. The d_{002} values display a range between 3.65 Å for the fibers carbonized at 100 °C to 3.39 Å for those carbonized at 2100 °C. With the increase of temperature, the d_{002} spacing decreases; for pure graphite this spacing is 3.354 Å *(136)*. For the fibers carbonized at 1000, 1100, and 1300 °C, the d_{002} values are larger than turbostratic carbon generated in PAN-based carbon fibers.

Thus, they possessed no measurable degree of graphitic crystallinity. For 1600 and 2100 °C carbonized fibers, the 2θ peak of (0 0 2) planes was located at 26.0° and 26.2°, respectively. The corresponding degrees of graphitization (g%) are 18% and 41% for these carbon fibers. The decreased interlayer spacing is achieved by eliminating the disordered structure, which allows the graphitic planes stack better, yielding a more graphitic structure. The crystalline thickness, L_c displays an increasing trend, which is in good agreement with the d-spacing values. The crystalline thickness increased from 10 to 34 Å with increasing temperature. The decrease of interlayer spacing allows good planar stacking, which improves the growth of crystalline size *(132)*. Figure 4.12 displays the azimuthal scans of (0 0 2) peaks of FSLP fibers carbonized at three different temperatures. The 1600°C and 2100°C carbonized fibers preserved the orientation with FWHM still around 112°. Also, the azimuthal scan of mesophase-pitch based carbon fibers (K1100) is plotted together for comparison, and it is evident that FSLP-based carbon fibers possess very low degree of orientation.

In general, lignin is recognized as a non-graphitizable precursor due to its highly branched structure with heterogeneity. Thus, lignin-based carbon fibers still possess low degree of graphitic crystallinity. The results in this study show evidence of increased structural ordering beyond 1600°C, which is attributed to the closer stacking of graphitic layers. However, even at higher temperatures, only small graphitic crystals formed in a predominantly turbostratic carbon matrix. Overall, a higher degree of graphitic structure can be created in lignin-based carbon fiber through high temperature treatment, but the inhomogeneous turbostratic structure still dominates within the carbon fibers.

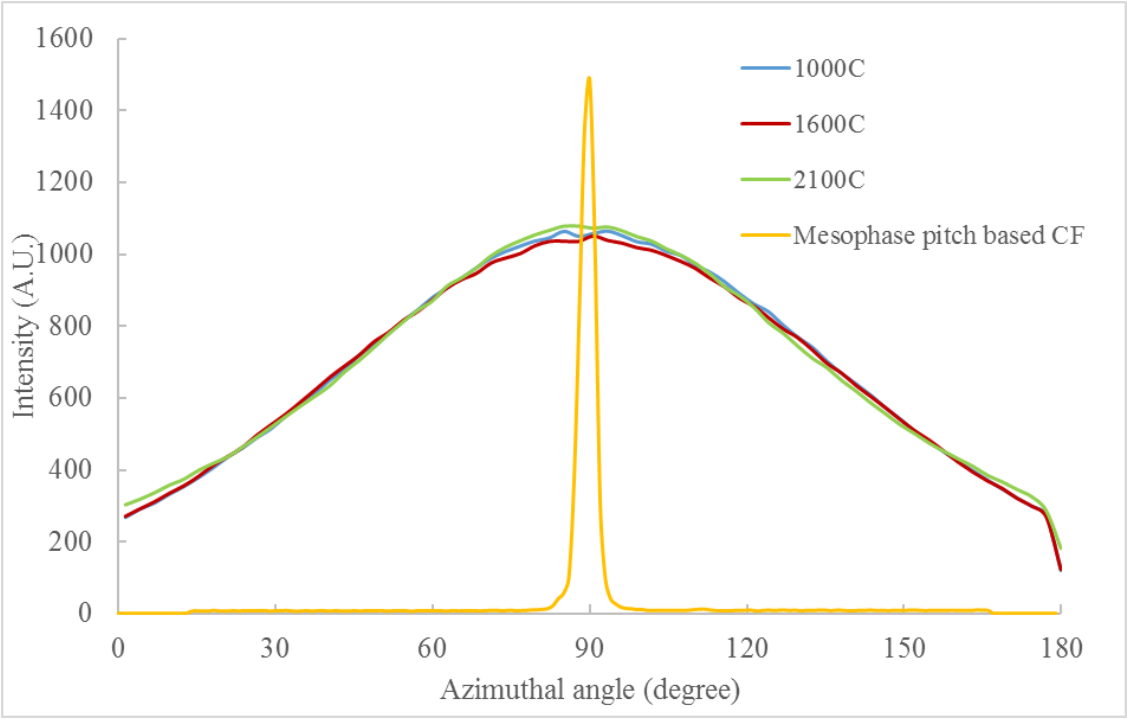

Figure 4.12 Representative azimuthal scans of the (0 0 2) peak of highest MW FSLP-based carbon fibers at three different carbonization temperatures.

Table 4.2 XRD results of highest MW FSLP-based carbon fibers.

Carbonization temperature (°C)	Peak position 2θ (002) (°)	d_{002} (Å)	Lc (002) (Å)	Degree of graphitization (%)
1000	24.2±0.2	3.65±0.03	10.7±0.4	-
1100	24.5±0.1	3.63±0.01	11.3±0.6	-
1300	25.2±0.7	3.53±0.09	14.9±0.7	-
1600	26.0±0.1	3.42±0.01	21.9±0.9	18%
2100	26.2±0.1	3.39±0.01	34.5±0.3	41%

4.3.4 TEM

The Figure 4.13 shows HR-TEM images of cross-section of FSLP-based carbon fibers. At low temperature of 1000 °C, the carbon fibers show fibrous texture without a preferred orientation (Figure 4.13 (a)). This indicates that the fibers are mainly composed of polyaromatic layers in turbostratic order in early carbonization stage. With the temperature increased to 1300 °C, a folded, entangled curvilinear sheets of layer planes are displayed within the fibers, shown in Figure 4.13 (b). Although the parallel orientation of the layered structure is improved, the fibers still present different degrees of disordered turbostratic structure. At 1600 °C, the crystalline domain still shows some degrees of misorientation, but the stacking layers become more parallel, and the interlayer spacing becomes smaller, which indicates that the stacked layers become more condensed and ordered. Even though the layers are not perfect, curving and folding still can be observed, these layers are parallel over a larger distance, showing an increased size of graphitic crystalline. At 2100 °C, the lamellar structure of carbon fibers becomes more ordered, and the stacks of layers increases slightly. This demonstrates that within some area, the transition between turbostratic and graphitic crystalline structure is beginning to occur. This is in agreement with previous XRD results. As the graphitization progresses, the crystalline domain becomes less disordered, but in some region, the structural defects still can be observed.

Figure 4.13 (e) shows the TEM image of commercial pitch-based carbon fiber, K1100, for comparison. The stacked layers are well ordered and parallel with a decreased interlayer spacing value. In general, the interlayer spacing values of the lignin-based

carbon fibers measured via TEM are consistent with that obtained by XRD. Note that the TEM only measures local d-spacing within a specific region, which cannot represent the average d-spacing of entire carbon fiber group.

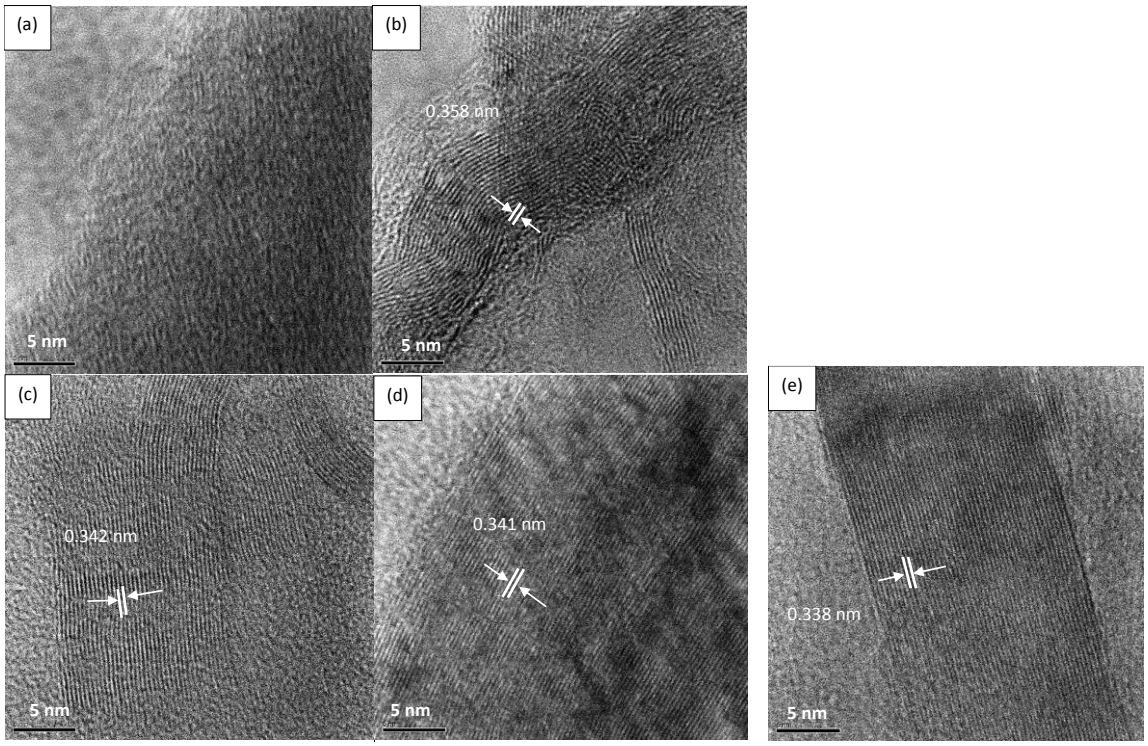

Figure 4.13 TEM micrographs of highest MW FSLP-based carbon fibers at (a) 1000°C (b) 1300°C (c) 1600 °C (d) 2100°C and mesophase pitch-based carbon fibers (e) K1100.

4.3.5 Effect of carbonization temperature on carbon fiber morphology

The images of carbon fiber cross-section and longitudinal surfaces observed by SEM are shown in Figure 4.14. The average equivalent diameters of carbon fibers treated at different temperatures were all below 6 μm, which is smaller than most of reported melt-spun lignin derived carbon fibers *(89-91)*. The resulting carbon fibers preserved the non-circular dog-bone shape cross section due to the finite diffusion rate during dry

spinning process. The longitudinal surface of fibers carbonized at 1000°C is relatively smooth. When carbonization temperature was increased to 1300°C and 1600°C, the surface of the carbon fiber becomes rough, and observable pores and defects (circled in Figure 4.14) with a diameter of tens of nm appears on the surface. When the carbonization temperature was increased to 2100°C, a more porous structure can be seen on the fiber surface. These surface defects were likely caused by the out-diffusion of non-carbonaceous elements during carbonization. As mentioned early, even though ALPHA process was able purify kraft lignin to some extent, the fractionated lignin precursor still processed about 0.06-0.08 wt% of impurities, which contains mostly metal salts generally presented in kraft lignin. The degradation, or out-diffusion of these impurities can lead to more surface defects at higher carbonization temperatures. Also, the surface defects may have been due to the impurities present in the environment during fiber spinning and heat-treatment. These defects will lead to decrease in the carbon fiber properties.

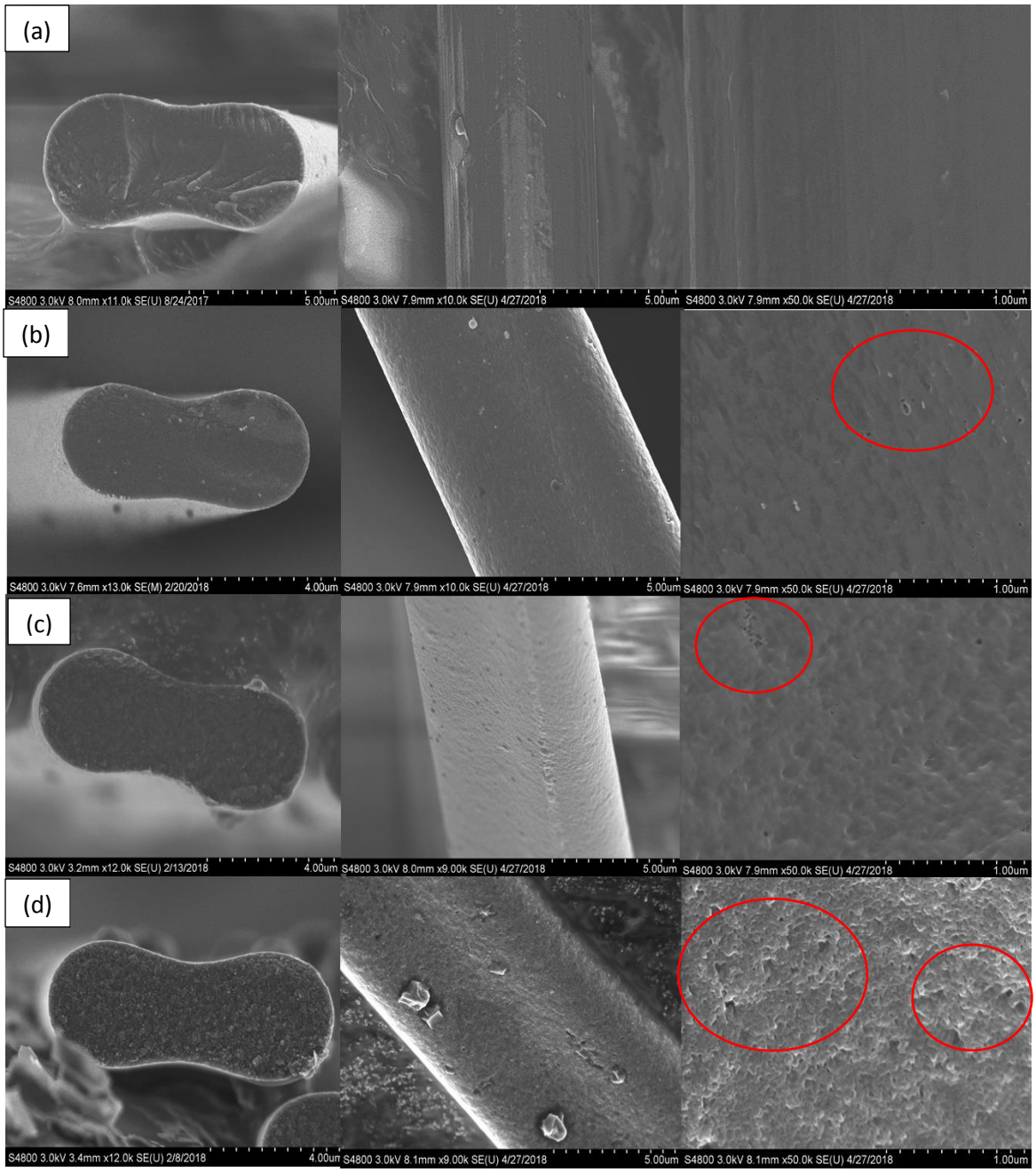

Figure 4.14 SEM micrographs of FSLP based carbon fibers carbonized at (a) 1000 °C (b) 1300 °C (c) 1600 °C (d) 2100 °C.

4.3.6 Electrical resistivity

In addition to mechanical properties of carbon fibers for reinforcement applications, electrical properties are also important for lignin-based carbon fibers, which could also been used as functional materials for other applications. Along the direction of fiber axis containing parallel graphitic layers, electrical conductivity is produced by the movement of electrons throughout the sp^2 array. Figure 4.15 displays the electrical resistivity values of highest MW FSLP-based carbon fibers prepared at temperatures between 1000°C and 2100°C. With the increase of carbonization temperatures, the electrical resistivity of carbon fibers gradually decreased from 95 to 28 μΩ·m. The improvement of conductivity is due to the increase to crystalline size within the carbon fibers. The Raman spectroscopy and X-ray diffraction results demonstrate that the graphitic crystalline grows, and the interlayer spacing decreases with increasing temperature, which is responsible for the observed decrease in electrical resistivity. Further improvement might be achieved by graphitization at higher temperature (2500-3000 °C). However, the electrical resistivity values of lignin-based carbon fibers are still much larger compared to pitch-based carbon fibers, for example, P-25 has electrical resistivity of 13 μΩ·m, and K1100 has of 1.25 μΩ·m. This is mainly due to the non-graphitic nature of carbon fibers produced from lignin, which causes turbostratic carbon structure with poorly oriented layers along fiber axis.

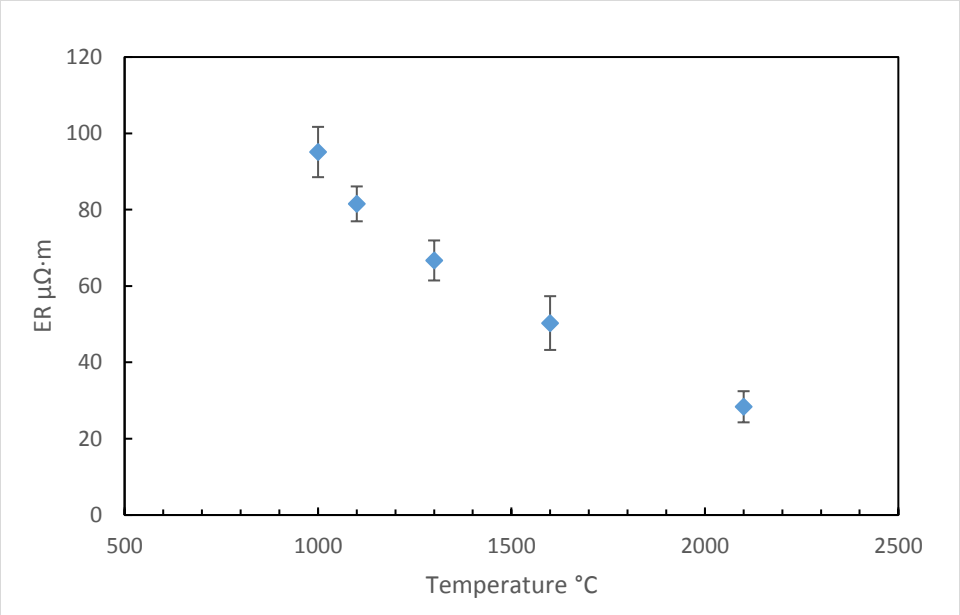

Figure 4.15 Electrical resistivity and of Highest MW FSLP carbon fibers carbonized at different temperatures.

4.3.7 Mechanical properties of FSLP-based carbon fiber

The stress-strain curves of different FSLPs-based carbon fibers are shown in Figure 4.16. All types of carbon fibers display a linear/elastic response to failure. The carbon fibers obtained from the medium and higher-MW FSLPs presented similar stress at failure (strength), slightly above 1.0 GPa, but different slopes (moduli). The carbon fibers obtained from the highest MW FSLPs display the largest tensile strength above 1.3 GPa. In contrast, carbon fibers derived from lignin fibers produced at 80 °C with undesired sharp crevices/defects possessed a tensile strength of only 0.6 GPa. While comparable to many of the prior carbon fibers reported in literature studies (derived from melt-spun lignin) *(68, 75, 89, 90)*, these fibers were not as good as those obtained from 30-45 °C dry-spun lignin fibers.

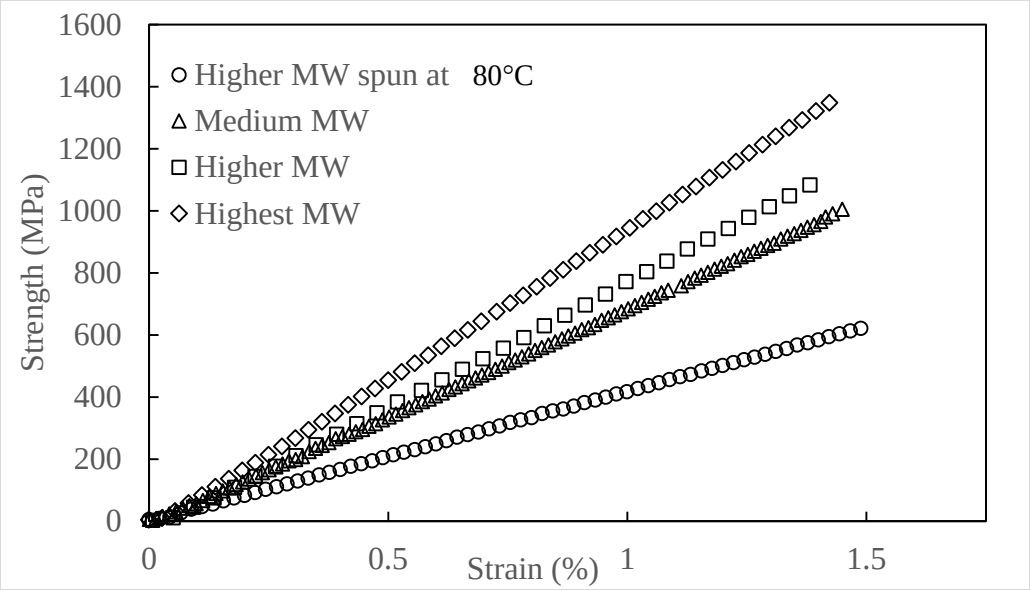

Figure 4.16 Representative tensile testing stress-strain curves of single FSLPs derived carbon fibers

The tensile properties of carbon fibers derived from the three MW grades of FSLPs are displayed in Table 4.3. Carbon fibers produced in the current study displayed increasing moduli values as the MW of the FSLPs increased resulting from a refinement of carbon structure. Enhanced graphitic content (better carbon layer formation) is known to enhance lattice-controlled properties such as modulus *(2, 3)*. Thus, carbon fibers produced from the medium- and higher-MW FSLPs displayed tensile moduli of 74±4 and 87±7 GPa, respectively, whereas the highest-MW FSLP displayed a tensile modulus of 98±5 GPa. The highest tensile strength of 1.39 ±0.23 GPa was also measured for carbon fibers produced from the highest-MW FSLP. These strength and modulus values of 1.39 and 98 GPa, respectively, represent the best-quality lignin-based carbon fibers produced to date. Another aspect that needs to be noted is the ash content. The ash content values reported in this study vary from 0.08-0.05 wt%, which is comparable to the best

experimental organosolv lignins. In previous research studies, it was reported that the strength of carbon fiber is very sensitive to the purity of lignin precursor, as metal salts can create defects during the heat treatment *(6)*. Overall, the good quality of FSLPs including both high purity and high molecular weight contributed to the enhanced mechanical properties of resulting carbon fibers.

Although the strength is almost 40% higher than the highest value reported in literature and the modulus has approached 100 GPa, it is noted that further improvement in these properties is needed for such fibers are to compete with low-cost PAN-derived CFs and low-cost glass fibers. To further increase the mechanical properties, both lignin source and the method of pretreatment within the ALPHA process need to be changed in order to generate superior FSLPs (ash content below 100 ppm, and MW higher than 30,000 g/mol), in turn, can help improve properties of resulting carbon fibers, as listed in Chapter 5 in future work.

Table 4.3 Tensile properties of carbon fibers obtained from medium, higher and highest MW of FSLPs.

Precursor Lignin	Tensile Strength (GPa)	Modulus (GPa)	Strain (%)	Equivalent Diameter (μm)
Medium MW	1.05±0.14	74±4	1.4±0.1	6.2±0.3
Higher MW	1.03±0.09	87±6	1.2±0.2	5.7±0.4
Highest MW	1.39±0.23	98±5	1.4±0.2	5.6±0.2

The mechanical properties of the highest MW lignin derived carbon fibers carbonized at different temperatures are displayed in Figure 4.17 and summarized in Table 4.4. With the increase in carbonization temperature, the fiber diameter and the

elongation at break decreased, while the modulus increased. The fibers carbonized at 1000 °C displayed the highest tensile strength of 1.39 GPa. Higher carbonization temperatures above 1000 °C resulted in a reduction in tensile strength due to defects generated at higher temperatures as metal-based impurities are evolved, as shown in Figure 4.14. In addition, since the carbonization in this study was done as a batch process, the exposure time of fibers to temperatures over 1000 °C is longer when the carbonization temperature increased. For carbonization at 2100 °C, the residence time above 1000 °C was 145 min longer than that of the fibers carbonized at 1000°C. The longer exposure time at higher temperature might cause additional defects to form as even trace amounts impurities in lignin precursor will evolve from the carbon fibers leaving behind micro-defects. Therefore, 1000 °C was found to be the best carbonization temperature for this type of lignin-based carbon fiber based on the highest tensile strength. However, the modulus increased with increasing of carbonization temperature. This is expected because of a higher graphitic structure is typically formed at higher carbonization temperatures, which enhances lattice-dominated properties such as modulus and electrical conductivity, but adversely affects the tensile strength.

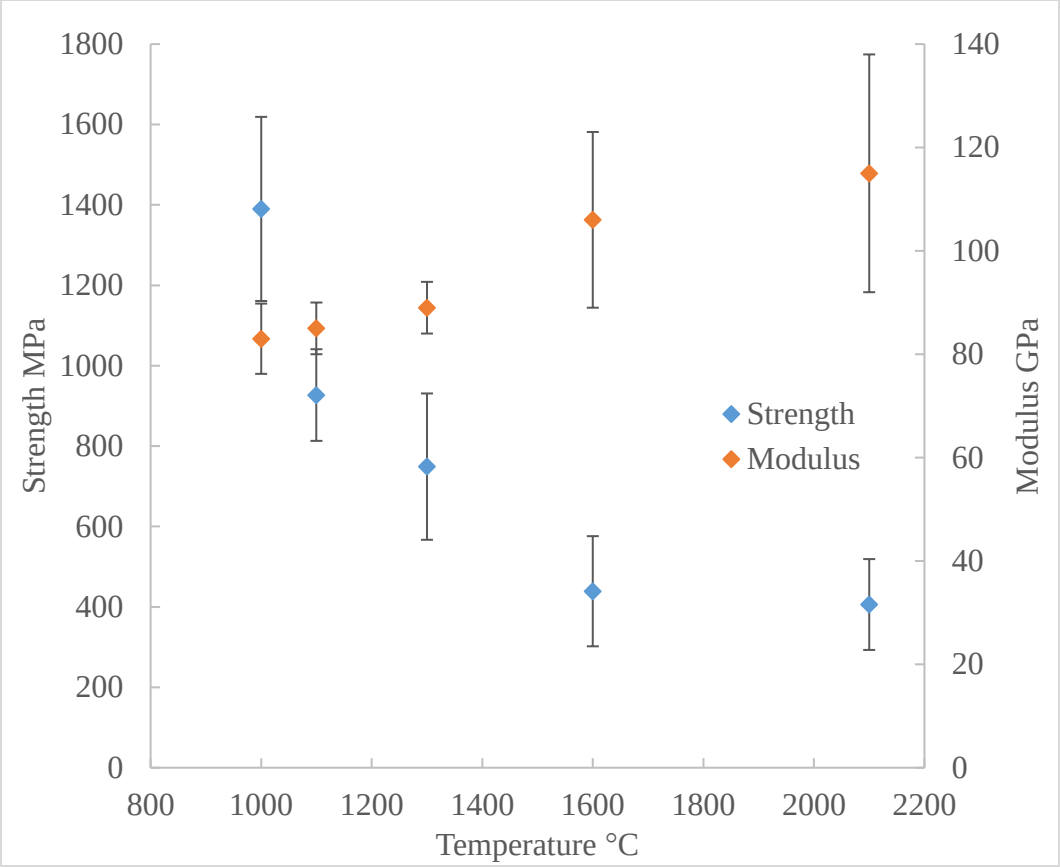

Figure 4.17 Tensile strength and modulus of highest-MW FSLP based carbon fibers at different carbonization temperatures.

Table 4.4. Tensile properties of highest MW lignin-based carbon fibers at different carbonization temperatures. (*Equivalent diameter was measured by SEM and image analysis. **The tensile modulus shown below was not compliance corrected).

Carbonization Temperature (°C)	Equivalent Diameter* (μm)	Tensile Strength (MPa)	Tensile Modulus (GPa)**	Strain of Failure (%)
1000	5.6±0.2	1390±229	83±6.8	1.7±0.2
1100	5.8±0.3	927±114	85±5	1.1±0.1
1300	5.5±0.2	749±182	86±5	0.9±0.2
1600	5.3±0.3	439±137	106±17	0.4±0.1
2100	5.2±0.3	406±113	115±23	0.4±0.1

4.4 Conclusions

The structural transition of FSLP fibers during thermal stabilization and carbonization was studied using ATR-FTIR and XRD. Thermal stabilization process leads to dehydration, demethylation, oxidation and cross-linking reactions. After carbonization, a turbostratic carbon structure was formed within the fibers although a better carbon-layered structure was formed within the carbon fibers as the MW of FSLP increased. At low carbonization temperatures in the range 1000-1600°C, the lignin-based carbon fibers display low degree of graphitic crystallinity structure as observed by Raman spectroscopy, XRD and TEM. Carbonization temperatures above 2000 °C improved the layer plane order and spacing within carbon fibers. However, the lignin-based carbon fibers did not show a true 3-D graphitic structure, in contrast to that observed in pitch-based carbon fibers even at a carbonization temperature above 2000°C, indicating that even the highest MW lignin was a non-graphitizable material. The electrical conductivity of the carbon fibers improved with increasing of carbonization temperatures (from 1000 to 2100°C). However, the lignin-based carbon fibers had low conductivity compared to that of pitch or even PAN-based carbon fibers, indicating a very low graphitic crystalline structure in these fibers. These results are consistent with those obtained by Raman spectroscopy and XRD.

The resultant carbon fibers at 1000°C from the highest-MW FSLP, which comprised 10% of the feed lignin, possessed the highest average tensile strength of 1.39±0.23 GPa – almost 40% stronger than any lignin-based carbon fiber reported to date. However, it was observed that the fibers carbonized at temperatures above 1300°C

had rougher surface as compared with the fibers carbonized at 1000°C. The surface defects were likely caused by the out-diffusion of non-carbonaceous elements, such as the impurities in FSLPs. Thus, the tensile strength decreased due to the surface defects. However, the modulus increased because of the enhanced lattice structure (although not highly graphitic). As a result, for strength application, the best carbonization temperature for the current grade of FSLPs was 1000°C, at which the carbon fibers display the highest tensile strength. But for electrical applications where the mechanical properties are not essential, high MW of lignin and high carbonization temperature could facilitate the formation of graphitic microstructure. Results presented in this Chapter have been published in reference 94.

CHAPTER FIVE
CONCLUSIONS AND FUTURE WORK

5.1 Conclusions

This final chapter summarizes concluding remarks based on the findings presented in Chapter 2 through Chapter 4. In this research study, two types of low-cost lignin-based precursors were investigated, and the resulting carbon fibers derived from these two precursors display improved mechanical properties compared to those reported in previous literature studies.

In Chapter 2, a standard wet-spinning process of producing void-free lignin/PAN blend fibers was established. Rheological measurements and FTIR results confirm that lignin can be considered as a "diluent" in the blends because the shear viscosity decreases with an increase of lignin content, and there is no chemical reaction or crosslinking between PAN and lignin in the blends. As expected, higher solid content for lignin/PAN blend solutions can compensate for the reduced viscoelastic properties and facilitate the wet-spinning. However, the resulting L/P precursor fibers still possess micron-sized voids due to lignin leaching during spinning, and it was confirmed by UV-vis that lignin concentration in the coagulant bath increased as the wet-spinning continued. Therefore, reducing out-diffusion of lignin by controlling the coagulant composition was found to be an efficient method in comparison with gel-spinning reported in other studies. By incorporating 0.2 wt% lignin in the coagulant during wet-spinning, lignin out-diffusion was minimized as confirmed by UV-vis spectroscopy. Thus, the successful wet-spinning

of void-free L/P fibers containing up to 50 wt% lignin content was demonstrated, and a cost-effective route for producing carbon fibers from lignin/PAN blends was established.

After thermal oxidative stabilization of lignin/PAN precursor fibers at 300 °C and carbonization at 1200 °C, the resulting carbon fibers show no observable voids in cross-sections. Raman spectroscopy and WAXD results indicate that higher lignin content (from 25 to 50 wt%) leads to a lower degree of graphitic crystallinity, which reduced the tensile modulus but the tensile strength of resulting carbon fibers was not significantly affected. Thus, equi-gravimetric lignin content can be incorporated into PAN without further decreasing the strength.

The limitation of the above study is that the environmental issues posed by pure PAN precursors (viz. HCN release) are also posed by lignin/PAN blends (although to a smaller extent), and the improved mechanical properties are primarily from PAN. To increase the mechanical performance of pure lignin derived carbon fibers, solvent fractionation is necessary to isolate cleaned lignin fractions with high molecular weight. A liquid-liquid equilibrium system that forms between lignin and acetic acid/water was developed by Thies group and described in Chapter 3, and resulting in isolated lignin fractions with higher molecular weight (FSLPs) were provided for further processing. The dry-spinning process was established to spin the FSLPs with three different MW fractions. In the dry-spinning process, the viscosity was maintained constant by tuning temperature and lignin content of the spinning dope, and the pressure drop was kept below 3000 psi, which is a safe operation limit. Thus, a processable spinnability window was established. At spinning temperature range between 70-80°C, the lignin precursor

fibers displayed crenulated cross-sectional structure with 26% larger lateral surface area than that of equivalent circular fibers. At lower spinning temperature range of 30-45°C, which was found to be the best regime, the lignin fibers possessed dog-bone shaped cross-section with 19% larger lateral surface area. The lignin precursor fibers dry-spun from highest MW FSLPs possessed tensile strength of 50±10 MPa and a modulus of 4.4±0.2 GPa, which are higher than those for other lower MW FSLPs.

Tension was applied during thermos-oxidative stabilization step, and constant length was maintained during carbonization. FSLP-based carbon fibers were successfully produced. The effect of molecular weight of FSLPs on the carbon fiber microstructure was studied using Raman spectroscopy and WAXD. Overall, FSLP-based carbon fibers had low graphitic crystallinity, but higher MW of FSLPs contributed to a better-packed carbon-layer structure within the fibers. Higher carbonization temperature also improved the graphitic crystalline structure of FSLP-based carbon fibers. The d_{002} spacing reduced from 0.365 to 0.339 nm, and the crystalline size L_c increased from 10.7 to 34.5 nm when the carbonization temperature increased from 1000°C to 2100 °C. The electrical conductivity of the carbon fibers improved with increasing carbonization temperatures (from 1000 to 2100°C). Finally, tensile testing revealed that the, highest MW FSLP derived carbon fibers displayed tensile strength, modulus and strain-to-failure of 1.39±0.23 GPa, 98±5 GPa and 1.4±0.2%, respectively. These properties are among the highest reported in the literature to date.

5.2 Recommendations for future work

The lignin used in lignin/PAN blend solutions for wet-spinning, reported in Chapter 2, was as-received raw lignin without pre-treatment. The as-received lignin contains ~2% impurities, which cause defects during carbonization and lead to the reduction in tensile properties of carbon fibers. Therefore, it is recommended that purer grades of lignin with reduced the ash content (below 0.1 wt%) be used for further studies on lignin/PAN blends. Also, according to previous literature studies, fractionated high MW lignin can facilitate spinning of lignin/PAN blend solution. Some preliminary trials were done to mix high MW FSLP and PAN polymer, however, a homogeneous blend could not be obtained due to the incompatibility of high MW FSLP with DMSO. Therefore, other stronger solvent such as DMF and DMAc should be studied.

In Chapter 3, acetic acid/water mixture was utilized as solvent to fractionate lignin precursor and form spinning dope. However, other solvent/lignin systems, such as acetone could also be used to purify and isolate high MW lignin. In our prior studies, acetone was found to be an effective solvent for dry-spinning because it is more volatile than acetic acid (at any given temperature). Some preliminary work has been done to use acetone/water (85/15 wt%) mixture as solvent to dissolve high MW FSLP to form a dope for dry-spinning, which was performed at temperatures ranging from 30 to 45°C. The as-spun fibers display crenulated cross-section due to the fast diffusion of solvent. As described in Chapter 3, the lignin fibers dry-spun from acetic acid/water-FSLP solution at low temperature range (30-40°C) show smooth lateral surface but non-circular dog-bone cross-section. However, the lignin fibers dry-spun from acetone/water-FSLP solution at

30-45°C display displayed excessive crenulation that reduce tensile strength. Less concentrated (lower solid content) spinning solution was used to prevent the formation of dry extrudate, but that could not be drawn down due to the rapid evaporation of acetone. Up to 400% extension (% of original length) was achieved during thermal oxidation step, and the fibers were carbonized with constant length at 1000°C. The strength and modulus of the resulting carbon fibers were 1.2±0.2 GPa, and 71±8 GPa, respectively. The strength value is among the best quality carbon fibers derived solely from lignin, but lower than those for FSLP-based carbon fibers derived from acetic acid.

The lignin used in the current study was limited to softwood kraft lignin recovered from the SLRP process. To further investigate lignin fractionation via ALPHA and to increase the mechanical properties of lignin-based carbon fibers, both lignin source and the method of pretreatment within the ALPHA process need to be explored to obtain a superior lignin precursor. A preliminary study has been done using Biochoice lignin as a new softwood kraft lignin source. The same ALPHA conditions were applied to Biochoice lignin as what was applied to SLRP (described in Chapter 3). A strong 67/33 AcOH/water solution was used to isolate highest 10% of the feed lignin. The molecular weight 10,150 Da, as measured by the Thies group, was lower than the highest MW fraction from SLRP. Also, the ash content was 0.13 wt%, twice as high as that of the highest MW fraction from SLRP lignin. This is probably because the initial ash content of Biochoice lignin (before ALPHA-based fractionation) was twice that of raw SLRP lignin. Thus, the capability of reducing ash content via ALPHA needs to be improved. As a result, the Biochoice lignin is not considered as a good lignin source for improving

carbon fiber performance. The strength and modulus of carbon fibers derived from fractionated Biochoice lignin were only 869±178 MPa, and 51±7 GPa, respectively.

As described in Chapters 3 and 4, the carbonization was performed under constant length due to the limitation of batch operation. It is known that the carbon fibers obtained from a process where larger extension is observed during carbonization display better tensile properties because of a higher molecular orientation within the fibers. Therefore, when the lignin fibers are stabilized and carbonized on a continuous line, where fiber tension can be controlled to different levels in stepwise temperature zones, additional improvement in tensile strength and modulus can be expected.

Finally, to demonstrate the incorporation of FSLP-based carbon fibers in an epoxy matrix, mini-composites were produced that were nominally 1 cm wide and 5 cm long. Due to the mis-alignment of carbon fibers in the composite samples, the average volume fraction was limited to 13.8%, which is relatively low compared with commercial composites that can contain up to 60 vol% carbon fibers. The average tensile strength and modulus were 124 ±26 MPa and 15.4±1.4 GPa, respectively. Although these properties are well below the levels desired for high performance composites, these preliminary findings demonstrate the feasibility of producing composites from FSLP-based carbon fibers. Future investigations could be done to (i) produce FSLP-based carbon fibers in continuous form to achieve better alignment; (ii) improve interfacial properties of fibers and matrix.

In summary, this current research study developed lignin/PAN polymer blends and fractionated high MW lignin precursors for producing carbon fibers with enhanced mechanical performance. Wet-spinning of lignin/PAN blends and dry-spinning of FSLPs was conducted in a batch mode of this research. Subsequently, the precursor fibers were successfully converted to carbon fibers with tensile properties that are the highest reported for lignin-based carbon fibers. Above recommendation for lignin precursor and processing steps can help with the improvement in mechanical properties, and potentially push the application of lignin-based carbon fiber to composite industry.

REFERENCES

(1) Klett, A. S.; Payne, A. M.; Thies, M. C. Continuous-Flow Process for the Purification and Fractionation of Alkali and Organosolv Lignins. *ACS Sustainable Chemistry & Engineering* **2016**, *4*, 6689-6694.

(2) Fitzer, E.; Manocha, L. M. *Carbon reinforcements and carbon/carbon composites*; Springer Science & Business Media: Berlin, 2012.

(3) Chung, D. D.; Chung, D. *Carbon fiber composites*; Butterworth-Heinemann: Boston, 2012.

(4) Morales Sandoval, M. S. UV-Assisted Stabilization of Polyacrylonitrile-Based Carbon Fiber Precursors. Ph.D. Thesis and Dissertation, Clemson University, Clemson, SC, **2013**.

(5) Edie, D.; Diefendorf, R. *Carbon fiber manufacturing*; Noyes Publications: New York, 1993.

(6) Zhang, M. Carbon Fibers Derived from Dry-Spinning of Modified Lignin Precursors. Ph.D. Thesis and Dissertation, Clemson University, Clemson, SC, **2016**.

(7) Chand, S. Review carbon fibers for composites. *J. Mater. Sci.* **2000**, *35*, 1303-1313.

(8) Fitzer, E. Pan-based carbon fibers—present state and trend of the technology from the viewpoint of possibilities and limits to influence and to control the fiber properties by the process parameters. *Carbon* **1989**, *27*, 621-645.

(9) Ōtani, S. On the carbon fiber from the molten pyrolysis products. *Carbon* **1965**, *3*, 31IN335-3438.

(10) Newcomb, B. A. Processing, structure, and properties of carbon fibers. *Composites Part A: Applied Science and Manufacturing* **2016**, *91*, 262-282.

(11) Ogale, A. A.; Zhang, M.; Jin, J. Recent advances in carbon fibers derived from biobased precursors. *J Appl Polym Sci* **2016**.

(12) Edie, D. The effect of processing on the structure and properties of carbon fibers. *Carbon* **1998**, *36*, 345-362.

(13) MInus, M.; Kumar, S. The processing, properties, and structure of carbon fibers. *JOM Journal of the Minerals, Metals and Materials Society* **2005**, *57*, 52-58.

(14) Gupta, A.; Paliwal, D.; Bajaj, P. Acrylic precursors for carbon fibers. *Journal of Macromolecular Science, Part C: Polymer Reviews* **1991**, *31*, 1-89.

(15) Frushour, B. G.; Knorr, R. S. In *Acrylic fibers;* Handbook of Fiber Chemistry, Third Edition; CRC Press: New York, 2006.

(16) Frushour, B. G. Melting behavior of polyacrylonitrile copolymers. *Polymer Bulletin* **1984**, *11*, 375-382.

(17) Paiva, M.; Kotasthane, P.; Edie, D.; Ogale, A. UV stabilization route for melt-processible PAN-based carbon fibers. *Carbon* **2003**, *41*, 1399-1409.

(18) Bajaj, P.; Roopanwal, A. Thermal stabilization of acrylic precursors for the production of carbon fibers: an overview. *Journal of Macromolecular Science, Part C: Polymer Reviews* **1997**, *37*, 97-147.

(19) Morales Sandoval, M. S. UV-Assisted Stabilization of Polyacrylonitrile-Based Carbon Fiber Precursors. Ph.D. Thesis and Dissertation, Clemson University, Clemson, SC, **2013**.

(20) Tan, L.; Wan, A.; Pan, D. Pregelled gel spinning of polyacrylonitrile precursor fiber. *Mater Lett* **2011**, *65*, 887-890.

(21) Wang, Y.; Wang, C.; Bai, Y.; Bo, Z. Effect of the drawing process on the wet spinning of polyacrylonitrile fibers in a system of dimethyl sulfoxide and water. *J Appl Polym Sci* **2007**, *104*, 1026-1037.

(22) Rahaman, M. S. A.; Ismail, A. F.; Mustafa, A. A review of heat treatment on polyacrylonitrile fiber. *Polym. Degrad. Stab.* **2007**, *92*, 1421-1432.

(23) Dunham, M.; Edie, D. Model of stabilization for pan-based carbon fiber precursor bundles. *Carbon* **1992**, *30*, 435-450.

(24) Morgan, P. *Carbon fibers and their composites*; CRC press: Boca Raton, FL, 2005.

(25) Matsumoto, T. Mesophase pitch and its carbon fibers. *Pure and applied chemistry* **1985**, *57*, 1553-1562.

(26) Dienes, G. J. Mechanism for Self‐Diffusion in Graphite. *J. Appl. Phys.* **1952**, *23*, 1194-1200.

(27) Edie, D.; Fox, N.; Barnett, B.; Fain, C. Melt-spun non-circular carbon fibers. *Carbon* **1986**, *24*, 477-482.

(28) Riggs, D. M.; Shuford, R. J.; Lewis, R. W. In *Graphite fibers and composites;* Handbook of composites; Springer: 1982; pp 196-271.

(29) Stoller, H.; Butler, B.; Theis, J.; Lieberman, M. Carbon fiber reinforced-carbon matrix composites. *Composites: State of the art.(A 74-32483 15-18) New York, Metallurgical Society of AIME, Inc., 1974*, **1974**, 69-136.

(30) Frank, E.; Steudle, L. M.; Ingildeev, D.; Spörl, J. M.; Buchmeiser, M. R. Carbon fibers: precursor systems, processing, structure, and properties. *Angewandte Chemie International Edition* **2014**, *53*, 5262-5298.

(31) Zimmer, J.; White, J. Disclination structures in the carbonaceous mesophase. *Advances in liquid crystals* **1982**, *5*, 157-213.

(32) Buckley, J. D.; Edie, D. D. *Carbon-carbon materials and composites*; William Andrew: Park Ridge, NJ, 1993.

(33) Hino, T.; Naito, T.; Kuroda, H.; Tsushima, E.; Nomura, T. *High modulus pitch-based carbon fiber and method for preparing same* **1989**.

(34) Bermudez, V.; Lukubira, S.; Ogale, A. A. 1.3 Pitch Precursor-Based Carbon Fibers. **2018**.

(35) Gilberte, M. M. *Process of graphitizing" polynosic" regenerated cellulose fibrous textile and resulting fibrous graphite textile* **1967**.

(36) Ford, C. E.; Mitchell, C. V. *Fibrous graphite* **1963**.

(37) Goodhew, P.; Clarke, A.; Bailey, J. A review of the fabrication and properties of carbon fibres. *Materials Science and Engineering* **1975**, *17*, 3-30.

(38) Dumanlı, A. G.; Windle, A. H. Carbon fibres from cellulosic precursors: a review. *J. Mater. Sci.* **2012**, *47*, 4236-4250.

(39) McCorsley III, C. C. *Process for shaped cellulose article prepared from a solution containing cellulose dissolved in a tertiary amine N-oxide solvent* **1981**.

(40) Peng, S.; Shao, H.; Hu, X. Lyocell fibers as the precursor of carbon fibers. *J Appl Polym Sci* **2003**, *90*, 1941-1947.

(41) Friedfeld, B. Cost Assessment of Lignin-and PAN-Based Precursor for Low-Cost Carbon Fiber. *Presentation for the Automotive Composites Consortium* **2007**, *17*.

(42) Mathur, R.; Bahl, O.; Mittal, J. Advances in the development of high-performance carbon fibres from PAN precursor. *Composites Sci. Technol.* **1994**, *51*, 223-230.

(43) Gosselink, R.; De Jong, E.; Guran, B.; Abächerli, A. Co-ordination network for lignin—standardisation, production and applications adapted to market requirements (EUROLIGNIN). *Industrial Crops and Products* **2004**, *20*, 121-129.

(44) Sjostrom, E. *Wood chemistry: fundamentals and applications*; Elsevier: London, 2013.

(45) Ek, M.; Gellerstedt, G.; Henriksson, G. *Ljungberg Textbook: Pulp and Paper Chemistry and Technology*; Fibre and Polymer Technology, KTH: 2007.

(46) Chakar, F. S.; Ragauskas, A. J. Review of current and future softwood kraft lignin process chemistry. *Industrial Crops and Products* **2004**, *20*, 131-141.

(47) Carrott, P.; Carrott, M. R. Lignin–from natural adsorbent to activated carbon: a review. *Bioresour. Technol.* **2007**, *98*, 2301-2312.

(48) Muurinen, E. Organosolv pulping--A review and distillation study related to peroxyacid pulping. **2000**.

(49) Klett, A. S. Purification, Fractionation, and Characterization of Lignin from Kraft Black Liquor for Use as a Renewable Biomaterial. **2017**.

(50) Mullinder, J. Repap happy with Alcell results, in engineering phase for expansion. *Pulp Paper J* **1989**, *42*, 31.

(51) Sundquist, J. Chemical pulping based on formic acid: Summary of Milox research. *Paperi ja Puu* **1996**, *78*, 92-95.

(52) Jordan, R. Formic acid pulping. *PCT patent* **1982**, *82*, 01902.

(53) Herdle, L.; Pancoast, L.; MacClaren, R. Acetylation celluloses from pulping of wood in acetic acid. *Tappi* **1964**, *47*, 617-620.

(54) Sano, Y.; Umemoto, M.; Takahashi, A.; Sasaya, T. Phenorganosolv pulping, 2: Pulping of beechwood with acetic acid-water-phenols system. *Journal of the Japan Wood Research Society (Japan)* **1986**.

(55) Fengel, D.; Wegener, G. *Wood: chemistry, ultrastructure, reactions*; Walter de Gruyter: Berlin, 1983.

(56) Gellerstedt, G.; Lindfors, E. Structural changes in lignin during kraft cooking. Part 4. Phenolic hydroxyl groups in wood and kraft pulps. *Svensk Papperstidn* **1984**, *87*, R115-R118.

(57) Azadi, P.; Inderwildi, O. R.; Farnood, R.; King, D. A. Liquid fuels, hydrogen and chemicals from lignin: A critical review. *Renewable and Sustainable Energy Reviews* **2013**, *21*, 506-523.

(58) Biermann, C. J. *Essentials of pulping and papermaking.*; University of Michigan, 1993.

(59) Notley, S. M.; Norgren, M. Lignin: Functional biomaterial with potential in surface chemistry and nanoscience. *The Nanoscience and Technology of Renewable Biomaterials* **2009**, 173-206.

(60) Tomani, P. The lignoboost process. *Cellulose Chemistry & Technology* **2010**, *44*, 53.

(61) Kouisni, L.; Holt-Hindle, P.; Maki, K.; Paleologou, M. The lignoforce system: a new process for the production of high-quality lignin from black liquor. *J.Sci.Technol.For.Prod.Processes* **2012**, *2*, 6-10.

(62) Velez, J.; Thies, M. C. Solvated liquid-lignin fractions from a Kraft black liquor. *Bioresour. Technol.* **2013**, *148*, 586-590.

(63) Zhang, M.; Ogale, A. A. Carbon fibers from dry-spinning of acetylated softwood kraft lignin. *Carbon* **2014**, *69*, 626-629.

(64) Jönsson, A.; Nordin, A.; Wallberg, O. Concentration and purification of lignin in hardwood kraft pulping liquor by ultrafiltration and nanofiltration. *Chem. Eng. Res. Design* **2008**, *86*, 1271-1280.

(65) Arkell, A.; Olsson, J.; Wallberg, O. Process performance in lignin separation from softwood black liquor by membrane filtration. *Chem. Eng. Res. Design* **2014**, *92*, 1792-1800.

(66) Johansson, C. Purification of lignin fuel from kraft black liquor by diafiltration. *Department of chemical engineering, Lund university, Lund sweden* **2003**, 126-131.

(67) Thies, M. C.; Klett, A. S.; Bruce, D. A. Solvent and recovery process for lignin. U.S. Patent 10,053,482, August 21, 2018.

(68) Nordström, Y.; Norberg, I.; Sjöholm, E.; Drougge, R. A new softening agent for melt spinning of softwood kraft lignin. *J Appl Polym Sci* **2013**, *129*, 1274-1279.

(69) Liu, H.; Dai, Z.; Cao, Q.; Shi, X.; Wang, X.; Li, H.; Han, Y.; Li, Y.; Zhou, J. Lignin/Polyacrylonitrile Carbon Fibers: the Effect of Fractionation and Purification on Properties of Derived Carbon Fibers. *ACS Sustainable Chemistry & Engineering* **2018**.

(70) Otani, S.; Fukuoka, Y.; Igarashi, B.; Sasaki, K. *Method for producing carbonized lignin fiber* **1969**.

(71) Fukuoka, Y. Carbon fiber made from lignin (Kayacarbon). *Jap Chem Quart* **1969**.

(72) Baker, D. A.; Rials, T. G. Recent advances in low-cost carbon fiber manufacture from lignin. *J Appl Polym Sci* **2013**, *130*, 713-728.

(73) Brebu, M.; Tamminen, T.; Spiridon, I. Thermal degradation of various lignins by TG-MS/FTIR and Py-GC-MS. *J. Anal. Appl. Pyrolysis* **2013**, *104*, 531-539.

(74) Sudo, K.; Shimizu, K. A new carbon fiber from lignin. *J Appl Polym Sci* **1992**, *44*, 127-134.

(75) Sudo, K.; Shimizu, K.; Nakashima, N.; Yokoyama, A. A new modification method of exploded lignin for the preparation of a carbon fiber precursor. *J Appl Polym Sci* **1993**, *48*, 1485-1491.

(76) Uraki, Y.; Kubo, S.; Nigo, N.; Sano, Y.; Sasaya, T. Preparation of carbon fibers from organosolv lignin obtained by aqueous acetic acid pulping. *Holzforschung-International Journal of the Biology, Chemistry, Physics and Technology of Wood* **1995**, *49*, 343-350.

(77) Hu, T. Q. *Chemical modification, properties, and usage of lignin*; Springer: Boston, MA, 2002.

(78) Baker, F. Utilization of sustainable resources for materials for production of carbon fiber structural and energy efficiency applications. *Nordic Wood Biorefinery Conference.* **2011**, 22-24.

(79) Baker, F.; Baker, D.; Gallego, N. Carbon fiber from lignin. *Proceeding, Carbon* **2010**, 11-16.

(80) Kadla, J.; Kubo, S.; Venditti, R.; Gilbert, R.; Compere, A.; Griffith, W. Lignin-based carbon fibers for composite fiber applications. *Carbon* **2002**, *40*, 2913-2920.

(81) Kubo, S.; Kadla, J. F. Kraft lignin/poly (ethylene oxide) blends: effect of lignin structure on miscibility and hydrogen bonding. *J Appl Polym Sci* **2005**, *98*, 1437-1444.

(82) Qin, W.; Kadla, J. Carbon fibers based on pyrolytic lignin. *J Appl Polym Sci* **2012**, *126*.

(83) Norberg, I.; Nordström, Y.; Drougge, R.; Gellerstedt, G.; Sjöholm, E. A new method for stabilizing softwood kraft lignin fibers for carbon fiber production. *J Appl Polym Sci* **2013**, *128*, 3824-3830.

(84) Soutis, C. Carbon fiber reinforced plastics in aircraft construction. *Materials Science and Engineering: A* **2005**, *412*, 171-176.

(85) Zhang, M.; Ogale, A. A. Effect of temperature and concentration of acetylated‐lignin solutions on dry‐spinning of carbon fiber precursors. *J Appl Polym Sci* **2016**, *133*.

(86) Husman, G. Development and commercialization of a novel low-cost carbon fiber. *Presentation at 2012 DOE Hydrogen and Fuel Cells Program and Vehicle Technologies Program Annual Merit Review and Peer Evaluation Meeting.* **2012**.

(87) Xiaozhong Dong, Chunxiang Lu, Pucha Zhou, Shouchun Zhang, Liyong Wang and Denghua Li **Polyacrylonitrile/lignin sulfonate blend fiber for low-cost carbon fiber**. *RSC Advances* **2015**, 42259, DOI: 10.1039/c52ra01241d.

(88) Liu, H. C.; Chien, A.; Newcomb, B. A.; Liu, Y.; Kumar, S. Processing, structure, and properties of lignin-and CNT-incorporated polyacrylonitrile-based carbon fibers. *ACS Sustainable Chemistry & Engineering* **2015**, *3*, 1943-1954.

(89) Qu, W.; Liu, J.; Xue, Y.; Wang, X.; Bai, X. Potential of producing carbon fiber from biorefinery corn stover lignin with high ash content. *J Appl Polym Sci* **2018**, *135*.

(90) Hosseinaei, O.; Harper, D. P.; Bozell, J. J.; Rials, T. G. Improving Processing and Performance of Pure Lignin Carbon Fibers through Hardwood and Herbaceous Lignin Blends. *International journal of molecular sciences* **2017**, *18*, 1410.

(91) Qu, W.; Xue, Y.; Gao, Y.; Rover, M.; Bai, X. Repolymerization of pyrolytic lignin for producing carbon fiber with improved properties. *Biomass Bioenergy* **2016**, *95*, 19-26.

(92) Hosseinaei, O.; Harper, D. P.; Bozell, J. J.; Rials, T. G. Role of physicochemical structure of organosolv hardwood and herbaceous lignins on carbon fiber performance. *ACS Sustainable Chemistry & Engineering* **2016**, *4*, 5785-5798.

(93) Jin, J.; Ogale, A. A. Carbon fibers derived from wet‐spinning of equi‐component lignin/polyacrylonitrile blends. *J Appl Polym Sci* **2018**, *135*.

(94) Jin, J.; Ding, J.; Klett, A. S.; Thies, M. C.; Ogale, A. A. Carbon Fibers Derived From Fractionated–Solvated Lignin Precursors for Enhanced Mechanical Performance. *ACS Sustainable Chemistry & Engineering* **2018**.

(95) Bunsell, A. R.; Renard, J. *Fundamentals of fibre reinforced composite materials*; CRC Press: Boca Raton, FL, 2005.

(96) Seydibeyoğlu, M. Ö A novel partially biobased PAN-lignin blend as a potential carbon fiber precursor. *BioMed Research International* **2012**, *2012*.

(97) Middleman, S. *Fundamentals of polymer processing*; McGraw-Hill College: New York, 1977.

(98) Tadmor, Z.; Gogos, C. G. *Principles of polymer processing*; John Wiley & Sons: Hoboken, New Jersey, 2013.

(99) Daojie Dong, Ph.D. Thesis and Dissertations, University of Florida, Gainsville, FL, 1993.

(100) Advani, S. G. *Flow and rheology in polymer composites manufacturing*; Elsevier science: Amsterdam, 1994.

(101) Hayahara, T.; Takao, S. Relationship between polymer concentration and molecular weight in the viscosity behavior of concentrated solution. *Colloid & Polymer Science* **1968**, *225*, 106-111.

(102) Morales, M. S.; Ogale, A. A. UV‐induced crosslinking and cyclization of solution‐cast polyacrylonitrile copolymer. *J Appl Polym Sci* **2013**, *128*, 2081-2088.

(103) Wangxi, Z.; Jie, L.; Gang, W. Evolution of structure and properties of PAN precursors during their conversion to carbon fibers. *Carbon* **2003**, *41*, 2805-2812.

(104) Weisenberger, M.; Grulke, E.; Jacques, D.; Rantell, A. T.; Andrewsa, R. Enhanced mechanical properties of polyacrylonitrile/multiwall carbon nanotube composite fibers. *Journal of nanoscience and nanotechnology* **2003**, *3*, 535-539.

(105) Mikolajczyk, T.; Szparaga, G.; Bogun, M.; Fraczek‐Szczypta, A.; Blazewicz, S. Effect of spinning conditions on the mechanical properties of polyacrylonitrile fibers modified with carbon nanotubes. *J Appl Polym Sci* **2010**, *115*, 3628-3635.

(106) Baker, F.; Gallego, N.; Baker, D. Low cost carbon fiber from renewable resources. *EERE, US Dept of Energy Project ID# lm_03_baker* **2010**.

(107) Fang, W.; Yang, S.; Wang, X.; Yuan, T.; Sun, R. Manufacture and application of lignin-based carbon fibers (LCFs) and lignin-based carbon nanofibers (LCNFs). *Green Chem.* **2017**, *19*, 1794-1827.

(108) Li, Q.; Xie, S.; Serem, W. K.; Naik, M. T.; Liu, L.; Yuan, J. S. Quality carbon fibers from fractionated lignin. *Green Chem.* **2017**, *19*, 1628-1634.

(109) Klett, A.; Chappell, P.; Thies, M. Recovering ultraclean lignins of controlled molecular weight from Kraft black-liquor lignins. *Chemical Communications* **2015**, *51*, 12855-12858.

(110) Velez, J.; Thies, M. C. Liquid Lignin from the SLRPTM Process: The Effect of Processing Conditions and Black-Liquor Properties. *J. Wood Chem. Technol.* **2016**, *36*, 27-41.

(111) Lake, M.; Blackburn, J. C. A Process for recovering lignin. U.S. Patent US9260464B2, Feb. 2016.

(112) Aldaeus, F.; Schweinebarth, H.; Törngren, P.; Jacobs, A. Simplified determination of total lignin content in kraft lignin samples and black liquors. *Holzforschung* **2011**, *65*, 601-604.

(113) Ding, J.; Klett, A. S.; Gamble, J. A.; Tindall, G. W.; Thies, M. C. Liquid–liquid equilibrium compositions and global phase behavior for the lignin–acetic acid–water system at 70 and 95° C. *Fluid Phase Equilib.* **2018**.

(114) Jiang, G.; Nowakowski, D. J.; Bridgwater, A. V. A systematic study of the kinetics of lignin pyrolysis. *Thermochimica Acta* **2010**, *498*, 61-66.

(115) Imura, Y.; Hogan, R.; Jaffe, M. In *Dry spinning of synthetic polymer fibers;* Advances in Filament Yarn Spinning of Textiles and Polymers; Elsevier: 2014; pp 187-202.

(116) Huang, X. Fabrication and properties of carbon fibers. *Materials* **2009**, *2*, 2369-2403.

(117) Otani, C.; Polidoro, H.; Otani, S.; Craievich, A. Structure variations of carbonizing lignin. *Journal de Chimie Physique* **1984**, *81*, 887-891.

(118) Rodríguez-Mirasol, J.; Cordero, T.; Rodríguez, J. High-temperature carbons from kraft lignin. *Carbon* **1996**, *34*, 43-52.

(119) Johnson, D.; Tomizuka, I.; Watanabe, O. The fine structure of lignin-based carbon fibres. *Carbon* **1975**, *13*, 321-325.

(120) Kubo, S.; Kadla, J. F. Hydrogen bonding in lignin: a Fourier transform infrared model compound study. *Biomacromolecules* **2005**, *6*, 2815-2821.

(121) Mainka, H.; Hilfert, L.; Busse, S.; Edelmann, F.; Haak, E.; Herrmann, A. S. Characterization of the major reactions during conversion of lignin to carbon fiber. *Journal of Materials Research and Technology* **2015**, *4*, 377-391.

(122) Snowdon, M. R.; Mohanty, A. K.; Misra, M. A study of carbonized lignin as an alternative to carbon black. *ACS Sustainable Chemistry & Engineering* **2014**, *2*, 1257-1263.

(123) Goudarzi, A.; Lin, L.; Ko, F. K. X-ray diffraction analysis of kraft lignins and lignin-derived carbon nanofibers. *Journal of Nanotechnology in Engineering and Medicine* **2014**, *5*, 021006.

(124) Cao, J.; Xiao, G.; Xu, X.; Shen, D.; Jin, B. Study on carbonization of lignin by TG-FTIR and high-temperature carbonization reactor. *Fuel Process Technol* **2013**, *106*, 41-47.

(125) Köhnke, J.; Fürst, C.; Unterweger, C.; Rennhofer, H.; Lichtenegger, H. C.; Keckes, J.; Emsenhuber, G.; Liebner, F.; Gindl-Altmutter, W. Carbon microparticles from organosolv lignin as filler for conducting Poly (lactic acid). *Polymers* **2016**, *8*, 205.

(126) Ferrari, A. C.; Robertson, J. Interpretation of Raman spectra of disordered and amorphous carbon. *Physical review B* **2000**, *61*, 14095.

(127) Schreiber, M.; Vivekanandhan, S.; Mohanty, A. K.; Misra, M. Iodine treatment of lignin–cellulose acetate electrospun fibers: enhancement of green fiber carbonization. *ACS Sustainable Chemistry & Engineering* **2014**, *3*, 33-41.

(128) Wang, S.; Zhou, Z.; Xiang, H.; Chen, W.; Yin, E.; Chang, T.; Zhu, M. Reinforcement of lignin-based carbon fibers with functionalized carbon nanotubes. *Composites Sci. Technol.* **2016**, *128*, 116-122.

(129) Cuesta, A.; Dhamelincourt, P.; Laureyns, J.; Martinez-Alonso, A.; Tascón, J. D. Raman microprobe studies on carbon materials. *Carbon* **1994**, *32*, 1523-1532.

(130) Tuinstra, F.; Koenig, J. L. Raman spectrum of graphite. *J. Chem. Phys.* **1970**, *53*, 1126-1130.

(131) Ko, T. Raman spectrum of modified PAN‐based carbon fibers during graphitization. *J Appl Polym Sci* **1996**, *59*, 577-580.

(132) Rodríguez, J. J.; Cordero, T.; Rodríguez-Mirasol, J. In *Carbon Materials from Lignin and Their Applications;* Production of Biofuels and Chemicals from Lignin; Springer: 2016; pp 217-262.

(133) Liu, J.; Qu, W.; Xie, Y.; Zhu, B.; Wang, T.; Bai, X.; Wang, X. Thermal conductivity and annealing effect on structure of lignin-based microscale carbon fibers. *Carbon* **2017***, 121*, 35-47.

(134) Hagberg, J. *Carbon Fibres for Multifunctional Lithium-Ion Batteries* **2018**.

(135) Alway-Cooper, R. M.; Anderson, D. P.; Ogale, A. A. Carbon black modification of mesophase pitch-based carbon fibers. *Carbon* **2013***, 59*, 40-48.

(136) Franklin, R. E. The structure of graphitic carbons. *Acta Crystallogr.* **1951**, *4*, 253-261.

APPENDICES

A.1 Preparation of FSLP-based carbon fiber composite

To wrap up the carbon fiber characterization study, preliminary experiments were conducted to produce FSLP-based carbon fiber composites. Due to the limitation of batch-scale experiments, FSLP-based carbon fibers were produced in a small amount, so it was not possible to prepare ASTM standard type large composite samples. Instead, to demonstrate the incorporation of FSLP-based carbon fibers in an epoxy matrix, mini-composites were produced measuring nominally 1 cm × 5 cm, as shown in Figure A.1.

First, FSLP-based carbon fibers were cut into size of 5 cm long tow and aligned in a silicone mold, as displayed in Figure A.1 (a). Epoxy mixture (EPON 828 and EPIKURE^{TM} 9553) was mixed in a weight ratio of 100:15.4. The epoxy mixture was applied over the carbon fibers as shown in Figure A.1 (b). Then, a porous Teflon release film was placed on top to let the excess of epoxy flow out and get absorbed by a bleeder ply. The whole system was wrapped by a Teflon bagging film. A hole was made on the side of the bagging film to connect the vacuum pump, as displayed in Figure A.1 (c). The system was left to cure while applying vacuum for 24 hours. Once cured, the bagging material was removed and the composite was placed in air convection oven for 2 hours at 120°C. Figure A.1 (d) shows a cured FSLP-carbon fiber composite sample.

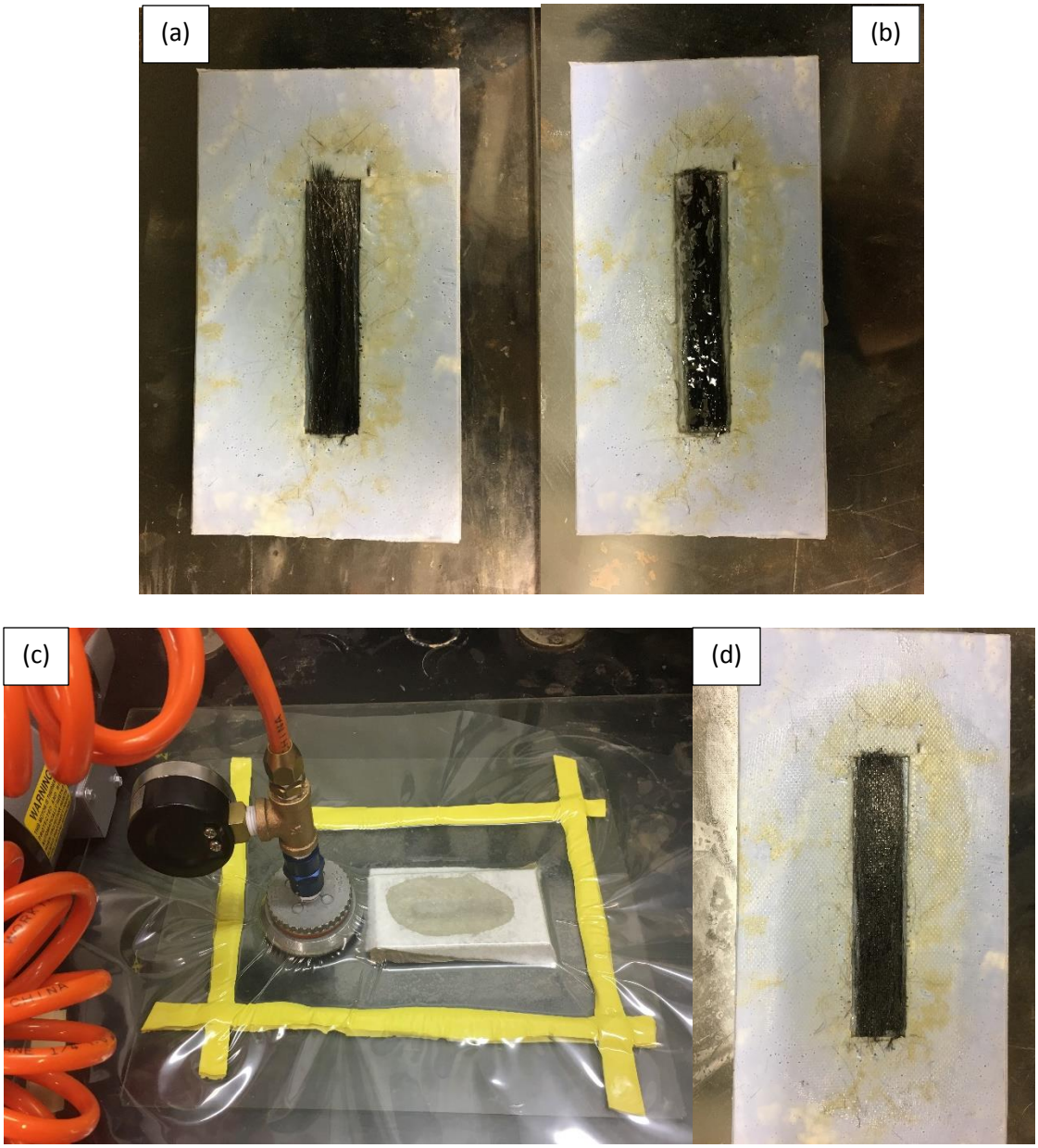

Figure A.1 The preparation of FSLP-based carbon fiber composite sample

For tensile test purpose, the end tabs were made on the composite samples to prevent the composite slipping out of the grips during the tensile test. About 1.5-2 cm long end tabs were made by applying fast cure epoxy glue on both side of the samples to prevent slippage, as shown in Figure A.2 (a).

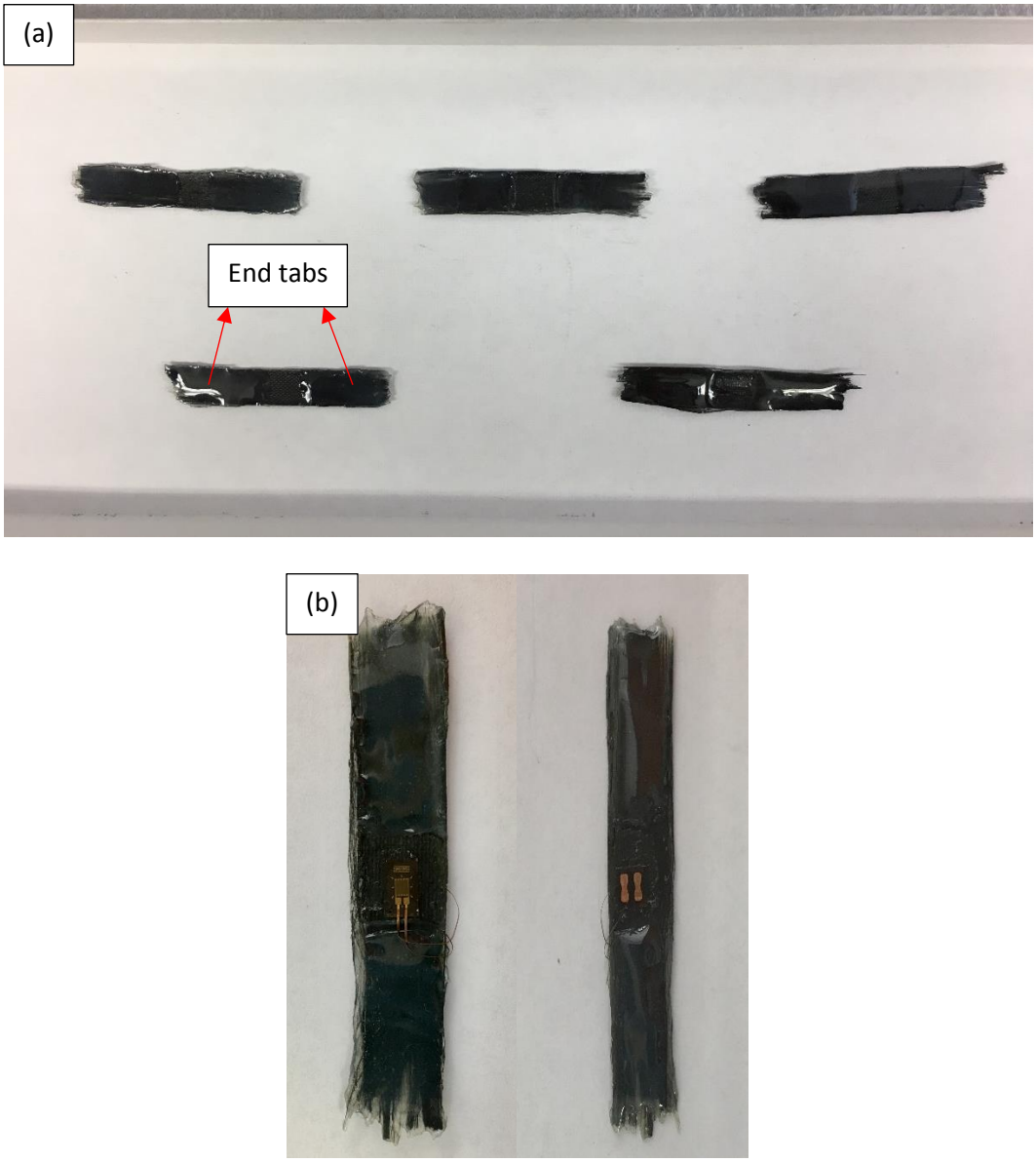

Figure A.2 FSLP-based carbon fiber composites with (a) end tabs (b) strain gauge

Strain gauge was applied to accurately measure the modulus of composite sample. A thin layer of LOCTITE super glue was applied on the surface of composite sample, which was 12 mm wide and 0.66 mm of thick, and strain gauge attached on it, as displayed in Figure A.2 (b). Once mounted on the sample, the strain gauge was connected to the P3 strain indicator and recorder, which can record the strain as stress is applied. The sample (with strain gauge) was mounted in the wedge-action grips of an ATS 900 testing machine, and the crosshead speed was set to 0.025 inch/min. The movement of crosshead pulls the sample apart, which increases its strain that is recorded by the gage. The P3 strain indicator converts the changing resistance to strain. The load was recorded using a 250-lb load cell in the ATS 900 testing machine. The thickness of the composite samples was measured under SEM, and illustrated in Figure A.3.

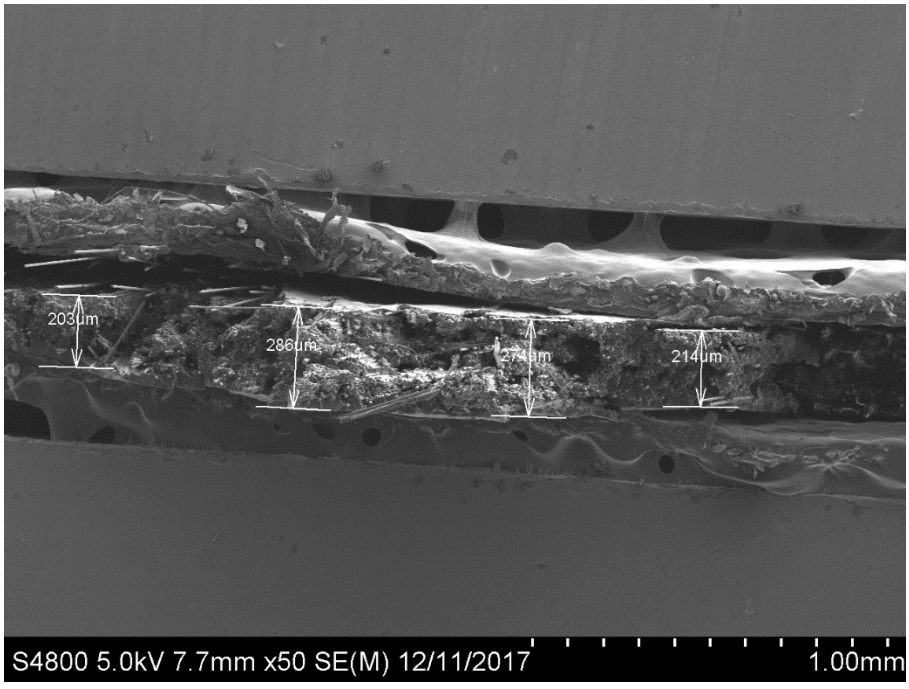

Figure A.3 SEM micrograph of the longitudinal cross-section of FSLP-based carbon fiber composite sample at low magnification

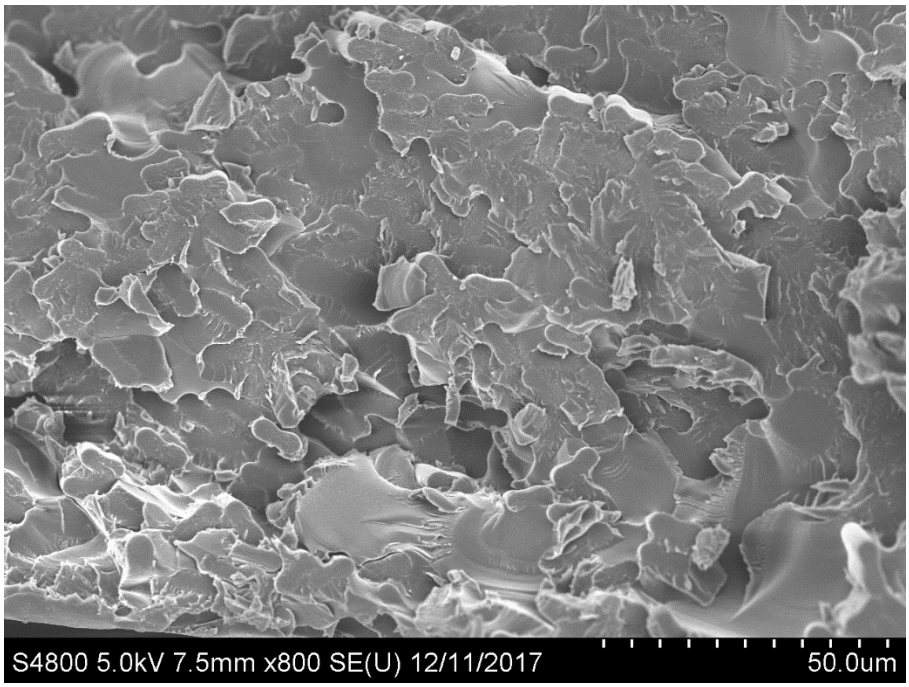

Figure A.4 SEM micrograph of the longitudinal cross-section of FSLP-based carbon fiber composite sample at high magnification

Figure A.4 displays the cross-section of the composite sample. The volume fraction was estimated by measuring the corresponding area of the carbon fibers with respect to the total inspected area using ImageJ. For FSLP-based carbon fiber composite, the average volume fraction was limited to approximately 13.8%, which is relatively low due to the mis-alignment of fibers in the composite samples. If the fibers were produced with large quantity in a continuous form, better alignment and a larger fiber volume fraction could be achieved.

The composite samples for tensile strength test broke a load of 60-85 lb (27.2-38.5 kg). The tensile strength could be obtained with the following equation, and the resulting stress- strain curve is displayed in Figure A.5.

$$\sigma_s = \frac{F}{A} = \frac{mg}{A} = \frac{38.5kg \times \frac{10N}{kg}}{0.01m \times (250 \times 10^{-6})m} = 154\ MPa$$

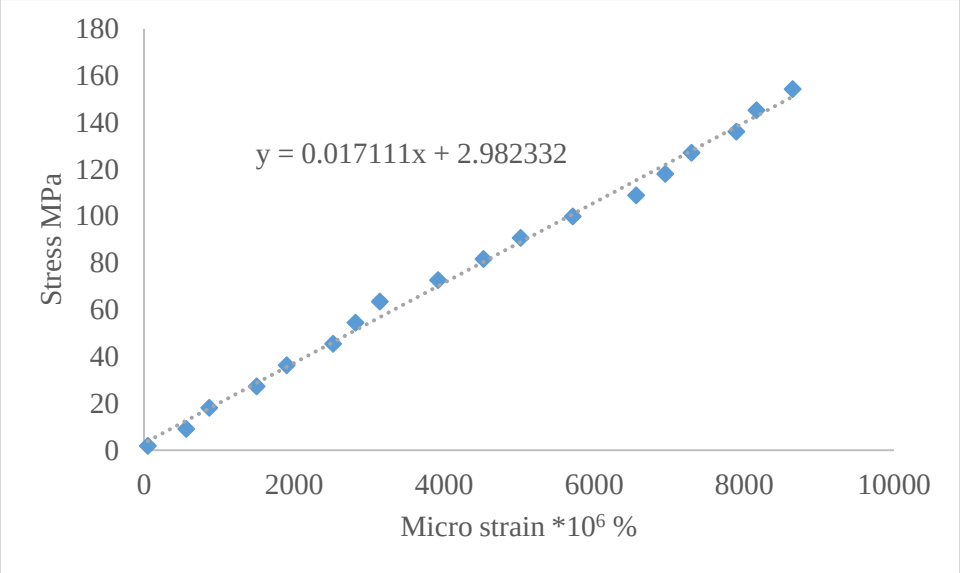

Figure A.5 Stress and micro strain plot of FSLP-based carbon fiber composite sample

$$E = 17.1Gpa$$

Three FSLP-based carbon fiber composites were tested. The average tensile strength and modulus were 124 ± 26 MPa and 15.4± 1.4 GPa, respectively.

The modulus of composite could also be predicted from rule-of-mixture by using resin properties in conjunction with fiber volume fraction.

$$E_c = E_f v_f + E_m v_m = E_f v_f + E_m(1 - v_f) = 85Gpa \times 0.138 + 3Gpa \times (1 - 0.138)$$
$$= 14.3Gpa$$

Using a resin modulus of 3 GPa, the unidirectional tensile modulus was predicted to be 14.3 GPa.